This is to certify that the

dissertation entitled

FINITE AMPLITUDE EFFECTS ON THE
DYNAMIC PERFORMANCE OF THE
CENTRIFUGAL PENDULUM VIBRATION
ABSORBER

presented by

Mehrnam Sharif-Bakhtiar

has been accepted towards fulfillment
of the requirements for

Ph.D. degree in Mechanical Engineering

Steven W Shaw
Major professor

Date 12/14/88

FINITE AMPLITUDE EFFECTS ON THE DYNAMIC PERFORMANCE OF THE CENTRIFUGAL PENDULUM VIBRATION ABSORBER

By:

Mehrnam Sharif-Bakhtiar

A THESIS

Submitted to
Michigan State University
in partial fulfillment of the requirements
for the degree of

DOCTOR OF PHILOSOPHY

Department of Mechanical Engineering

1989

ABSTRACT

FINITE AMPLITUDE EFFECTS ON THE DYNAMIC PERFORMANCE OF THE CENTRIFUGAL PENDULUM VIBRATION ABSORBER

By:

Mehrnam Sharif-Bakhtiar

The dynamic response of a centrifugal pendulum vibration absorber is studied. The thesis consists of two parts. First, the effects of the absorber's motion limiting stops on the overall response of the system is considered. The results of the analysis provide results on the existence and stability of the nonlinear periodic motions of the absorber mass based on various system parameters. Several properties which are inherent to the system are discovered in this analysis which have not been previously considered, including the coexistence of impacting and non-impacting motions at the *anti-resonance frequency* (the frequency for which the pendulum is designed).

For ranges of system parameters the stability of the symmetric periodic motions of the absorber mass break down due to pitchfork bifurcations and successive period doubling bifurcations ensue, leading to chaotic motions. The effect of detuning of the absorber is also considered.

In the second part of the study the nonlinear dynamic response of the system with damping in both the primary system and the pendulum is analyzed using the method of harmonic balance and Floquet theory. Periodic solutions are approximated by the first harmonic of the response; the resulting frequency response curves agree well with the simulations of the full nonlinear equations of motion. Particular attention is paid to the response at the anti-resonance frequency. Cases are demonstrated for which there exists more than one stable steady-state periodic motion of the system in the neighborhood of the anti-resonance frequency; this particular property of the system is due to nonlinear effects and cannot be captured through the traditional linear analysis. Furthermore, it is shown that for ranges of system parameters, the only stable periodic response of the system at the anti-resonance frequency is one of much larger amplitude than predicted by the linear analysis. The effects of system parameters on the shifting of the anti-resonance frequency and on the corresponding carrier amplitude are also considered.

The results obtained in the first part of the analysis confirm the conclusion that motion limiting stops for the absorber can be effectively employed when placed at amplitudes larger than the steady-state response predicted from the linearized analysis of the system at the anti-resonance frequency. The impact dynamics of the CPVA with motion limiting stops can be quite complicated when the system is subject to excitation frequencies above the anti-resonance frequency and can include chaotic motions. If the system is driven out of the region of validity for linearization, nonlinear effects can lead to catastrophic failures.

The results obtained in the second part of the analysis depict how the true response of the system can be drastically different than what is predicted from the linear analysis. Hence, as far as design applications of the CPVA are concerned, the response of the CPVA obtained through a linearized analysis of the system should by no means serve as the basis for the design, but rather as a first trial which is to be modified further through either experimental or nonlinear analysis of the system. Nonlinear characteristics of the system such as the shifting of the anti-resonance frequency and the jump phenomena must be considered in the design of the CPVA since, if ignored, the absorber's effectiveness can be reduced or result in larger oscillatory amplitudes in the primary system.

This work is dedicated to my family.

ACKNOWLEDGEMENTS

The author wishes to extend his deepest gratitude and appreciation to his advisor, Dr. Steven W. Shaw for his invaluable guidance and assistance throughout the course of his study along with the preparation of this manuscript.

Sincere thanks are also extended to the other members of the author's Doctoral Guidance committee, Dr. Ronald C. Rosenberg, Dr. Brian S. Thompson, Dr. Shui-Nee Chow, Dr. Alan Haddow, and Dr. Konstantin Mischaikow.

TABLE OF CONTENTS

LIST OF FIGURES

CHAPTER 1
INTRODUCTION

1.1- History and Literature Survey

The centrifugal pendulum vibration absorber (CPVA for short), although patented previously in France, was independently conceived and put into practice by E. S. Taylor in 1935 in order to eliminate torsional vibrations of geared radial aircraft-engine-propeller systems [1]. This was the first presentation of pendulous absorbers in the United States. The device, however, is useful in a broader range of applications for the reduction of torsional oscillations in rotating shafts of large engines and machinery which are subjected to torsional disturbances of frequencies proportional to the nominal speed of the shaft. Due to the relatively short length of the pendulum required to function as an effective absorber, the device was not suitable for small engines such as automotive engines until 1942 when the absorber was modified and incorporated into the design of internal combustion engines in order to alleviate the torsional vibrations of the crank shaft. This was done by integrating the absorber with the crankshaft counterbalance masses [2]. The effective radius of the pendulum in this case is the difference between the bushing's inner radius and the mating pin's radius (*i.e.*, the clearance in the journal bearing) which can be made as small as necessary.

In general, the reduction of torsional vibrations in rotating shafts such as automotive crank shafts is achieved using one of three different classes of dampers or absorbers [3]. These are the frictional dampers [4], tuned absorbers [5], and pendulous absorbers, where the CPVA belongs to this latter class.

In frictional dampers, the torsional vibration of the crank shaft is damped uniformly throughout the whole range of operational frequency of the system. Its effectiveness depends on its moment of inertia and the fluid viscosity which is used as the damping element. The main disadvantage of such a device is the substantial increase in the overall weight of the engine and the need to dissipate the heat generated by the damper. On the other hand, tuned absorbers, like linear spring-mass absorbers, are effective only for the fixed, narrow bandwidth of the frequency for which they are designed and, except in a few specialized cases, tuned absorbers find limited applications in the design of rotating shafts due to the variation of the speed of the crank shaft and consequently, the excitation frequency applied on the shaft.

The CPVA, however, is essentially a tuned absorber whose natural frequency varies in direct proportion to the rotational speed of the crankshaft. It also introduces no additional weight increase to the design of the system in many applications, and hence the CPVA becomes an attractive alternative to the reduction of torsional vibrations in engines and it makes the detailed study of its dynamic performance worthwhile.

The centrifugal pendulum vibration absorber has been successfully employed to overcome induced vibrations on the cabin and cockpit of helicopters which are due to the transmission of vibration from the main rotor hub of the craft. W. F. Paul [6] has noted an experiment on commercial and USAF versions of the Sikorsky S-61 helicopters where an airframe vibratory stress reduction of as much as 4:1 was achieved, and cockpit and cabin vibrations of $\pm 0.1g$ were recorded through the use of the CPVA indicating a substantial improvement over the recorded data of the operation of the rotor without the absorbers..

After the original idea of E. S. Taylor [1] to devise the CPVA, numerous research studies have been undertaken in order to exploit the potential advantages of the centrifugal absorber. A few instances are cited in the papers discussed below.

Zdanowich [8] presents an alternative approach to describe the mechanics of reduction of the carrier amplitude to zero at ω_{AR} through the notion of the **effective inertia** of the carrier. It is shown in [8] that at the anti-resonance frequency, the effective inertia of the carrier with respect to the sinusoidal excitation tends to infinity and therefore there will be no oscillation of the carrier.

Den Hartog [9] observed in 1947 that for a rotor, translational vibration of the rotor mass center in two orthogonal directions and torsional vibrations could be simultaneously reduced to zero by employing three pendula fixed to the rotor and disposed about the circumference of the rotor at 120 degrees with respect to one another. However, as noted by T. C. Lim [10], Den Hartog's analysis is not free of flaws in the sense that, although the rotor mass center translational acceleration in the direction of the applied force can be reduced to zero, the rotating pendula will always induce vibrations transverse to the line of action of the applied force. This problem may be solved by employing several such sets of pendula along the shaft.

Robert Plunkett [11] has carried out a rather detailed survey on the study and application of the CPVA along with other modes of vibration absorption through the appropriate use of the damping characteristics in materials and vibration isolation. The author is indebted to Plunkett's work [11] for providing some of the resources on the subject. Zdanowich and Wilson [8] present a description of application of CPVA prior to WWII. Harker [12] gives charts and design guidelines for the use of practical design; Meyer and Saldin [13] show an application of the absorber to turbine buckets and Reed [14], like Den Hartog [9], indicates the possibility of applying the principle to nonrotating machinery.

Some of the credit for the novel application of the idea of the CPVA goes to Sarazin [15] and to Chilton and Reed [16] who in 1930 proposed the idea of bifilar pendula as absorbers. Butler [17] elaborates on the notion of having the absorber's center of mass in the bifilar construction move on a noncircular trajectory. H. H. Denman in 1988 illustrated in [18] that such modification in the design of the absorber can be beneficial to the overall response of the system. Crossley studies the nonlinear response of the CPVA due to the wide angle of swing of the absorber in free [19] and the forced [20] modes of response, respectively. W. L. Miao and T. Mouzakis [21] present an experimental study on the nonlinear characteristics of the bifilar absorber mounted on the rotor hub of a helicopter. This idea originates from Kelly's work [22] who proposed the notion of application of CPVA to helicopter rotors to overcome excessive torsional vibrations of the mainframe of the helicopter. Mouzakis [23] discusses the interesting notion of a *monofilar* absorber which inherently possesses two distinct frequencies at which the absorber can be employed effectively.

1.2- Objectives

One of the major difficulties in the design and application of the CPVA is excessively large amplitudes of oscillation of the absorber which can occur during operation [19, 20]. In other words, absorbers that are thought to be properly designed can exhibit dynamics that are inconsistent with the original analysis. An example is cited by Newland [7] where an engine was designed with pendula calculated to swing through 45 degrees. During tests it was found that the vibration absorbers were not functioning properly and on dismantling the engine they were found to have been oscillating through a much larger angle than expected, damaging the stops which were set at 75 degrees amplitude.

Most of the literature on the subject of CPVA is based on the linear analysis of the system (see references [1-5], [8], [10] and, [30], for example). The studies of the nonlinear response are more limited (see Newland [7], Crossley [19, 20], Paul [6] and, Den Hartog [9]), and there are many dynamic properties of the system which remain to be explored. The increasing use of mathematical tools such as bifurcation theory [26] and the Poincarè map [27], to study nonlinear systems, along with the advent of high speed computing systems, makes it possible to undertake a more thorough study of the response of the CPVA. This report aims at shedding light on some of the nonlinear dynamic properties of the CPVA which have not been considered before.

The study is composed of two parts. In the first, an attempt is made to alleviate the large amplitude oscillation problem of the absorber by limiting its maximum angle of swing to a prescribed value. This is carried out by incorporating rigid constraints in the design of the CPVA. The resulting dynamics are dealt with in detail in chapter two.

In the second part of the study the objective is to better understand the dynamics of the CPVA without the constraints. To this effect, higher order nonlinear and damping terms are retained in the equations of motion of the system and their effects on the response of the system are studied. This is covered in chapter three of the thesis. Chapter 4 contains an overview of the results, some conclusions, and suggestions for further work.

In order to carry out the numerical computations of the analysis, the following system parameters are used throughout the study:

Crank radius, $R = 2.24$ *in.*

Crank polar moment of inertia, $J = 772.28$ *lb.in*^{2}.

Absorber effective length, $r = .561$ *in.*

Absorber mass, $m = 25.6$ *lbm.*

Crank rotational speed, $\Omega = 1000$ *RPM.*

The above dimensions might are chosen to be in the range of practical applications.

1.3- Full Nonlinear Equations of Motion

Figure (1) depicts a schematic view of the CPVA as applied in practice. The pendulous absorber is employed as a bifilar pendulum (Figure 2a) in which the absorber is mounted on the carrier through two pivoting arms. In addition, the absorber itself has a finite moment of inertia which can effect the dynamics of the system. However, in the following it is demonstrated that such bifilar configuration can be modeled as a simple pendulum (Figure 2b) provided certain geometric relations hold [7]. This is done through a comparison of the equations of motions of the models.

Referring to Figure (2a), which is a schematic view of a bifilar pendulum absorber, the expression for the velocity of the mass center of the absorber mass can be written as:

$$\overline{v}_{CG}=[(b+h)\psi'\cos\psi+l(\phi'-\psi')\cos(\psi+\phi)]\overline{i}+$$

$$+[-(b+h)\psi'\sin\psi+l(\phi'-\psi')\sin(\psi+\phi)\overline{j} \quad . \tag{1.1.1}$$

Denoting the inertia of the absorber with respect to its center of gravity by I_p, the kinetic energy of the bifilar system can be written as:

$$\overline{KE}=\frac{1}{2}(I+I_p)\psi'^2+$$

$$+\frac{1}{2}m\,[\psi'^2(b+h)^2+(\phi'-\psi')^2l^2-2\psi'(\phi'-\psi')l(b+h)\cos\phi] \tag{1.1.2}$$

Lagrange's equation can be written as:

$$\frac{d}{d\tau}\left(\frac{\partial\overline{KE}}{\partial\dot{q}_i}\right)-\frac{\partial\overline{KE}}{\partial q_i}+\frac{\partial PE}{\partial q_i}=Q_{r_{i_{nc}}} \qquad i=1,2 \tag{1.1.3}$$

where τ denotes time, q_1 and q_2 represent the generalized coordinates ψ and

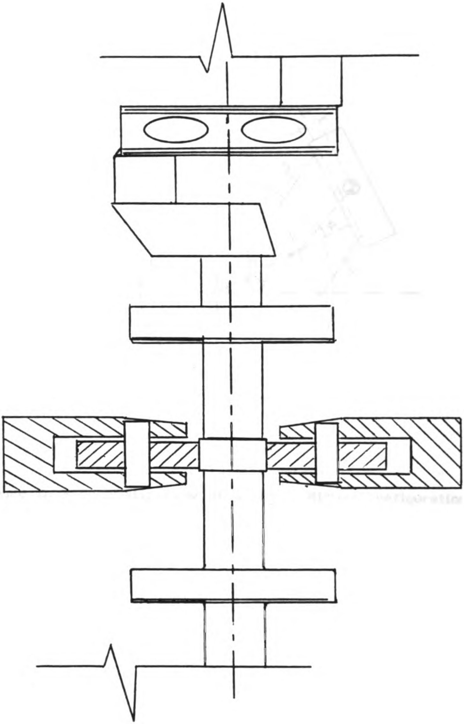

Figure 1 - Schematic View of a CPVA as Used in Practical Applications

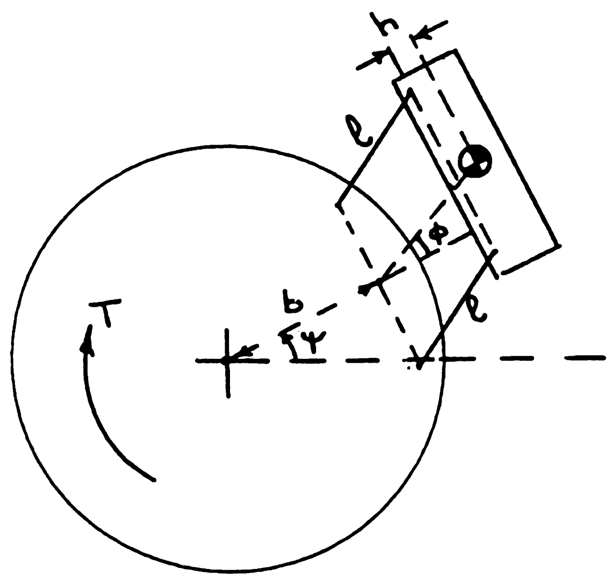

Figure 2a - Schematic view of a CPVA; Bifilar configuration

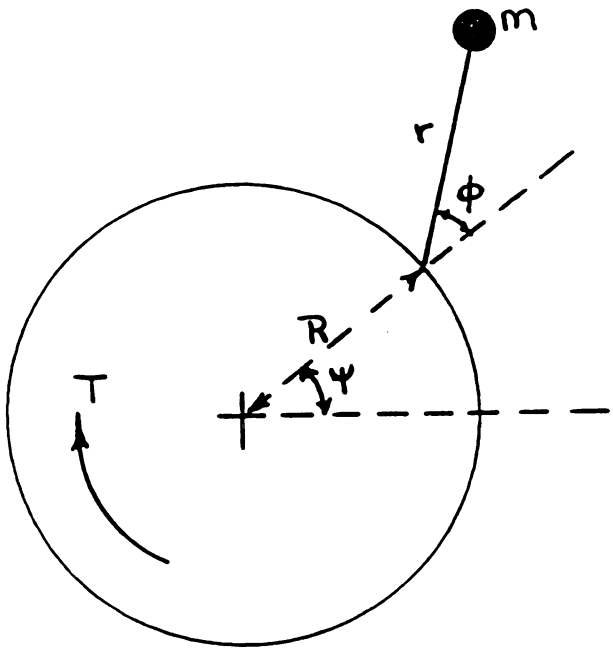

Figure 2b - Schematic view of a CPVA; Simple Pendulum Configuration

ϕ, and $Q_{r_{i_{nc}}}$, i=1,2 are generalized forces being $-C_p\phi'$ for the absorber and $-C_c\psi'+T(\tau)$ for the carrier, $T(\tau)$ represents the torsional excitation on the carrier and C_c and C_p are the damping values of the carrier and the absorber, respectively. The effect of gravity on the system is negligible for even moderate rotational speeds and hence the potential energy is zero, PE=0. Hence, the equations of motion for the bifilar pendulum vibration absorber system can be written as:

$$[(I+I_p)+m(b+h)^2+ml^2+2m(b+h)l\cos\phi]\psi''$$

$$-ml((b+h)\cos\phi+l)\phi''+$$

$$+m(b+h)l\phi'^2\sin\phi-2m(b+h)l\psi'\phi'\sin\phi+C_c\psi'=T(\tau) \tag{1.1.4a}$$

$$-ml((b+h)\cos\phi+l)\psi''+ml^2\phi''+C_p\phi'+m(b+h)l\psi'^2\sin\phi=0 \tag{1.1.4b}$$

Referring to Figure (2b), the relation for the absolute velocity of the absorber mass can be written as:

$$\bar{v}_c=\bar{v}_c+\bar{v}_{p/c}$$

where subscripts c and p stand for the carrier and the pendulum, respectively. Since

$$\bar{v}_c=(R\psi'\sin\psi)\bar{i}-(R\psi'\sin\psi)\bar{j}$$

and,

$$\bar{v}_{p/c}=[-r(-\psi'+\phi')\sin(\psi+\phi)]\bar{i}+[r(-\psi'+\phi')\cos(\psi+\phi)]\bar{j}$$

then,

$$\bar{v}_p = [R\,\psi'\sin\psi + r(\psi' - \phi')\sin(\psi+\phi)]\bar{i} + [-R\,\psi'\cos\psi +$$

$$+ r(\psi' - \phi')\cos(\psi+\phi)]\bar{j}, \qquad (1.1.5a)$$

and hence,

$$v_p^2 = R^2\psi'^2 + r^2(\psi' - \phi')^2 + 2Rr\,\psi'(\psi' - \phi')\cos\phi \qquad (1.1.5b)$$

Thus, the kinetic energy of the system of Figure (2b) can be written as:

$$KE = \frac{1}{2}J\psi'^2 + \frac{1}{2}mv_m^2$$

or

$$KE = \frac{1}{2}(J+mR^2)\psi'^2 + \frac{1}{2}mr^2(\psi' - \phi')^2 + mRr\,\psi'(\psi' - \phi')\cos\phi \qquad (1.1.6)$$

where J is the polar moment of inertia of the carrier, m is the absorber mass, R and r are the effective carrier and the pendulum radii, respectively, and ψ and ϕ are the angular displacements of the carrier and the pendulum, respectively, as denoted in Figure (2).

Neglecting the effects of gravity on the system, and applying Lagrange's equation, the equations of motion for the simple pendulum absorber of Figure (2b) can be written as:

$$[J + mR^2 + mr^2 + 2mRr\cos\phi]\psi'' - mr(R\cos\phi + r)\phi'' + mRr\,\phi'^2\sin\phi -$$

$$-2mRr\,\psi'\,\phi'\sin\phi + C_c\,\psi' = T(\tau) \qquad (1.1.7a)$$

$$-mr(R\cos\phi + r)\psi'' + mr^2\phi'' + C_p\,\phi' + mRr\,\psi'^2\sin\phi = 0 \qquad (1.1.7b)$$

where ( )$'$ denotes differentiation with respect to time, τ, and $T(\tau)$ represents the excitation on the carrier.

Comparison of equations (1.1.4) and (1.1.7) reveals that the bifilar pendulum vibration absorber of Figure (2a) can be dynamically modeled as the simple pendulum vibration absorber of Figure (2b) provided the following geometric conditions hold:

$$J = I + I_p$$

i.e., the inertia of the carrier in Figure (2b) should be the total inertia of the carrier and the pendulum. Also,

$$r = l$$

$$R = b + h$$

i.e., the effective radius of the carrier in Figure (2b) should be the sum of the distance from the center of the carrier to the line joining the pivot points of the bifilar absorber, plus the distance from the center of gravity of the bifilar absorber to the line joining its pivot points (see Figure 2a). This equivalent modeling of the bifilar absorber by a simple pendulum absorber is possible primarily due to the fact that there is no rotation of the bifilar absorber about its center of gravity.

Considering the above analysis, from hereafter the simple pendulum model of the CPVA will be used for obvious reasons of simplicity, while it is understood that the necessary geometric conditions hold between the simple pendulum model used with its corresponding bifilar type.

By referring to the equations of motion for the CPVA (equations 1.1.7) one can observe that the angular displacement of the carrier, ψ, does not appear in either of the equations (1.1.7). This renders the variable ψ ignorable and consequently, when written in first order form, the equations represent a third order system, *i.e.*, one equation each for $\dot{\psi}$, ϕ and, $\dot{\phi}$. Hence, the solution of the equations of motion yields $\dot{\psi}$ where upon integration the angular displacement of the carrier, ψ, can be obtained up to an arbitrary constant.

1.4- The Undamped, Linear System

As a first attempt to the solution of the problem under study, the dynamic response of an undamped, linear system is studied in this section. Obviously, a true model of the actual system should incorporate the effects of damping and also the effects of nonlinearities. However, a study of this simple model provides insight into the overall dynamic response of the system and yields approximate results to the actual nonlinear, damped system. Furthermore, a linear undamped model of the CPVA is often a valid model of the actual system since for very low absorber and carrier damping values (as is typically the case) and small amplitudes of the oscillation of the absorber, the CPVA can be modeled as a linear, undamped system with an acceptable degree of accuracy. Also, introduction of damping and nonlinear effects into the model can be looked upon, in an asymptotic sense, as perturbations on the linear system.

In order to carry out the linear analysis, certain assumptions are made to simplify the equations of motion, they are as follows:

1. The angular displacement of the absorber, ϕ, is small enough that

$$\sin\phi=\phi \quad , \quad \cos\phi=1 \ .$$

2. The dampings in the carrier, C_c, and the pendulum, C_p, are negligible.
3. The excitation is of the form

$$T(\tau)=T_0\sin\omega\tau \tag{1.2.1}$$

4. The motion of the carrier, ψ, is a steady-state, constant rotation plus a small sinusoidal oscillation, *i.e.*,

$$\psi=\Omega\tau+\theta \tag{1.2.2}$$

5. Terms involving products of ϕ, θ and their time derivatives are negligible.

Substitution of assumptions 1 through 5 into the equations of motion (1.1.7) results in the *undamped*, *linearized* equations of motion as follows:

$$[J+m(R+r)^2]\theta''-mr(R+r)\phi''=T_0\sin\omega\tau \tag{1.2.3a}$$

$$-mr(R+r)\theta''+mr^2\phi''+mRr\Omega^2\phi=0 \tag{1.2.3b}$$

Now we assume a sinusoidal system response:

$$\phi=\phi_0\sin\omega\tau \tag{1.2.4a}$$

$$\theta=\theta_0\sin\omega\tau \tag{1.2.4b}$$

where the relative phase (0 or π) is accounted for in the signs of θ_0 and ϕ_0. Using equations (1.2.2) and (1.2.4), equations for the amplitudes ϕ_0 and ψ_0 can be obtained:

$$-[J+m(R+r)^2]\omega^2\psi_0+mr(R+r)\omega^2\phi_0=T_0 \tag{1.2.5a}$$

$$mr(R+r)\omega^2\psi_0-mr^2\omega^2\phi_0+mRr\Omega^2\phi_0=0 \tag{1.2.5b}$$

Equations (1.2.5) are the ***amplitude*** relations for the linearized model of the CPVA. The natural frequencies and mode shapes of the system are determined to be:

$$\omega_1=0 \quad , \quad \omega_2=\left(\frac{R\Omega^2}{Jr}[J+m(R+r)^2]\right)^{1/2} \tag{1.2.6}$$

and

$$v_1=\begin{pmatrix}\infty\\ c\end{pmatrix} \ , \ c \ arbitrary, \tag{1.2.7a}$$

$$v_2=\begin{pmatrix}1\\ I_1\end{pmatrix} \ , \ I_1=\frac{-[J+m(R+r)^2]}{mr(R+r)} \tag{1.2.7b}$$

In words, the mode shape represented by equation (1.2.7a) which correponds to the $\omega_1=0$ natural frequency, indicates a rigid-body mode in which the angular displacement of the carrier tends to infinity while the absorber retains a finite angle with respect to the $\phi=0$ reference line. The second mode, equation (1.2.7b), is associated with the nontrivial natural frequency of the system and corresponds to the case where the carrier and the absorber are oscillating out of phase.

Note that from equation (1.2.5b), the steady-state amplitude ratio equation can be written as:

$$\frac{\psi_0}{\phi_0}=\frac{\omega^2-\Omega^2\frac{R}{r}}{\left(\frac{R+r}{r}\omega^2\right)} \quad . \tag{1.2.8}$$

This implies that if the frequency of the torsional excitation, ω, on the carrier is $j\Omega$, $j=1,2,3,\ldots$, then the pendulum can be tuned such that $j=(R/r)^{1/2}$, thereby reducing the oscillatory amplitude of the carrier to zero. In fact, such disturbances whose frequencies are multiples of the rotational speed of the carrier, Ω, are typical in internal combustion engines. This particular frequency for which the absorber is designed is called the ***anti−resonance frequency*** and is denoted by ω_{AR}. Hence,

$$\omega_{AR}=\Omega\left(\frac{R}{r}\right)^{1/2} \quad . \tag{1.2.9}$$

Note that ω_{AR} varies in direct proportion to Ω, the nominal rotational speed of the carrier. The term $j=(R/r)^{1/2}$ is called the *order* of the engine torque and in most practical applications, torques of order half the number of cylinders of the engine are the most dominant ones. For instance, for a four cylinder, four-stroke automotive engine (the type of engine considered in this report), the order $j=2$ torque, *i.e.*, the second harmonic of the excitation, carries a substantial portion of the overall torque.

Figures (3a) and (3b) illustrate the frequency response of the carrier and the absorber, respectively, as obtained based on the undamped linearized CPVA model. Note that at the anti-resonance frequency, ω_{AR}, while the carrier amplitude of oscillation is reduced to zero, the absorber has a finite amplitude of oscillation described by

$$\phi_0 \big|_{\omega=\omega_{AR}} = \frac{T_0}{mRr\Omega^2(R+r)} \quad .$$

At the anti-resonance frequency the torque exerted by the absorber on the carrier is equal in magnitude and opposite in direction to that of the external excitation torque, hence resulting in a net zero torque on the carrier.

In order to better understand the dynamics of the CPVA under the given excitation and damping conditions, and to grasp a general overview of the mechanics of the system, the next section is devoted to the steady-state response of the system under various simple but basic excitation and damping conditions. The solutions presented therein will provide the basis for further analysis of the system, as the various expansion processes described in the following chapters will be done about the appropriate steady-state solutions demonstrated in the next section.

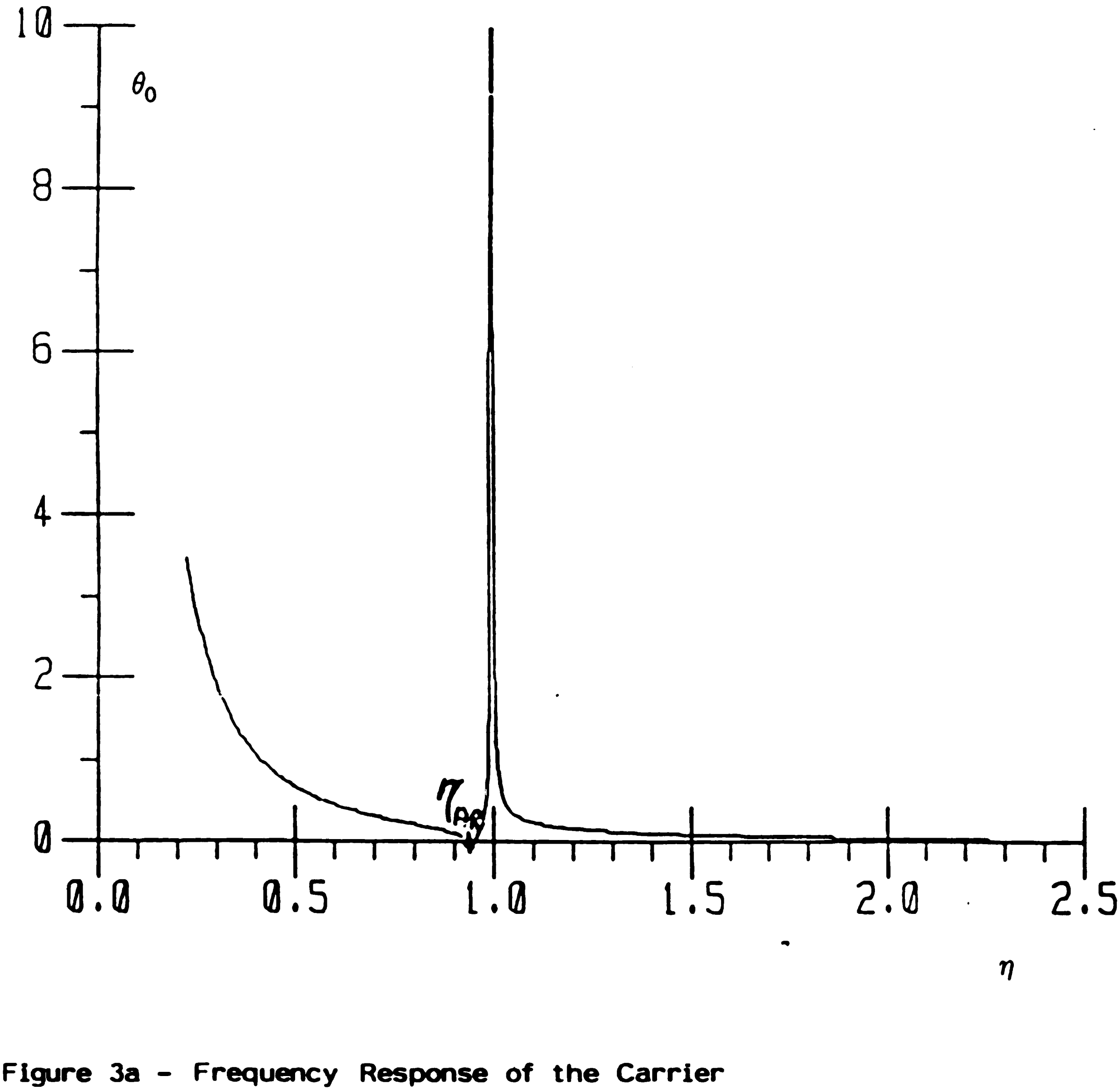

Figure 3a - Frequency Response of the Carrier

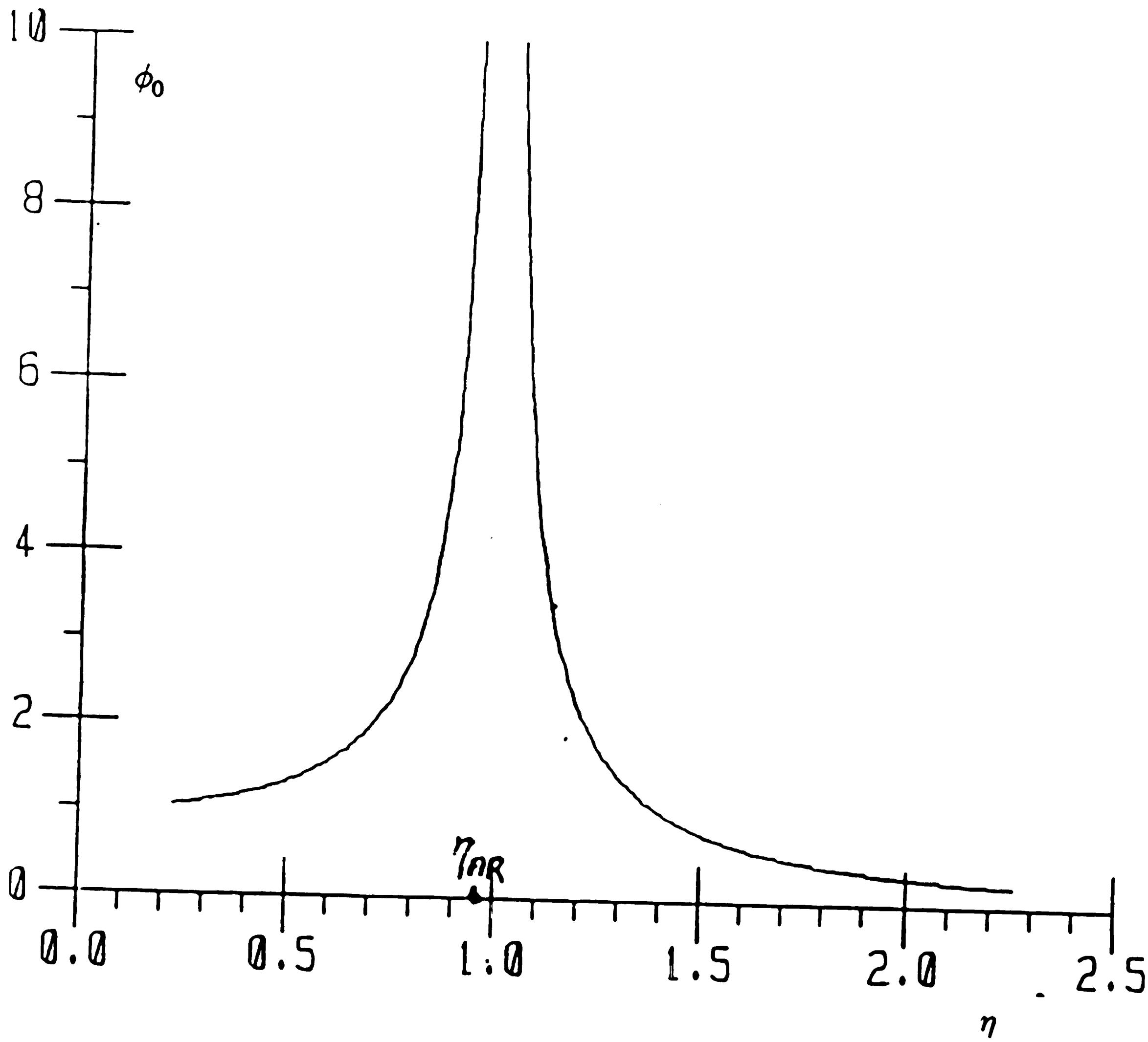

Figure 3b - Frequency Response of the Pendulum

1.5- Steady-State Dynamics of the CPVA for Various Combinations of Damping and Nonoscillatory Excitation

In this section the steady-state solutions of the nonlinear equations of motion are obtained for various damping and constant torque conditions. The steady-state response of the system in the absence of any oscillating component of the torque is presented in the following in order to provide the nominal operating conditions for the case of no applied periodic torques. These operating conditions are used as a basis for linearization and for nonlinear expansions throughout the thesis.

By referring to the equations of motion (1.1.7) and letting $T(\tau)=T_0$, a constant torque, the equations of motion can be rewritten as

$$[J+mR^2+mr^2+2mRr\cos\phi]\psi'' - mr(R\cos\phi+r)\phi'' + mRr\phi'^2\sin\phi -$$

$$-2mRr\psi'\phi'\sin\phi + C_c\psi' = T_0 \tag{1.3.1a}$$

$$-mr(R\cos\phi+r)\psi'' + mr^2\phi'' + C_p\phi' + mRr\psi'^2\sin\phi = 0 \tag{1.3.1b}$$

Depending on whether C_c, C_p or, T_0 are taken to be zero in equations (1.3.1), the following eight different cases can be outlined.

1. $C_c=C_p=0$; $T_0\neq0$

This renders the equations of motion (1.3.1) as

$$[J+mR^2+mr^2+2mRr\cos\phi]\psi'' - mr(R\cos\phi+r)\phi'' + mRr\phi'^2\sin\phi -$$

$$-2mRr\psi'\phi'\sin\phi = T_0 \tag{1.3.2a}$$

$$-mr(R\cos\phi+r)\psi'' + mr^2\phi'' + mRr\psi'^2\sin\phi = 0 \tag{1.3.2b}$$

In order to find the steady-state solutions of the CPVA corresponding to equations (1.3.2), let

$$\psi'' = \alpha \ , \ \alpha = constant$$

$$\phi'' = \phi' = 0$$

Hence, integrating these latter equations with respect to time, τ, yields,

$$\psi' = \alpha\tau + \Omega$$

and

$$\phi = constant \quad .$$

Substitution of these equation into equations (1.3.2) yields,

$$[J + mR^2 + mr^2 + 2mRr\cos\phi]\alpha = T_0 \tag{1.3.3a}$$

$$-mr(R\cos\phi + r)\alpha + mRr(\alpha\tau + \Omega)^2\sin\phi = 0 \tag{1.3.3b}$$

Assuming ϕ is small enough that one can write $\cos\phi = 1$, equation (1.3.3a) yields an expression for α as

$$\alpha = \frac{T_0}{J + m(R + r)^2} \quad .$$

Note that this case corresponds to the first mode of the CPVA obtained in equation (1.2.6) and (1.2.7a) implying that the angular displacement of the carrier, ψ, tends to infinity while the pendulum makes a small but finite angle with the $\phi=0$ line (see Figure 2b) at $\tau=0$. This angle tends to zero as ψ tends to infinity. To be specific, from equation (1.3.3b) one can write

$$R\,\alpha\tau^2\sin\phi = R + r \quad .$$

In other words ϕ varies in time in such a way that the above relation holds for all time τ implying that $\phi \longrightarrow 0$ as $\tau \longrightarrow \infty$.

2. $C_c = C_p = T_0 = 0$

Under these conditions, by letting

$$\psi''=0 \quad , \quad \psi'=\Omega \quad , \quad \Omega \text{ constant} \tag{1.3.4a}$$

$$\phi''=\phi'=0 \quad , \quad \phi=constant \tag{1.3.4b}$$

equation (1.3.1b) is identically zero and equation (1.3.1a) yields

$$mRr\Omega^2 \sin\phi=0$$

implying

$$\Omega=0 \quad , \quad \phi \text{ arbitrary}$$

or

$$\phi=n\pi \quad , \quad \Omega \text{ arbitrary.}$$

where the first of these two solutions is the trivial static configuration and the second corresponds to the case where the carrier is rotating with a constant angular velocity while the pendulum remains at $\phi=0$ ($\phi=\pi$ is unstable).

3. $C_c \neq 0$, $C_p = T_0 = 0$

Using the assumptions outlined in equations (1.3.4), equations (1.3.1a,b) yield

$$C_c \Omega=0 \quad => \quad \Omega=0 \quad ,$$

and

$$mRr\Omega^2 \sin\phi=0 \quad => \quad \phi \text{ arbitrary.}$$

In other words, the carrier comes to a stop with the absorber at an arbitrary angle.

4. $C_c, C_p \neq 0$, $T_0=0$

Letting

$$\psi''=0 \quad , \quad \psi'=\Omega \quad , \quad \Omega=constant$$

$$\phi''=0 \quad , \quad \phi'=\phi'_0 \quad , \quad \phi_0'=constant \ ,$$

equation (1.3.1a) yields

$$\Omega=0$$

and from (1.3.1b) one obtains

$$C_p\phi_0' + mRr\Omega^2\sin\phi=0$$

implying

$$\phi'=0 \quad , \quad \phi=arbitrary.$$

which is the same as case 3 above.

5. $C_p \neq 0 \quad , \quad C_c=T_0=0$

Using the same assumptions as equations (1.3.3), equation (1.3.1a) is identically zero and equation (1.3.1b) yields

$$\Omega=0 \quad or \quad \phi=n\pi \quad .$$

again implying the same result as that of case 3 above.

6. $C_c=0 \quad , \quad C_p, T_0 \neq 0$

Letting

$$\psi''=\alpha \quad , \quad \alpha=constant$$

$$\phi''=\phi'=0$$

the solutions turn out to be identical to those considered in the case 1.

7. $C_c=0$, $C_p, T_0 \neq 0$ Using equations (1.3.3), equation (1.3.1a) yields

$$\Omega=\frac{T_0}{C_c}$$

and from equation (1.3.1b),

$$\phi=n\,\pi \quad .$$

implying the carrier rotating with a constant angular velocity Ω fixed by the relation $\Omega=\frac{T_0}{C_c}$ while the absorber remains at $\phi=0$ or π (the $\phi=\pi$ solution is inherently unstable).

8. $C_c, C_p, T_0 \neq 0$

Substitution of assumptions (1.3.3) into equations (1.3.1) yields the equations of motion identical to those of the previous case 7.

One can readily see (for obvious reasons) that in all the cases considered above, none admit an oscillatory solution to the problem. Furthermore, one can see that the carrier damping, C_c, has a significant effect in determining the rate of steady rotation of the carrier (cases 7 and 8), for in the absence of C_c (cases 1, 2, 5 and, 6) the carrier's velocity either tends to zero or infinity as $\tau \rightarrow \infty$. Note in cases 3 and 4 that, although C_c is nonzero, the other determining parameter, namely, T_0, is set to zero and $\Omega=0$ results. The pendulum damping, C_p does not show any significant effect on the steady-state response of the system.

It should be noted that in the chapter 2 the linearization of the equations of motion will be carried out about the system parameters corresponding to case 6 and the nonlinear expansion of chapter 3 will correspond to the system parameters outlined in case 8 above.

CHAPTER 2

EFFECT OF MOTION LIMITING STOPS ON THE DYNAMIC RESPONSE OF THE CPVA

Figure (4) shows a schematic view of a CPVA with rigid constraints which are employed in order to limit the maximum allowable amplitude of oscillation of the absorber to a prescribed value, denoted as β. The objective of the design is to have the absorber oscillate freely between the two constraints in normal operation without coming into contact with the stops, except possibly during transient motions.

In order to achieve this objective, the response of the absorber in relation to the constraints and the range of parameters for which impacting and/or non-impacting periodic motions exist is to be considered. In particular, the possibility of ***coexistence*** of linear non-impacting and nonlinear, impacting motions at the anti-resonance frequency is of interest. Such coexistence can, in fact, occur and cannot be predicted without a detailed consideration of impacting motions. An absorber which is thought to be properly designed (*i.e.*, using only linear analysis and the addition of stops at amplitudes larger than the steady-state amplitudes predicted by the linear theory) may encounter impacting steady-state dynamics.

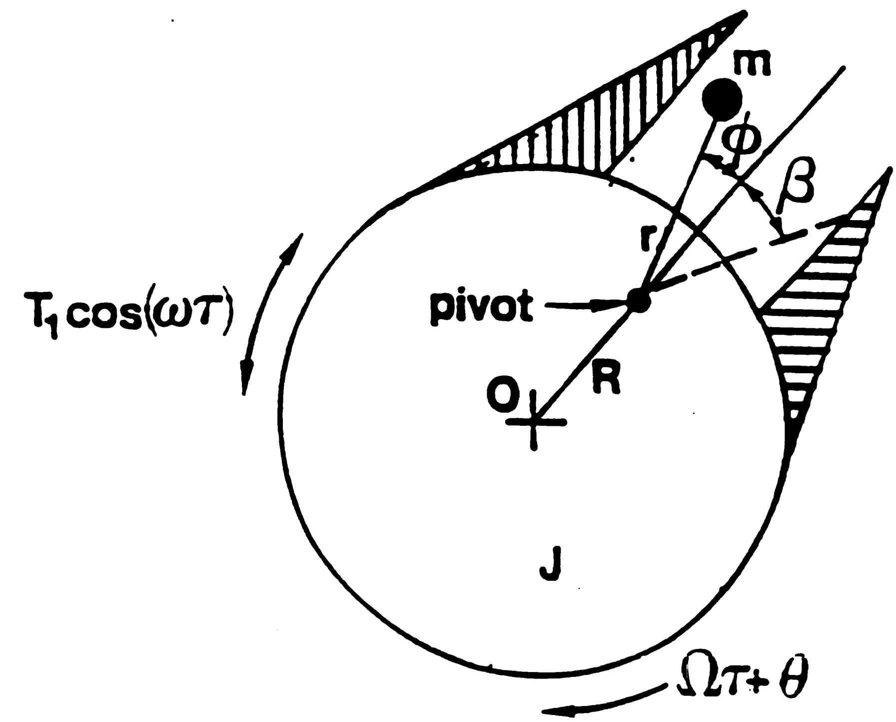

Figure 4 - Schematic View of a CPVA with Rigid Constraints

It is shown in the following that such coexistence occurs only for damping characteristics of the absorber too large for practical applications of the absorber. This result cannot be obtained without a detailed investigation to determine the range of system parameters for which such multi-steady-state dynamic behavior can occur. Also, should the system be subjected to a higher frequency disturbance than predicted, the response of the absorber with constraints can be quite complicated as shown in the following.

In addition, all previous studies of the CPVA have been carried out based on the assumption that the absorber does not come into contact with motion-limiting stops. Hence the analysis is done without considering any possible vibro-impact behavior in the system, even though such stops (often referred to as *snubbers*) are employed in all practical implementations of the CPVA.

The aim of this part of the study is to achieve a better understanding of these issues and to determine the range of system parameters for which a linear absorber with stops can function satisfactorily.

2.1- Equations of Motion and Assumptions

The full nonlinear equations of motion, equations (1.1.7) are rewritten here as

$$[J+mR^2+mr^2+2mRr\cos\phi]\psi''-mr(R\cos\phi+r)\phi''+$$

$$+mRr\phi'^2\sin\phi-2mRr\psi'\phi'\sin\phi+C_c\psi'=T(\tau) \tag{2.1.1a}$$

$$-mr(R\cos\phi+r)\psi''+mr^2\phi''+C_p\phi'+mRr\psi'^2\sin\phi=0 \tag{2.1.1b}$$

where the definition of all of the terms in equations (2.1.1) above can be found following equations (1.1.7). Equations (2.1.1) are valid for the case when the pendulum is not in contact with either of the constraints, *i.e.*, $|\phi|<\beta$.

At impact, $|\phi|=\beta$, use is made of the total angular momentum of the system. The total angular momentum of the carrier is in the direction perpendicular to the plane of Figure (4), *i.e.*, out of the paper, and can be written as

$$H_c=-J\psi' \quad . \tag{2.1.2a}$$

The vector angular momentum of the pendulum mass is given by

$$\overline{H}_p=\overline{\rho}\times m\overline{v}_p \quad ,$$

with

$$\overline{v}_p=[R\psi'\sin\psi+r(\psi'-\phi')\sin(\psi+\phi)]\,\overline{i}+$$

$$+[-R\psi'\cos\psi+r(\psi'-\phi')\cos(\psi+\phi)]\,\overline{j} \quad ,$$

being the velocity of the pendulum mass and

$$\bar{\rho}=\bar{R}+\bar{r}$$

$$=[R\cos\psi+r\cos(\psi+\phi)]\ \bar{i}+[R\sin\psi+r\sin(\psi+\phi)]\ \bar{j}\quad ,$$

being the position vector of the pendulum mass. The angular momentum of the absorber is also in the $\bar{k}$ direction (outwards, perpendicular to the plane of the paper) is given by

$$H_p=-m(R^2+r^2+2Rr\cos\phi)\psi' +mr(R\cos\phi+r)\phi' \quad . \tag{2.1.2b}$$

Consequently, the total angular momentum of the CPVA in the $\bar{k}$ direction can be written as:

$$H=H_c+H_p \quad ,$$

or

$$H=-[J+m(R^2+r^2+2Rr\cos\phi]\psi' +mr(R\cos\phi+r)\phi' \quad . \tag{2.1.3}$$

Assuming that at impact the contact time is small enough that the law of the conservation of the total angular momentum of the system can be instantaneously applied, one can write,

$$H^+=H^-$$

or

$$k_1\psi'^+ +k_2\phi'^+ =k_1\psi'^- +k_2\phi'^- \tag{2.1.4}$$

where superscripts - and + refer to the times just prior and after impact, respectively, and,

$$k_1=-[J+m(R^2+r^2+2Rr\cos\beta)] \quad , \tag{2.1.5a}$$

$$k_2=mr(R\cos\beta+r) \quad . \tag{2.1.5b}$$

Another relation describing the dynamics of impact can be determined by the usual definition of the coefficient of restitution, e. This can be written as:

$$e = \frac{v_{p_n}^{+} - v_{c_n}^{+}}{v_{c_n}^{-} - v_{p_n}^{-}} \tag{2.1.6}$$

where v denotes absolute velocity and subscripts p, c and, n refer to the points of contact on the pendulum, the carrier and, the direction normal to the line of impact, respectively.

To find the expressions for v_{p_n} and v_{c_n}, reference is made to Figure (5) which shows the pendulum at impact with one of the constraints. For the sake of clarity, only one of the constraints is shown. Rewriting equation (1.1.5a) which is in reference to the $(\bar{i}\ ,\ \bar{j})$ coordinate system of Figure (5), yields

$$\bar{v}_p = [R\,\psi'\sin\psi + r(\psi' - \phi')\sin(\psi+\phi)]\ \bar{i} +$$

$$+[-R\,\psi'\cos\psi + r(\psi' - \phi')\cos(\psi+\phi)]\ \bar{j} \quad . \tag{2.1.7}$$

Equation (2.1.7) can be written in terms of the $(\bar{n}\ ,\ \bar{t})$ coordinate system as

$$\begin{pmatrix} v_{p_n} \\ v_{p_t} \end{pmatrix} = \bar{R} \begin{pmatrix} v_{p_i} \\ v_{p_j} \end{pmatrix} \tag{2.1.8a}$$

where $\bar{R}$ is the so-called rotation matrix having the form,

$$\bar{R} = \begin{pmatrix} -\sin\xi & \cos\xi \\ -\cos\xi & -\sin\xi \end{pmatrix} \tag{2.1.8b}$$

where $\xi = \psi + \alpha$ and where the angle α can be observed from Figure (5) and its explicit form is presented below. From equations (2.1.7) and (2.1.8) one obtains,

$$v_{p_n} = -R\,\psi'\cos\alpha + r(-\psi' + \phi')\cos(\beta - \alpha) \tag{2.1.9}$$

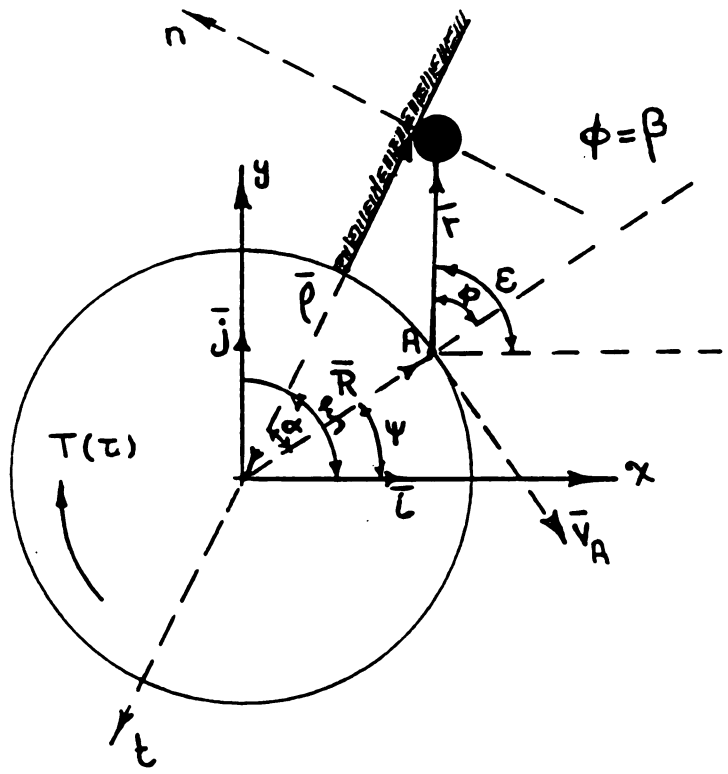

Figure 5 - Schematic View of a CPVA with the Pendulum at Impact

similarly, since

$$\overline{v}_c = \overline{\psi}\,' \times \overline{\rho}$$

$$= (\rho\psi\,' \sin\xi)\ \overline{i} - (\rho\psi\,' \cos\xi)\ \overline{j} \quad , \tag{2.1.10a}$$

$$\overline{\rho} = [\overline{R}\cos\psi + r\cos(\psi+\phi)]\ \overline{i} + [R\sin\psi + r\sin(\psi+\phi)]\ \overline{j} \tag{2.1.10b}$$

$$\overline{\psi}\,' = -\psi\,'\ \overline{k} \tag{2.1.10c}$$

then

$$v_{c_n} = -\rho\psi\,' \tag{2.1.11}$$

where ρ is the magnitude of $\overline{\rho}$ and the angle β can be observed from Figure (5) as well.

Substitution of equations (2.1.9) and (2.1.11) into equation (2.1.6) yields:

$$e = \frac{(k_3+\rho)\psi\,'^{+} + k_4\phi\,'^{+}}{-(k_3+\rho)\psi\,'^{-} - k_4\phi\,'^{-}} \quad , \tag{2.1.12}$$

where

$$k_3 = -R\cos\alpha - r\cos(\beta-\alpha) \quad , \tag{2.1.13a}$$

$$k_4 = r\cos(\beta-\alpha) \quad , \tag{2.1.13b}$$

$$\alpha = \tan^{-1}\left(\frac{r\sin\beta}{R + r\cos\beta}\right) \quad , and \tag{2.1.13c}$$

$$\rho = [(R + r\cos\beta)^2 + r^2\sin^2\phi]^{1/2} \quad . \tag{2.1.13d}$$

Equations (2.1.4) and (2.1.12) can be solved simultaneously, for $\phi\,'^{+}$ (or $\psi\,'^{+}$) in terms of the variables prior to impact, *i.e.*, $\psi\,'^{-}$ and $\phi\,'^{-}$, to yield,

$$\phi\,'^{+} = k_8\psi\,'^{-} + k_9\phi\,'^{-} \quad , \tag{2.1.14}$$

where

$$k_8=\frac{k_1k_5(1+e)}{k_2k_5-k_1k_4} \quad , \tag{2.1.15a}$$

$$k_9=\frac{k_3k_5+ek_1k_4}{k_2k_5-k_1k_4} \quad ,\text{and} \tag{2.1.15b}$$

$$k_5=k_3+\rho \quad . \tag{2.1.15c}$$

One can readily observe that equations (2.1.14) in conjunction with equations (2.1.15) are complicated enough so to obscure the true dynamics of the absorber and the carrier at impact. An alternative, and more enlightening, approach employs the geometrical properties of the system to simplify the equations of impact obtained above. Referring to Figure (5) it can be seen that

$$k_3+\rho=-[R\cos\alpha+r\cos(\alpha-\beta)]+\rho$$

$$=-(R\cos\alpha+r\cos\alpha\cos\beta+r\sin\alpha\sin\beta)+\rho \quad .$$

Considering

$$\cos\alpha=\frac{R+r\cos\beta}{\rho} \quad ,$$

$$\sin\alpha=\frac{r\sin\beta}{\rho} \quad ,$$

and equation (2.1.13d), one obtains

$$k_3+\rho=0 \quad ,$$

which renders equation (2.1.12) as

$$e=-\frac{\phi'^+}{\phi'^-} \quad ,$$

or

$$\phi'^+=-e\phi'^- \quad . \tag{2.1.16}$$

which is a familiar equation of impact for a single mass system. This simple result is a natural consequence of the fact that ϕ is a relative coordinate.

Returning to the free-flight (*i.e.*, non-impacting) mode of the system, the following assumptions are then made to simplify the free-flight equations of motion (2.1.1) (see Figure 4):

1. The carrier runs at nearly constant speed Ω with a small time-dependent variation, *i.e.*,

$$\psi(\tau)=\Omega\tau+\theta(\tau) \quad ,$$

2. The carrier damping is assumed negligible,

$$C_c=0 \quad .$$

3. ϕ is small enough so that $\sin\phi=\phi$, $\cos\phi=1$ are valid approximations.
4. Second and higher order terms of θ, ϕ and their derivatives can be neglected (*i.e.*, linearize the free-flight equations of motion).
5. The applied torque is sinusoidal in time.

Incorporation of the above assumptins renders the equations of motion (2.1.1) as,

$$[J+m(R+r)^2]\theta'' - mr(R+r)\phi'' = T(\tau) = T_1\cos\omega\tau \tag{2.1.17a}$$

$$-mr(R+r)\theta'' + mr^2\phi'' + C_p\phi' + mRr\Omega^2\phi = 0 \tag{2.1.17b}$$

Eliminating the θ'' variable between equations (2.1.17a) and (2.1.17b) one obtains,

$$Jmr^2\phi'' + C_p[J+m(R+r)^2]\phi' +$$
$$+mRr\Omega^2[J+m(R+r)^2]\phi = mr(R+r)T_1\cos\omega\tau \tag{2.1.18}$$

Rescaling equation (2.1.18) by redefining time and angular displacement as (see [28]),

$$t=\left(\frac{R\,\omega^2}{Jr}[J+m((R+r)^2]\right)^{1/2}\tau \tag{2.1.19a}$$

$$x=\frac{\phi}{\beta} \quad , \tag{2.1.19b}$$

equation (2.1.18) can be put into the following nondimensional form:

$$\ddot{x}+2\lambda\dot{x}+x=K\cos\eta t \tag{2.1.20a}$$

where

$$\lambda=C_p\left(\frac{R\,\Omega^2}{Jr}[J+m(R+r)^2]\right)^{1/2}$$

is the nondimensional damping ratio,

$$K=\frac{(R+r)T_1}{R\,\Omega^2\beta[J+m(R+r)^2]}$$

is the nondimensional excitation amplitude,

$$\eta=\omega\left(\frac{R\,\Omega^2}{Jr}[J+m(R+r)^2\right)^{-\frac{1}{2}}$$

is the nondimensional excitation frequency and, an over-dot denotes differentiation with respect to the rescaled, dimensionless time, t.

As stated previously, equation (2.1.20a) is valid when the pendulum is not in contact with the constraints, *i.e.*, $|x|<1$. For impacts, ($|x|=1$), equation (2.1.16) is also rescaled to yield equation (2.1.20b) as

$$\dot{x}^{+}=-e\dot{x}^{-} \quad , \quad |x|=1 \quad . \tag{2.1.20b}$$

It should be noted that the rescaling (equations 2.1.19) that led to equations (2.1.20) renders the anti-resonance frequency (equation 1.2.9) as

$$\eta_{AR}=\left(1+\frac{m}{J}(R+r)^2\right)^{-\frac{1}{2}} \quad . \tag{2.1.21}$$

This is the nondimensional frequency at which $\theta=0$ for the undamped, linear response, *i.e*, it is the desired operating frequency.

The original equations of motion (2.1.1) were in coupled form. Use of the assumptions (1) through (5) with the nonlinear equations of motion resulted in a set of linear equations (2.1.17) describing the motion of the pendulum between the constraints which were easily decoupled. In addition, the impact equations can be expressed in an uncoupled form (equation 2.1.16) and consequently equations (2.1.20a) and (2.1.20b) fully describe the motion of the pendulum for a given set of initial conditions and parameter values. The dynamics of the carrier can then be determined using equations (2.1.17a) or (2.1.17b). In particular, equation (2.1.17a) yields,

$$\theta'' = \frac{mr(R+r)\phi'' + T_1 \sin\omega\tau}{J + m(R+r)^2} \tag{2.1.22a}$$

and successive integrations with respect to time, τ, results in an expression for θ' and θ as,

$$\theta' = \frac{mr(R+r)\phi' - \dfrac{T_1}{\omega}\cos\omega\tau}{J + m(R+r)^2} \tag{2.1.22b}$$

and

$$\theta = \frac{mr(R+r)\phi - \dfrac{T_1}{\omega^2}\sin\omega\tau}{J + m(R+r)^2} \quad . \tag{2.1.22c}$$

The constants of integration in equations (2.1.22b) and (2.1.22c) are taken to be zero without any loss of generality since the addition of a nonzero constant to equation (2.1.22b) would result in a term like $c\tau$ (c a nonzero constant) whereas θ in assumption (1) is assumed to be a small variation about the steady-state rotation, and this component of ψ is already accounted for by Ω in $\psi = \Omega\tau + \theta$. Also, the addition of a nonzero constant to equation (2.1.22c) would indicate a trivial phase shift in the value of θ and a simple change of variables would result in the same expression as (2.1.22c).

Equation (2.1.20a) can be solved for a set of initial conditions. Such solutions are valid only for excitation amplitudes which result in amplitudes of the response (*i.e.*, $x_{\max}$) less than unity. In other words, any solution of equation (2.1.20a) which yields $x_{\max}>1$ is considered to be invalid since such condition implies that the absorber is passing ***through*** the rigid constraints. Given a set of initial conditions $(x_0, t_0, \dot{x}_0)$, the steady-state amplitude of the linear free-flight equations, X, obtained from the solution of equation (2.1.20a), can be written as

$$X = \frac{K}{[(1-\eta)^2 + 4\lambda^2\eta^2]^{1/2}} \quad .$$

Thus, for this solution to be valid, the torque intensity, K must satisfy the following inequality:

$$K < K_{cr} = [(1-\eta)^2 + 4\lambda^2\eta^2]^{1/2} \quad .$$

since K_{cr} renders X as unity. For $K > K_{cr}$ the desired steady-state solution will not exist.

2.2- Impacting, Periodic Response

2.2.1- Methods of Analysis

In the following, equations are derived for the existence and stability of certain periodic motions. The type of impacting motions described here are the symmetric, double-impact periodic motions (SDIP, for short) which have one impact for every half cycle of the excitation. A brief discussion will also be presented on the existence of pairs of anti-symmetric double impact periodic motions which are brought forth as a consequence of the breakdown of the stability of certain SDIP motions. This will be discussed towards the end of the chapter.

To study the existence and stability of SDIP motions, it is convenient to write equations (2.1.20a) in first order form as

$$\dot{x}=y$$

$$\dot{y}=-\lambda y+K\cos\eta t \tag{2.2.1}$$

$$\dot{t}=1$$

where the three variables (x,y,t) determine the state of the system for those solutions restricted to $|x|<+1$ in the three-dimensional phase space. Reference is made to Figure (6), which illustrates the phase trajectory of a double-impact motion in the $(x\ ,\ y)$ plane. Starting at point A (corresponding to the absorber coming in contact with the constraint at $x=+1$ with positive velocity), the impact equation (2.1.20b) is used to obtain the time and velocity at point B in Figure (6), *i.e.*,

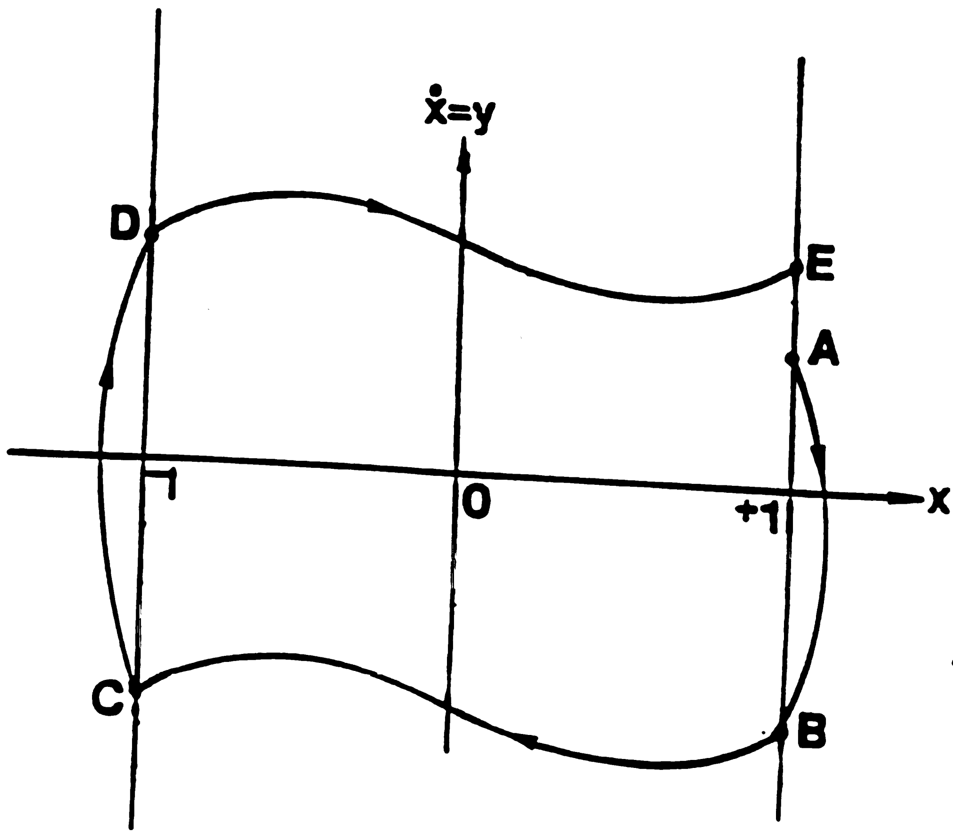

Figure 6 - Phase Trajectory of a Double-Impact Motion

$$y_B = -e y_A \tag{2.2.2a}$$

$$t_B = t_A \tag{2.2.2b}$$

(in Figure 6 the trajectory from A to B is actually exactly on $x=+1$, but is shown as is for clarity. Likewise for the C to D trajectory at $x=-1$). The motion from point B to point C is governed by the free-flight equations (2.2.1). The solution of (2.2.1) with initial conditions corresponding to point B is valid until $x=-1$ again. Since double-impact orbits are of interest here, it is then assumed that the next impact after point B occurs at point C with $x=-1$ as shown in Figure (6). Excluded, for the present, are orbits that leave the rigid constraints at $x=+1$ and next impact at $x=+1$ again. For the motion of interest, the time and velocity at point B ($t_B, y_B < 0$) uniquely, although implicitly, determine the time and velocity at point C ($t_C, y_C < 0$) through the expressions,

$$x(t_C;+1,t_B,y_B) = -1 \quad , \tag{2.2.3a}$$

and,

$$\dot{x}(t_C;+1,t_B,y_B) = y_C \tag{2.2.3b}$$

where $x(t;+1,t_B,y_B)$ is the explicit solution of equation (2.1.20a) with initial conditions corresponding to the state of the absorber at point B, *i.e.*, $x=+1$, $t=t_B$, $y=y_B$. Equation (2.2.3a) can be inverted to yield t_C as a function of (t_B,y_B), *i.e.*,

$$t_C = t_C(t_B,y_B) \quad , \tag{2.2.4}$$

where t_C is the first root of equation (2.2.3a) for which $t_C > t_B$. Substitution of this equation into equation (2.2.3b) yields an expression for y_C as a function of (t_B,y_B), *i.e.*,

$$y_C = y_C(t_B,y_B) \quad . \tag{2.2.4b}$$

By referring to Figure (6), the motion continues to point D via the impact rule:

$$y_D = -e y_C \tag{2.2.5a}$$

$$t_D = t_C \quad . \tag{2.2.5b}$$

The free-flight motion from point D to point E is again governed by equation (2.1.20a), where the time and velocity at E are uniquely determined from those at D, same as the case of the motion from point B to point C. Hence, the following conditions can be written:

$$x(t_E;-1,t_D,y_D) = +1 \tag{2.2.6a}$$

and

$$\dot{x}(t_E;-1,t_D,y_D) = y_C \quad . \tag{2.2.6b}$$

and when equation (2.2.6a) is inverted, one obtains,

$$t_E = t_E(t_D,y_D) \tag{2.2.7a}$$

where t_E is the first root of equation (2.2.6a) for which $t_E > t_D$. Then, from equations (2.2.2a) and (2.2.7a) we have y_E as follows:

$$y_E = y_E(t_D,y_D) \quad . \tag{2.2.7b}$$

In reference to equations (2.2.2) through (2.2.7), one can observe that a two-impact cycle has been completed taking the motion from one impact at $x=+1$ to the next similar impact at $x=+1$. From these considerations it is seen that by making use of the equations (2.2.2), (2.2.4), (2.2.5) and (2.2.7) the time and velocity at point A in the cycle uniquely determines those at point E, *i.e.*,

$$t_E = t_E(t_A,y_A) \quad , \tag{2.2.8a}$$

$$y_E = y_E(t_A,y_A) \quad . \tag{2.2.8b}$$

In this sense each excursion from x=+1 to x=−1 and back is reduced to the simple recursion relation of equation (2.2.8). This recursion is a natural consequence of equations (2.1.20a) and (2.1.20b) and it will be used in the following to study the motions of the absorber. One should note that explicit expressions for above relations such as equations (2.2.8) are not available in explicit form since such a task would imply inverting several transcendental functions, making the process impossible. In spite of this, explicit solutions for the existence of SDIP motions are obtained in the following through certain conditions which govern the nature of the SDIP motions.

The idea of studying dynamical systems using recursion relations, or maps, has its origins in the works of Poincarè [27]. To this effect, the mapping given by equations (2.2.8) will be referred to as the *Poincarè Map* for the system being studied. By considering the phase space (x,y,t) with $x \leq 1$, it is seen that this method determines how points with $x=+1$, $y>0$ are eventually mapped back to $x=+1$, $y>0$ under the governing equations of motion. Formalizing this, one can define a *Poincare`Section* for this case as

$$\Sigma=\left\{(x,y,t) : x=+1,\ y>0\right\} \quad , \tag{2.2.9}$$

and the attendant *Poincarè Map*, $\mathbf{P}$, which is a rule taking points in Σ back into Σ, *i.e.*,

$$\mathbf{P}=\Sigma\rightarrow\Sigma \quad ,\textit{or equivalently} \quad (t_{i+1}\ ,\ y_{i+1})=\mathbf{P}\,(t_i\ ,\ y_i) \quad , \tag{2.2.10}$$

where

$$(t_i\ ,\ y_i)\epsilon\Sigma \quad .$$

Points in the set Σ correspond to those states in which the absorber is just coming into contact with the constraint at $x=+1$. For instance, points A and E in Figure (6) are in Σ . The mapping **P** is equivalent to equations (2.2.8) for those points in Σ which result in excursions like the one shown in Figure (6). It is noteworthy to mention that some points in Σ may be mapped back to Σ without any encounter at $x=-1$, in which case rules other than those given by equations (2.2.8) must be used. In addition, some points in Σ may be mapped onto $|x|=1$, $y=0$ in which case discontinuities in **P** may arise (see [28,29] for details).

Periodic motions of the absorber mass may be studied using **P** as follows. Each iterate of **P** corresponds to an impact of the absorber mass with the constraint at $x=+1$ and relates the condition (time and velocity) at the previous impact to those of the subsequent one. A motion which repeats itself after k impacts at $x=+1$ necessarily satisfies the condition

$$(\bar{t}+\frac{2\pi n}{\eta},\bar{y})=\mathbf{P}^{k}(\bar{t},\bar{y}) \tag{2.2.11}$$

where $\mathbf{P}^k$ indicates that **P** has been applied k times (*i.e.*, defining $\mathbf{P}^{j+1}(\,.\,)=\mathbf{P}(\mathbf{P}^{j}(\,.\,))$, $\mathbf{P}^{0}(\,.\,)=(\,.\,)$ is sufficient to define $\mathbf{P}^{k}(\,.\,)$). Equation (2.2.11) corresponds to a $2k$ impact motion of period $\frac{2\pi n}{\eta}$ in which the absorber mass repeats its motion after k impacts at $x=+1$, during which n cycles of the forcing pass. Such a motion is referred to as a *subharmonic of order n*. The point $(\bar{t},\bar{y})$ is referred to as a *periodic point* of **P**.

Such a periodic motion may be either stable or unstable. The stability of periodic points can be investigated by tracing in time the dynamics of small perturbations on the initial conditions for the periodic point $(\bar{t},\bar{y})$. This procedure can be discretized by observing the effects of perturbations using the Poincarè map. Consider a small disturbance (ξ,ν), where $(t,y)=(\bar{t}+\xi,\bar{y}+\nu)$ and $|\xi|,|\nu|<<1$, imposed on the periodic point. Its state is observed after subsequent returns to the Poincarè section, Σ. Since local stability is of interest here, linearizing about $(\bar{t},\bar{y})$ one obtains,

$$(\xi_{i+1},\nu_{i+1})=\mathbf{DP}\,(\xi_i,\nu_i) \quad , \quad |\xi|,|\nu|<<1 \tag{2.2.12}$$

where (ξ,ν) is the perturbation and **DP** is the first derivative of the Poincarè map, **P**, evaluated at the periodic point $(\bar{t},\bar{y})$. Using the notation employed in Figure (6), the matrix **DP** can be written as:

$$\mathbf{DP}=\left.\begin{pmatrix} \dfrac{\partial t_E}{\partial t_A} & \dfrac{\partial t_E}{\partial y_A} \\ \dfrac{\partial y_E}{\partial t_A} & \dfrac{\partial y_E}{\partial y_A} \end{pmatrix}\right|_{(\bar{t},\bar{y})} \tag{2.2.13a}$$

and the above matrix, for convenience, is denoted as

$$\mathbf{DP}=\left.\left(\frac{\partial(t_E,y_E)}{\partial(t_A,y_A)}\right)\right|_{(\bar{t},\bar{y})} \quad . \tag{2.2.13b}$$

Hence, the problem of stability of periodic points is reduced to the study of the eigenvalues of the **DP** matrix. If both eigenvalues of the **DP** have moduli less than one then $(\bar{t},\bar{y})$ is stable. If any of the eigenvalues has a modulus greater than one, then $(\bar{t},\bar{y})$ is unstable (see [26, 31, 32] for example). As system parameters are varied, the periodic point changes continuously as do its associated eigenvalues, λ_1 and λ_2. *Local Bifurcations* occur as eigenvalues pass through the unit circle in the complex plane, *i.e.*, when $|\lambda_i|=1$, $i=1,2$ [26]. It is shown in the following that the **DP** matrix has a determinant with magnitude less than one for motions of interest and thus only $\lambda=\pm1$ bifurcations are possible. No Hopf bifurcations occur in which λ_1 and λ_2 pass through the unit circle as a complex conjugate pair. Period doubling, or flip bifurcations occur for $\lambda_i=-1$. Bifurcations corresponding to $\lambda_i = +1$, saddle-node and pitchfork bifurcations, also occur. These are discussed in the following.

2.2.2- Symmetric, Double-Impact Motions- Existence

Necessary conditions for the existence of an SDIP motion can be obtained by matching end conditions which require that a periodic, symmetric, double-impact motion exist. The conditions to be solved use the known linear solution for the motion of the absorber during the free-flight motion and the symmetry of a SDIP motion and are given by

$$x(\bar{t}=\frac{\pi n}{\eta};+1,\bar{t},-e\bar{y})=-1 \tag{2.2.14a}$$

$$\dot{x}(\bar{t}+\frac{\pi n}{\eta};+1,\bar{t},-e\bar{y})=-\bar{y} \tag{2.2.14b}$$

$$|x(t;+1,\bar{t},-e\bar{y})|<1 \quad \text{for} \quad t\epsilon(\bar{t},\bar{t}+\frac{\pi n}{\eta}) \tag{2.2.14c}$$

where x is the explicit solution of equation (2.1.20a). For a SDIP motion with a corresponding fixed point $(\bar{t},\bar{y})$ on the Poincarè section, Σ, equation (2.2.14a) states that starting at $x=+1$ and after a time-lapse equal to exactly $\frac{\pi n}{\eta}$ (*i.e.*, half of the n number of periods of the excitation), the absorber should be at $x=-1$ at which point the velocity, by equation (2.2.14b), must equal $-\bar{y}$. Condition (2.2.14c) merely states that the mathematical solution of the displacement of the absorber, x, should remain within the physical boundaries of the model, *i.e.*, the absorber cannot penetrate into the constraints.

It is worth mentioning that for very low frequencies of excitation, η, say $\eta<0.5$, the results corresponding to solutions of conditions (2.2.14) are in fact what are called ***penetrating*** motions which are consistent with the mathematical modeling of the system but are physically not realizable. These solutions satisfy conditions (2.2.14a) and (2.2.14b) but violate (2.2.14c).

Also, note that due to the symmetric nature of the SDIP motion only odd orders of the subharmonics can exist. The reason for this is that the excitation that takes the absorber from $x=+1$ to $x=-1$ should be equal and opposite in direction to the one that brings the pendulum back to $x=+1$, implying $n=2i+1$ (i integer) periods of the forcing are necessary to sustain a SDIP motion for one full cycle.

For a typical set of initial conditions (x_0,t_0,y_0), such a solution can be written, for the underdamped case, $\lambda<1.0$, as

$$x(t;x_0,t_0,y_0)=\frac{e^{-\lambda(t-t_0)}}{\Lambda}\Big([x_0-C\cos(\eta t_0-\overline{\alpha})]\Lambda\cos(\Lambda(t-t_0))+$$

$$+\Lambda\cos\Lambda(t-t_0)+(\lambda x_0+y_0-C\lambda\cos(\eta t_0-\overline{\alpha})+$$

$$+C\eta\sin(\eta t_0-\overline{\alpha}))\sin(\Lambda(t-t_0))\Big)+C\cos(\eta t-\overline{\alpha}) \tag{2.2.15}$$

where

$$C=\frac{K}{[(1-\eta)^2+4\lambda^2\eta^2]^{1/2}} \quad , \tag{2.2.16a}$$

$$\overline{\alpha}=\tan^{-1}\left(\frac{2\lambda\eta}{1-\eta^2}\right) \quad , \tag{2.2.16b}$$

$$\Lambda=\sqrt{1-\lambda^2} \quad . \tag{2.2.16c}$$

Equations (2.2.14a,b) can be solved for $(\overline{t},\overline{y})$ as follows. Substitution of equation (2.2.15) into (2.2.14a) yields

$$\frac{E}{\Lambda}\Big((1-Cc_\eta)\Lambda\overline{c}+(\lambda-C\lambda c_\eta-e\overline{y}+C\eta s_\eta)\overline{s}\Big)-Cc_\eta=-1 \tag{2.2.17a}$$

where

$$E = e^{\frac{-\lambda\pi n}{\eta}} \tag{2.2.18a}$$

$$\bar{c} = \cos\frac{\Lambda\pi n}{\eta} \quad , \quad \bar{s} = \sin\frac{\Lambda\pi n}{\eta} \tag{2.2.18b}$$

$$c_\eta = \cos(\eta\sigma - \bar{\alpha}) \quad , \quad s_\eta = \sin(\eta\sigma - \bar{\alpha}) \tag{2.2.18c}$$

$$\sigma = \bar{t}\ mod(\frac{2\pi}{\eta}) \quad . \tag{2.2.18d}$$

Differentiation of equation (2.2.15) with respect to time, t, yields the expression for $\dot{x}(t;x_0,t_0,y_0)$ as:

$$\dot{x}(t;x_0,t_0,y_0) = \frac{e^{-\lambda(t-t_0)}}{\Lambda}\Big([y_0 + C\eta\Lambda\sin(\eta t_0 - \bar{\alpha})]\Lambda\cos(\Lambda(t-t_0)) +$$

$$+ (-x_0 - \lambda y_0 + C\cos(\eta t_0 - \bar{\alpha}) - C\lambda\eta\sin(\eta t_0 - \bar{\alpha}))\sin(\Lambda(t-t_0))\Big) -$$

$$-C\eta\sin(\eta t - \bar{\alpha}) \tag{2.2.18e}$$

Application of condition (2.2.14b) to equation (2.2.18e) results in equation (2.2.17b) as

$$\frac{E}{\Lambda}\Big([-e\bar{y} + C\eta s_\eta]\Lambda\bar{c} + [-1 + \lambda e\bar{y} + Cc_\eta - C\lambda\eta s_\eta]\bar{s}\Big) +$$

$$+C\eta s_\eta = -\bar{y} \tag{2.2.17b}$$

Any solution $(\bar{t},\bar{y})$ of equations (2.2.17), which is a fixed point of the Poincarè map, **P**, corresponds to a SDIP motion in the phase space if condition (2.2.14c) holds. Equation (2.2.17) can be solved for $(\bar{t},\bar{y})$ by solving for c_η and s_η, which appear linearly in these equations to yield:

$$c_\eta = \cos(\eta\sigma - \bar{\alpha}) = \frac{(1+e)\bar{s}}{ECJ_1}\bar{y} + \frac{1}{C} \tag{2.2.19a}$$

$$s_\eta = \sin(\eta\sigma - \bar{\alpha}) = \frac{J_2}{C\eta J_1}\bar{y} \tag{2.2.19b}$$

where

$$J_1 = -\Lambda(1+E^{-2}+2\overline{c}E^{-1}) \tag{2.2.20a}$$

and

$$J_2 = \Lambda E^{-1}(1-e)\overline{c} + \lambda E^{-1}(1+e)\overline{s} + \Lambda E^{-2} - \Lambda e \quad . \tag{2.2.20b}$$

Equations (2.2.19a) and (2.2.19b) can be squared and added together using $c_\eta^2 + s_\eta^2 = 1$ to yield the following quadratic equation which can be used to solve for $\overline{y}$ in terms of the system parameters:

$$\left(\frac{(1+e)^2\overline{s}^2}{(ECJ_1)^2} + \frac{J_2^2}{(C\eta J_1)^2} \right)\overline{y}^2 + \frac{2(1+e)\overline{s}}{EC^2J_1}\overline{y} + \frac{1}{C^2} = 0 \tag{2.2.21a}$$

The solutions for $\overline{y}$ are:

$$\overline{y} = \frac{J_1^2C^2\left(-\frac{(1+e)\overline{s}}{J_1C^2E} \pm \Delta^{1/2} \right)}{\frac{(1+e^2)\overline{s}^2}{E^2} + \frac{J_2^2}{\eta^2}} \tag{2.2.21b}$$

where

$$\Delta = \frac{\frac{(1+e)^2\overline{s}^2}{E^2} + \frac{J_2^2}{\eta^2}(1-\frac{1}{C^2})}{(J_1C)^2} \quad . \tag{2.2.22}$$

The corresponding phase at impact for this motion can be obtained once $\overline{y}$ is known using the definitions of c_η and s_η given in equations (2.2.19).

2.2.3- Symmetric, Double-Impact Motions- Stability

To obtain the stability characteristics of the fixed point $(\overline{t},\overline{y})$, the first derivative of the Poincarè map, **DP**, must be determined. Since explicit, closed-form expressions for the Poincarè map are not available, the following implicit differentiation procedure is used to obtain an expression for the matrix **DP** (see [28], for example).

Using the chain rule and the notation defined in equation (2.2.13), one can write

$$\mathbf{DP} = \left(\frac{\partial(t_E, y_E)}{\partial(t_A, y_A)}\right) =$$

$$= \left(\frac{\partial(t_E, y_E)}{\partial(T_D, y_D)}\right)\left(\frac{\partial(t_D, y_D)}{\partial(t_C, y_C)}\right)\left(\frac{\partial(t_C, y_C)}{\partial(t_B, y_B)}\right)\left(\frac{\partial(t_B, y_B)}{\partial(t_A, y_A)}\right) \tag{2.2.23}$$

By referring to equations (2.2.2) and (2.2.5) it is easily seen that

$$\left(\frac{\partial(t_B, y_B)}{\partial(t_A, y_A)}\right) = \left(\frac{\partial(t_D, y_D)}{\partial(t_C, y_C)}\right) = \begin{pmatrix} 1 & 0 \\ 0 & -e \end{pmatrix} . \tag{2.2.24}$$

The remaining two matrices are computed using implicit differentiation as follows. Differentiating equation (2.2.3a) with respect to t_B one obtains

$$\frac{\partial t_C}{\partial t_B} = \frac{e^{-\lambda(t_C - t_B)}}{\Lambda y_C}\Big(y_B \Lambda \cos(\Lambda(t_C - t_B)) + (-1 + C\cos(\eta t_B - \overline{\alpha}) -$$

$$-\lambda y_B - 2C\lambda\eta \sin(\eta t_B - \overline{\alpha}) - C\eta^2 \cos(\eta t_B - \overline{\alpha}))\sin(\Lambda(t_C - t_B))\Big) \tag{2.2.25a}$$

Differentiating equation (2.2.3a) with respect to y_B yields

$$\frac{\partial t_C}{\partial y_B} = \frac{-e^{-\lambda(t_C - t_B)}}{\Lambda y_C}\sin(\Lambda(t_C - t_B)) \tag{2.2.25b}$$

Noting that,

$$\frac{\partial y_C}{\partial t_B} = \frac{\partial y_C}{\partial t_C} \cdot \frac{\partial t_C}{\partial t_B} + \frac{d y_C}{d t_B} \tag{2.2.25c}$$

and

$$\frac{\partial y_C}{\partial y_B} = \frac{\partial y_C}{\partial t_C} \cdot \frac{\partial t_C}{\partial y_B} + \frac{d y_C}{d y_B} , \tag{2.2.25d}$$

the unknown terms on the right-hand-sides of equations (2.2.25c) and

(2.2.25d) can be computed using equation (2.2.3b) as follows:

$$\frac{\partial y_C}{\partial t_C} = \ddot{x}(t_C;+1,t_B,y_B)$$

$$= K\cos\eta t_C - 2\lambda y_C - 1 \quad , \tag{2.2.25e}$$

and

$$\frac{dy_C}{dy_B} = \frac{e^{-\lambda(t_C-t_B)}}{\Lambda}\Big(-\lambda\sin(\Lambda(t_C-t_B)) + \lambda\cos(\Lambda(t_C-t_B))\Big) \quad , \tag{2.2.25f}$$

and

$$\frac{dy_C}{dt_B} = \frac{e^{-\lambda(t_C-t_B)}}{\Lambda}\Big([2\lambda y_B + 2C\lambda\eta\sin(\eta t_B-\overline{\alpha}) + 1 -$$

$$-C\cos(\eta t_B-\overline{\alpha}) + C\eta^2\cos(\eta t_B-\overline{\alpha})]\Lambda\cos(\Lambda(t_C-t_B)) +$$

$$+(-\lambda + C\lambda\cos(\eta t_B-\overline{\alpha}) + (1-2\lambda^2)y_B + (1-2\lambda supu\, 2)C\eta\sin(\eta t_B-\overline{\alpha}) -$$

$$-C\eta\sin(\eta t_B-\overline{\alpha}) - C\lambda\eta^2\cos(\eta t_B-\overline{\alpha}))\sin(\Lambda(t_C-t_B))\Big) \quad . \tag{2.2.25g}$$

Furthermore, differentiation of equation (2.2.6a) with respect to t_D and y_D and differentiation of equation (2.2.6b) with respect to t_E yields:

$$\frac{\partial t_E}{\partial t_D} = \frac{e^{-\lambda(t_E-t_D)}}{\Lambda}\Big(y_D\Lambda\cos(\Lambda(t_E-t_D)) + (1 + C\cos(\eta t_D-\overline{\alpha}) -$$

$$-2C\lambda\eta\sin(\eta t_E-\overline{\alpha}) - C\eta^2\cos(\eta t_D-\overline{\alpha})y_D\lambda\sin(\Lambda(t_E-t_D))\Big) \tag{2.2.26a}$$

and

$$\frac{\partial t_E}{\partial y_D} = \frac{-e^{-\lambda(t_E-t_D)}\sin(\Lambda(t_E-t_D))}{\Lambda y_E} \tag{2.2.26b}$$

respectively. In addition, we have

$$\frac{\partial y_E}{\partial t_E} = \ddot{x}(t_E;-1,t_D,y_D)$$

$$=K\cos\eta t_E-2\lambda y_E-1 \quad . \tag{2.2.26c}$$

employing

$$\frac{\partial y_E}{\partial t_D}=\frac{\partial y_E}{\partial t_E}\cdot\frac{\partial t_E}{\partial t_D}+\frac{dy_E}{dt_D} \tag{2.2.26d}$$

and

$$\frac{\partial y_e}{\partial y_D}=\frac{\partial y_E}{\partial t_E}\cdot\frac{\partial t_E}{\partial y_D}+\frac{dy_E}{dy_D} \quad , \tag{2.2.26e}$$

equations (2.2.6a) and (2.2.6b) can be utilized to compute the remaining unknown terms on the right-hand-sides of equations (2.2.26d) and (2.2.26e) as

$$\frac{dy_E}{dt_D}=\frac{e^{-\lambda(t_E-t_D)}}{\Lambda}\Big((2y_D\lambda+2C\lambda\eta\sin(\eta t_D-\overline{\alpha})-1-$$

$$-C\cos(\eta t_D-\overline{\alpha})+C\eta^2\cos(\eta t_D-\overline{\alpha}))\Lambda\cos(\Lambda(t_E-t_D))+(\lambda+$$

$$+y_D(1-2\lambda^2)+(1-\eta^2)C\lambda\cos(\eta t_D-\overline{\alpha})-2\lambda^2\sin(\eta t_D-\overline{\alpha}))\sin(\Lambda(t_E-t_D))\Big) \tag{2.2.26f}$$

and

$$\frac{dy_E}{dy_D}=\frac{e^{-\lambda(t_E-t_D)}}{\Lambda}\Big(\Lambda\cos(\Lambda(t_D-t_E))-\lambda\sin(\Lambda(t_D-t_E)\Big) \quad . \tag{2.2.26g}$$

Substitution of equations (2.2.24) through (2.2.26) into equation (2.2.23) yields the final expression for matrix **DP** as,

$$\mathbf{DP}=[\ d_{ij}\ ] \quad , \quad i,j=1,2 \quad , \tag{2.2.27}$$

where

$$d_{11}=p_1p_2-ep_3p_4 \quad , \tag{2.2.28a}$$

$$d_{12}=-ep_1p_5+e^2p_3p_6 \quad , \tag{2.2.28b}$$

$$d_{21}=p_2p_7-ep_4p_8 \tag{2.2.28c}$$

and

$$d_{22} = -ep_5p_7 + e^2p_6p_8 \quad , \tag{2.2.28d}$$

where

$$p_1 = \frac{E}{\Lambda\bar{y}}[\bar{s} - Cc_\eta\bar{s} + 2C\lambda\eta s_\eta\bar{s} + e\bar{y}\Lambda\bar{c} + C\eta^2c_2\bar{s} - e\bar{y}\lambda\bar{s}] \quad ,$$

$$p_2 = \frac{E}{\Lambda\bar{y}}[-\bar{s} + Cc_\eta\bar{s} + \lambda e\overline{ys} - 2C\lambda\eta s_\eta\bar{s} - e\bar{y}\Lambda\bar{c} - c\eta^2c_\eta\bar{s}] \quad ,$$

$$p_3 = -\frac{E}{\Lambda\bar{y}}\bar{s}$$

$$p_4 = (1 - 2\lambda\bar{y} - K\cos\eta t)p_2 + \frac{E}{\Lambda}[-\lambda\bar{s} + C\lambda c_\eta\bar{s} -$$

$$-(1-2\lambda^2)e\overline{ys} - 2\bar{y}\Lambda\lambda\bar{c} + (1-2\lambda^2)C\eta s_\eta\bar{s} + 2C\Lambda\lambda\eta s_\eta\bar{c} +$$

$$+\Lambda\bar{c} - C\eta s_\eta\bar{s} - C\Lambda c_\eta\bar{c} - C\lambda\eta^2c_\eta\bar{s} + C\Lambda\eta^2c_\eta\bar{c}] \quad ,$$

$$p_5 = \frac{E\bar{s}}{\Lambda\bar{y}} - p_3 \quad ,$$

$$p_6 = (1 + 2\lambda\bar{y} - K\cos\eta t)p_3 + \frac{E}{\Lambda}(-\lambda\bar{s} + \Lambda\bar{c}) \quad ,$$

$$p_7 = (K\cos\eta t - 2\lambda\bar{y} - 1)p_1 + \frac{E}{\Lambda}(\lambda\bar{s} - C\lambda c_\eta\bar{s} + e\bar{y}(1-2\lambda^2)\bar{s} +$$

$$+2e\bar{y}\Lambda\lambda\bar{c} - (1-2\lambda^2)C\eta s_\eta\bar{s} - 2C\Lambda\lambda\eta s_\eta\bar{c} - \Lambda\bar{c} +$$

$$+C\eta s_\eta\bar{s} + C\eta s_\eta\bar{s} + C\Lambda c_\eta\bar{c} + C\lambda\eta^2c_\eta\bar{s} - C\Lambda\eta^2c_\eta\bar{c}) \quad ,$$

and

$$p_8 = (K\cos\eta t - 2\lambda\bar{y} - 1)p_3 + \frac{E}{\Lambda}(-\lambda\bar{s} + \Lambda\bar{c}) \quad .$$

Consequently, the expressions for the eigenvalues of the **DP** matrix can be written as

$$\lambda_{1,2} = \frac{1}{2}\left((d_{11}+d_{22}) \pm [(d_{11}+d_{22})^2 + 4(d_{11}+d_{22})(d_{11}d_{22}+d_{12}d_{21})]^{1/2}\right) \quad . \tag{2.2.29}$$

These calculations involve no approximations in the mathematics.

2.3- Results

2.3.1- Frequency Response

Figure (7) is a typical plot of $\bar{y}$ vs. η depicting the stable and unstable response branches for $n=1$, that is, motions with the same period as the excitation, and Figure (8) depicts a similar plot for $n=1$ and the subharmonic orders $n=3$ and 5. Superimposed on Figure (7) is the non-impacting, or linear branch of the response curve. This branch depicts the maximum velocity (at $x=0$) of motions for which there are no impacts and the absorber simply oscillates between the two constraints. Figure (9a), (9b), and (9c) depict the variation of $\bar{y}$ as system parameters $\bar{K}$, $\bar{\lambda}$ and, e, *i.e.*, the excitation amplitude, the damping ratio and, the coefficient of restitution, respectively, are varied. Figure (10) illustrates the dynamic behavior of the absorber and the carrier for a typical stable impacting motion, specifically point A in Figure (7).

By referring to Figure (7) and moving horizontally from the right towards decreasing values of the frequency, η, one observes the following. For excitation frequencies around η=2.25, the only possible motion is the linear one (or possibly the $n=3$ subharmonic) up to a point where stable and unstable SDIP motions with $n=1$ motions emerge in a saddle-node bifurcation. This point corresponds to the excitation frequency for which real roots appear for the quadratic equation in terms of $\bar{y}$, that is,

$$\Delta=0$$

where Δ is as defined in equation (2.2.22). Equivalently, in terms of the driving amplitude, these saddle-node bifurcations occur at

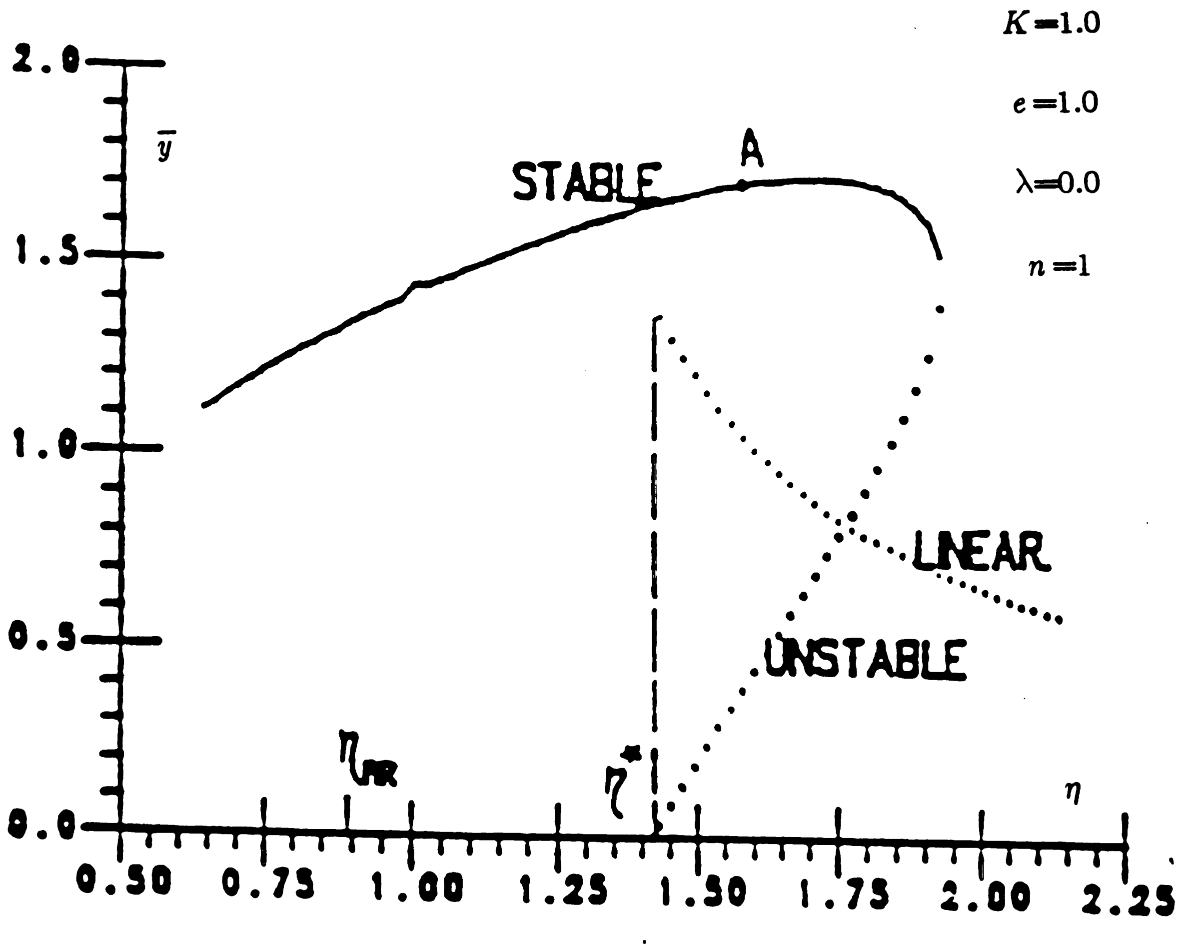

Figure 7 - Frequency Response of the Absorber

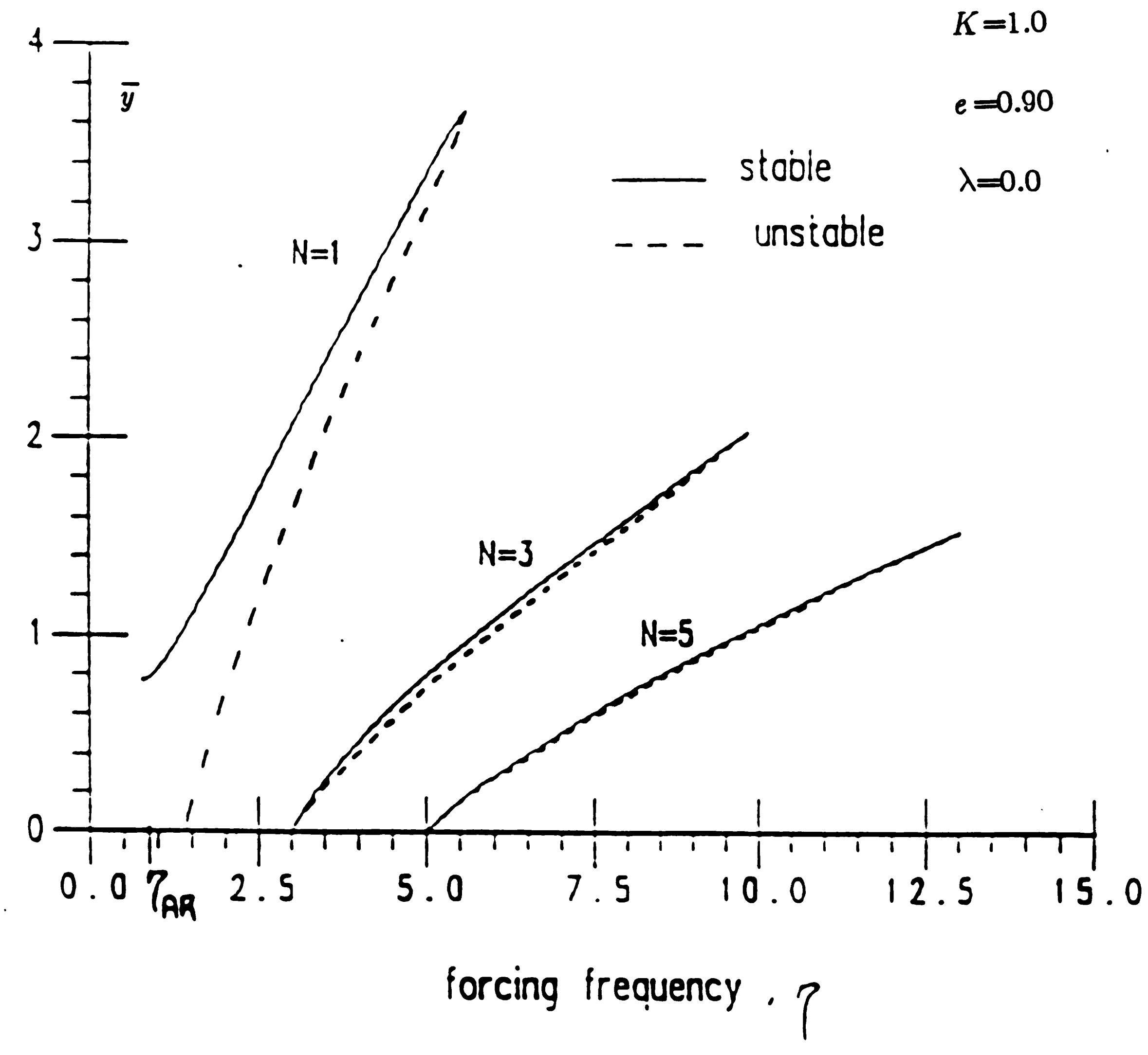

Figure 8 - Frequency Response of the Absorber; Subharmonic Orders and the Primary Response

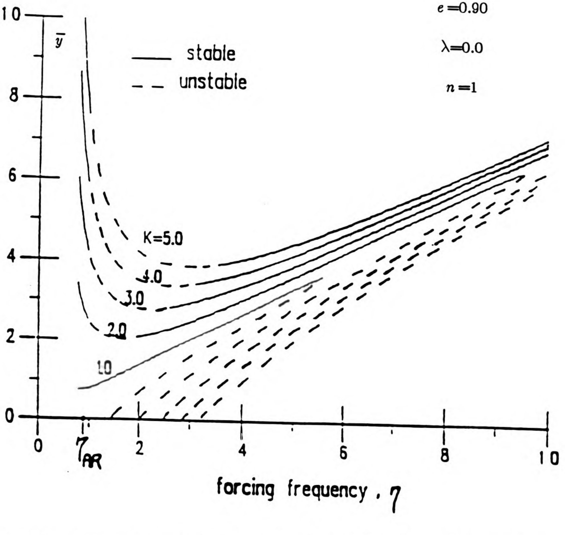

Figure 9a - Variation of the Response of the Absorber with Respect to the Excitation Amplitude

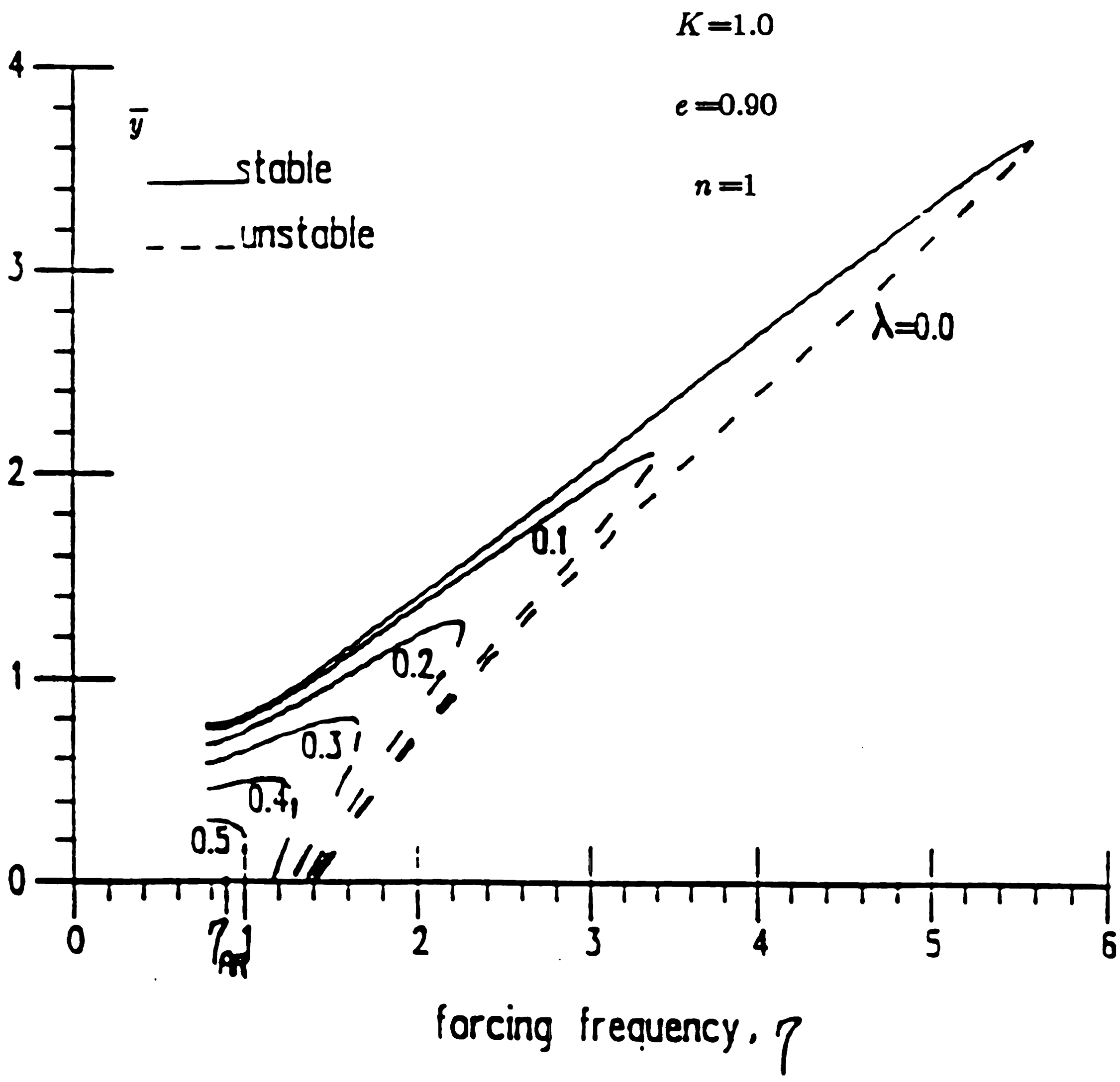

Figure 9b - Variation of the Response of the Absorber with Respect to the Absorber Damping

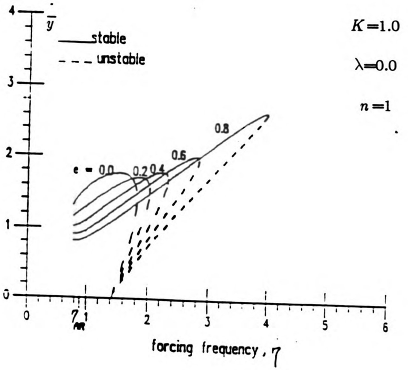

Figure 9c - Variation of the Response of the Absorber with Respect to the Coefficient of Restitution

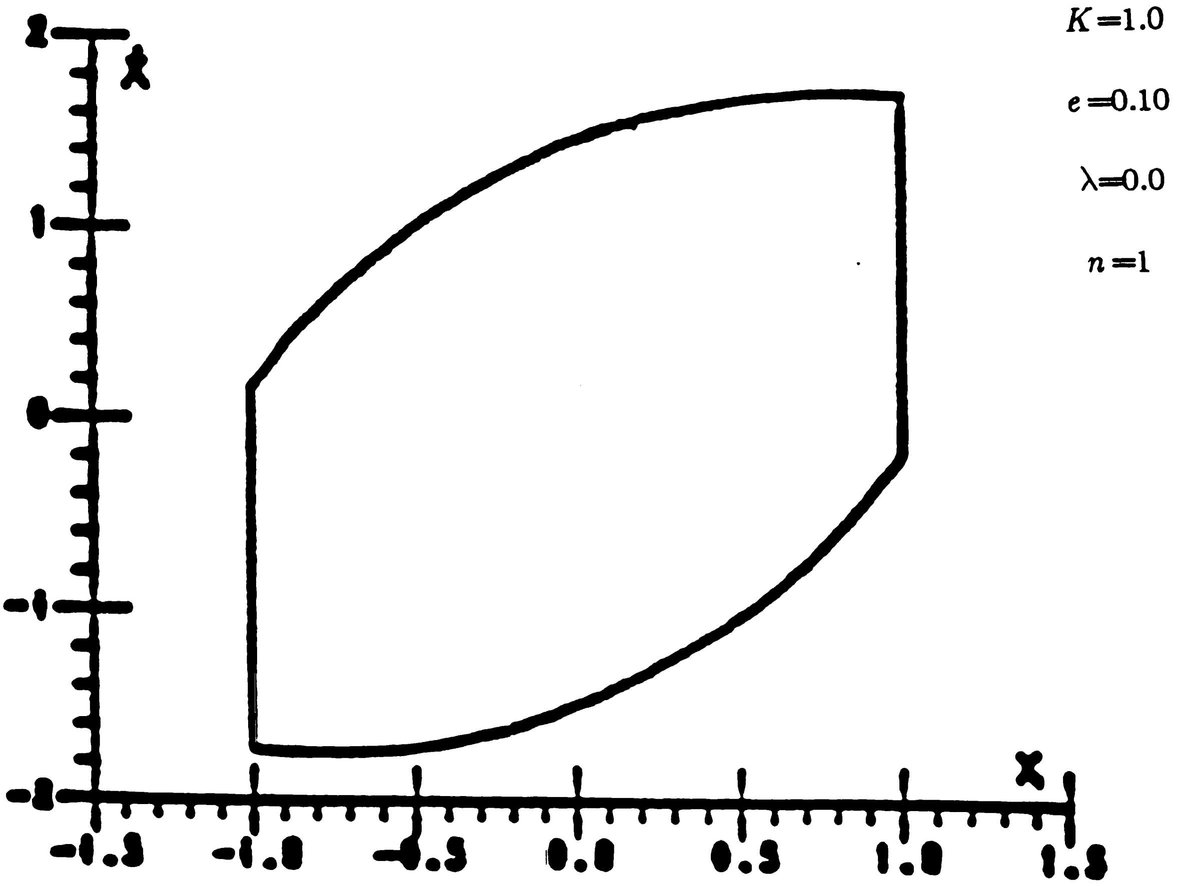

Figure 10a - Phase Trajectory of the Absorber Depicting an SDIP Motion

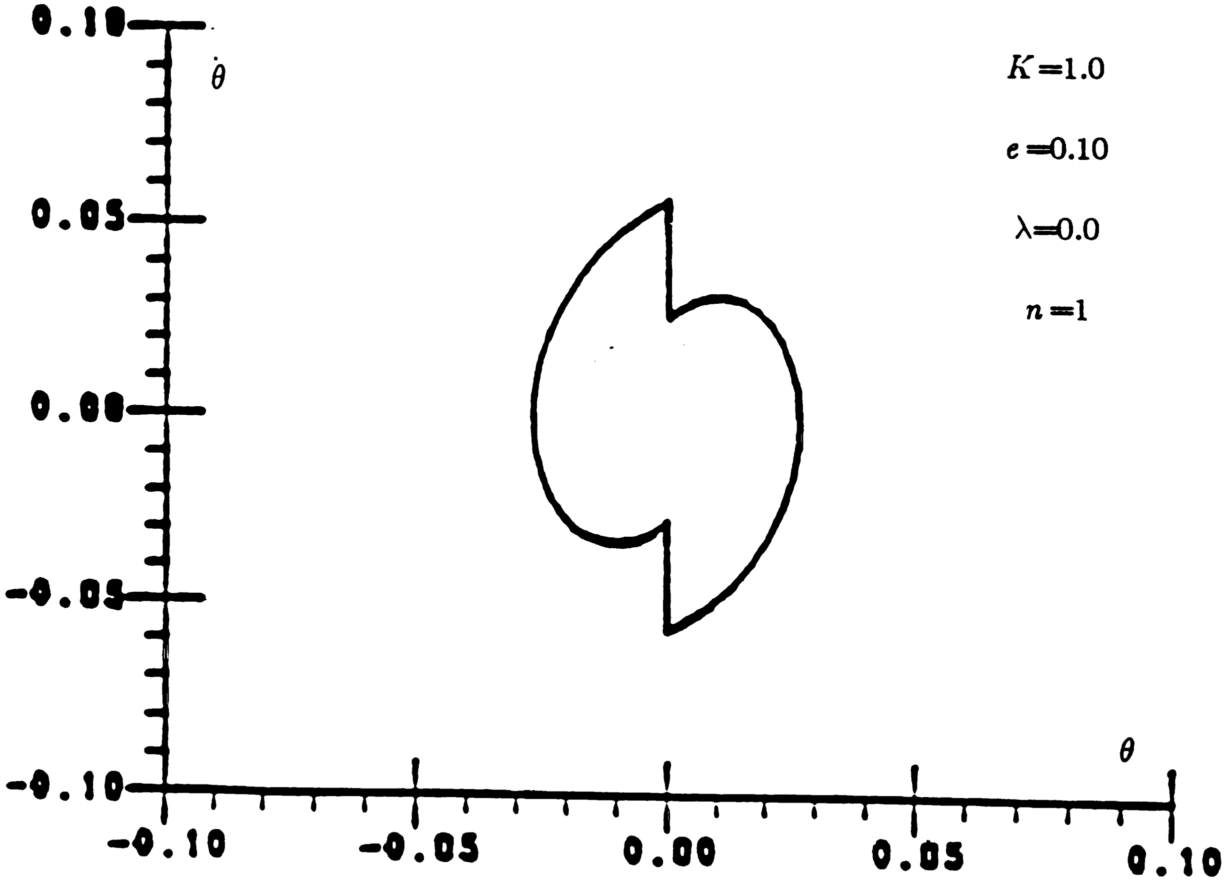

Figure 10b - Phase Trajectory of the Carrier Depicting an SDIP Motion

$$K=J_2E\left(\frac{(1-\eta^2)^2+4\lambda^2\eta^2}{(1+e^2)\eta^2\bar{s}^2+J_2^2E^2}\right)^{1/2} .$$

As the frequency is decreased further, the steady-state amplitude of the linear branch, $y_{\max}$, increases to a point where the motion just touches the constraints at $|x|=1$. This occurs in Figure (7) at a frequency denoted by η^* at which the linear motion with $x_{\max}=1$ coexists along with an unstable SDIP motion having $\bar{y}=0$. That these two motions are in fact coincident at $\eta=\eta^*$ can be shown as follows. For an SDIP motion with $n=1$ to satisfy $\bar{y}=0$, equation (2.2.21b) yields, using the minus branch,

$$\Delta^{1/2}+\frac{(1+e)\bar{s}}{J_1C^2E}=0$$

or, equivalently,

$$-(1+e)\bar{s}+J_1C^2E\,\Delta^{1/2}=0 .$$

If the steady-state amplitude of the linear branch is unity then from equation (2.2.15) it follows that $C=1$. It can be demonstrated that the above condition holds *only* for $C=1$ by using equations (2.2.20a) and (2.2.22) for J_1 and Δ, respectively, as follows:

$$J_1C^2E\,\Delta^{1/2}=\left(CE\left[E^{-2}(1+e)^2\bar{s}^2+\eta^{-2}J_2^2(1-C^{-2})\right]^{1/2}\right)_{C=1}$$

$$=-(1+e)\bar{s} .$$

Any further decrease of the frequency results in the merging and annihilation of the stable linear and the unstable SDIP motions in a degenerate saddle-node bifurcation at $\eta=\eta^*$.

A point of interest about the transformation of linear motions into impacting SDIP orbits is that as the amplitude of the oscillation of the absorber is increased in the linear (non-impacting) range, eventually the amplitude, $|x|$, will equal 1.0, *i.e.*, the motion just grazes the stops while still retaining its linear character. An attempt to further increase the amplitude of the linear motion of the absorber by changing a parameter will destroy the non-impacting motion. However, contrary to what one might intuitively expect, the transformation from linear to nonlinear orbits will not be a smooth one and there will be jump discontinuity (see Figure 7). In other words, a stable SDIP motion with $\bar{y}=\epsilon$, $0<\epsilon<<1$, will not emerge from the linear motion as η is decreased past η^*. This occurs since the stable linear motion with $x_{\max}=1$ and an unstable SDIP motion with $\bar{y}=0$ *annihilate* each other in a saddle-node bifurcation. The overall result is that as parameters are varied, a linear motion does not smoothly transform into an SDIP motion.

It is possible for the stable SDIP response to become unstable in a symmetry-breaking pitchfork bifurcation which results in an anti-symmetric pair of periodic motions. These motions can, as η is decreased further, undergo period doubling bifurcations which result in chaotic dynamics for the system. This is described in more detail towards the end of the chapter.

2.3.2- The Response at the Anti-resonance

An extensive study was carried out to determine the possibility of coexistence of impacting and non-impacting motions at the anti-resonance frequency. To this effect, a fine grid of points in the parameter (K,λ,e) space was searched to detect the occurrence of such coexistence. Figure (11) is a plot showing the coexistence points for different values of K in the (λ,e) space.

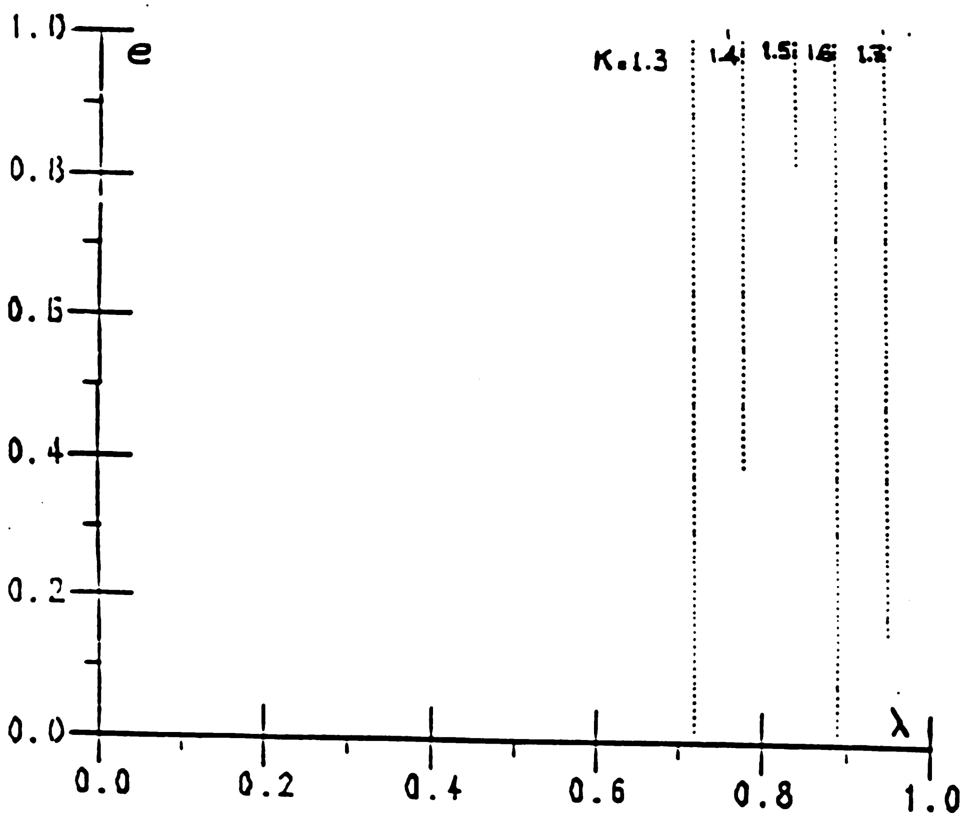

Figure 11 - Coexistence of Linear and Nonlinear Motions at the Anti-resonance Frequency

The occurrence of coexistence at the anti-resonance frequency is crucial from a design point of view since the dynamic behavior of the pendulum, and consequently the carrier, depend on the intial conditions and slight disturbances could take the motion from non-impacting to impacting motions and vice versa. As can be observed from Figure (11), coexistence at the anti-resonance frequency occurs only at unreasonably large values of the damping ratio, $\lambda>0.7$. This places the issue outside the realm of practical applications. The upper bound for K can be obtained by requiring that a linear, non-impacting motion exist at the anti-resonance frequency, *i.e.*, $C\leq 1$ at $\eta=\eta_{AR}$. Employing the definition of C from equation (2.2.16a), this implies that the excitation amplitude should be limited as follows:

$$K\leq K_{cr}(\lambda)=\left\{(1-\eta_{AR}^2)^2+4\lambda^2\eta_{AR}^2\right\}^{1/2}$$

for the existence of a linear motion. The function $K_{cr}(\lambda)$ is bounded above by 0.50 over the range of realistic damping ratios, $0\leq\lambda\leq 0.25$.

Figure (12) depicts a case revealing the coexistence of all three types of motions, namely, the stable and unstable SDIP motions and the linear, non-impacting motion at $\lambda=0.80$, as a function of the coefficient of restitution, e.

The effect of detuning can also be studied in this context. Detuning refers to the presence of disturbances with slightly different excitation frequencies than the frequency for which the absorber is designed. The primary focus of the study of the detuning in this report is to investigate the sensitivity of the occurrence of coexistence at the operating frequency. In other words, if the excitation frequency is not exactly at the anti-resonance frequency, η_{AR}, will this significantly affect the likelihood of coexistence? Figures (13) and

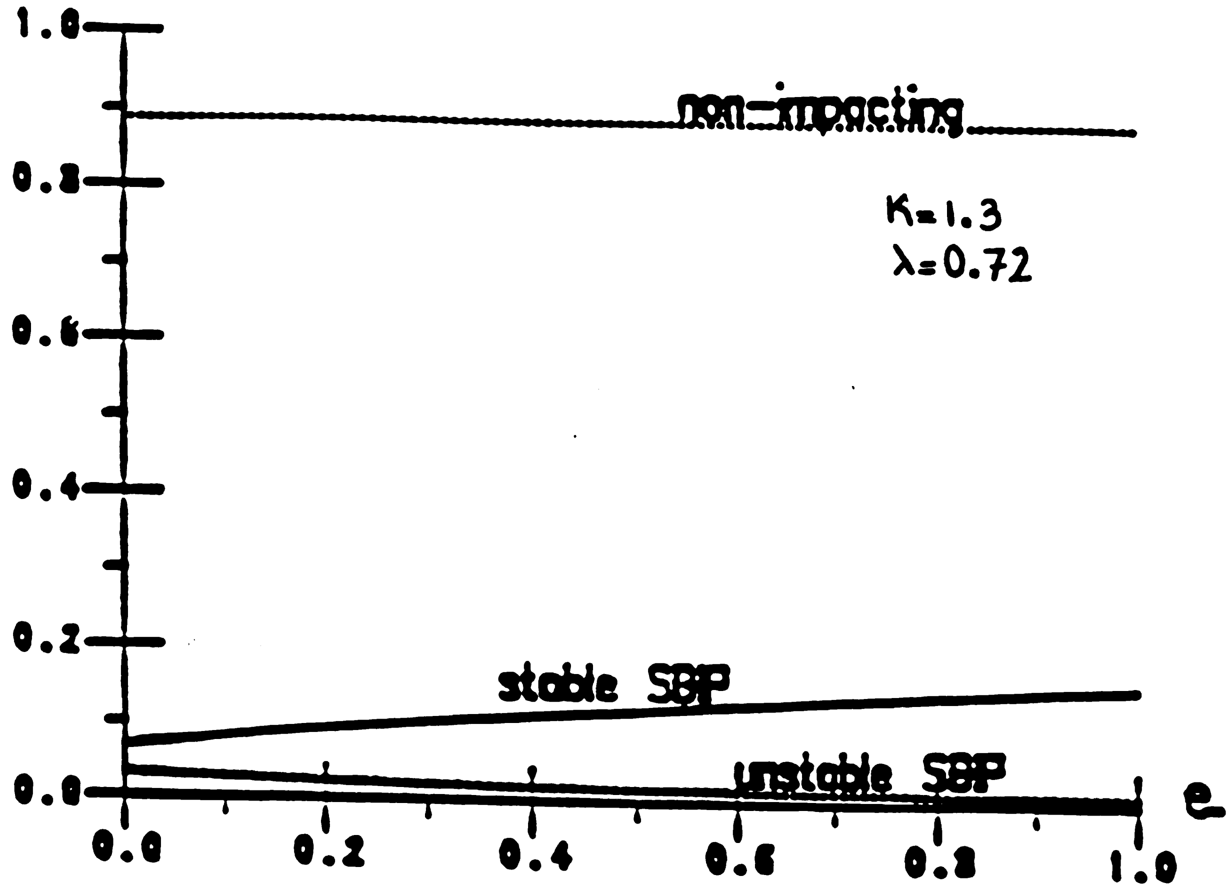

Figure 12 - The Types of Motions Coexisting at the Anti-resonance Frequency

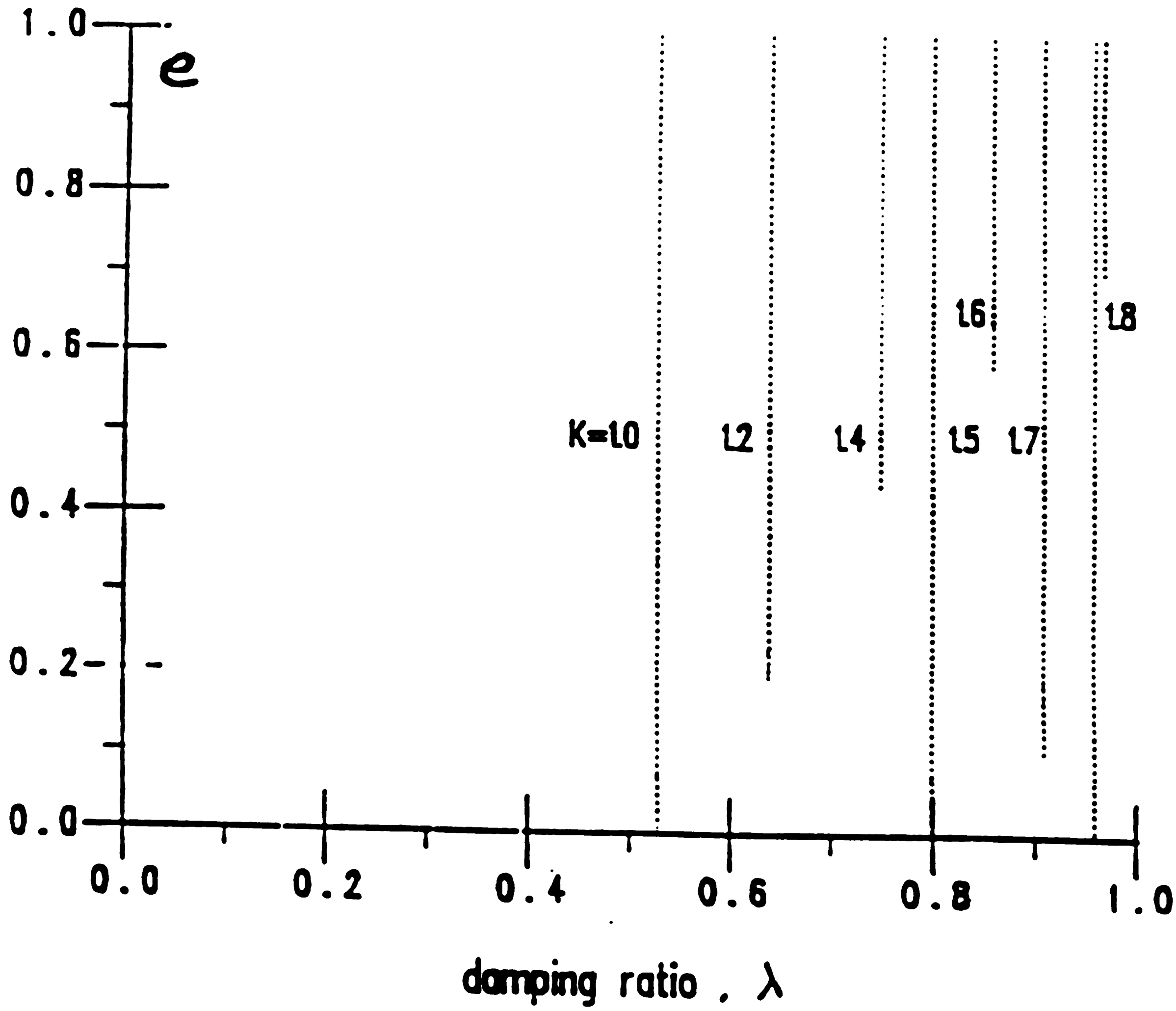

Figure 13a - Coexistence Corresponding to +5% Deviation from the Anti-resonance Frequency

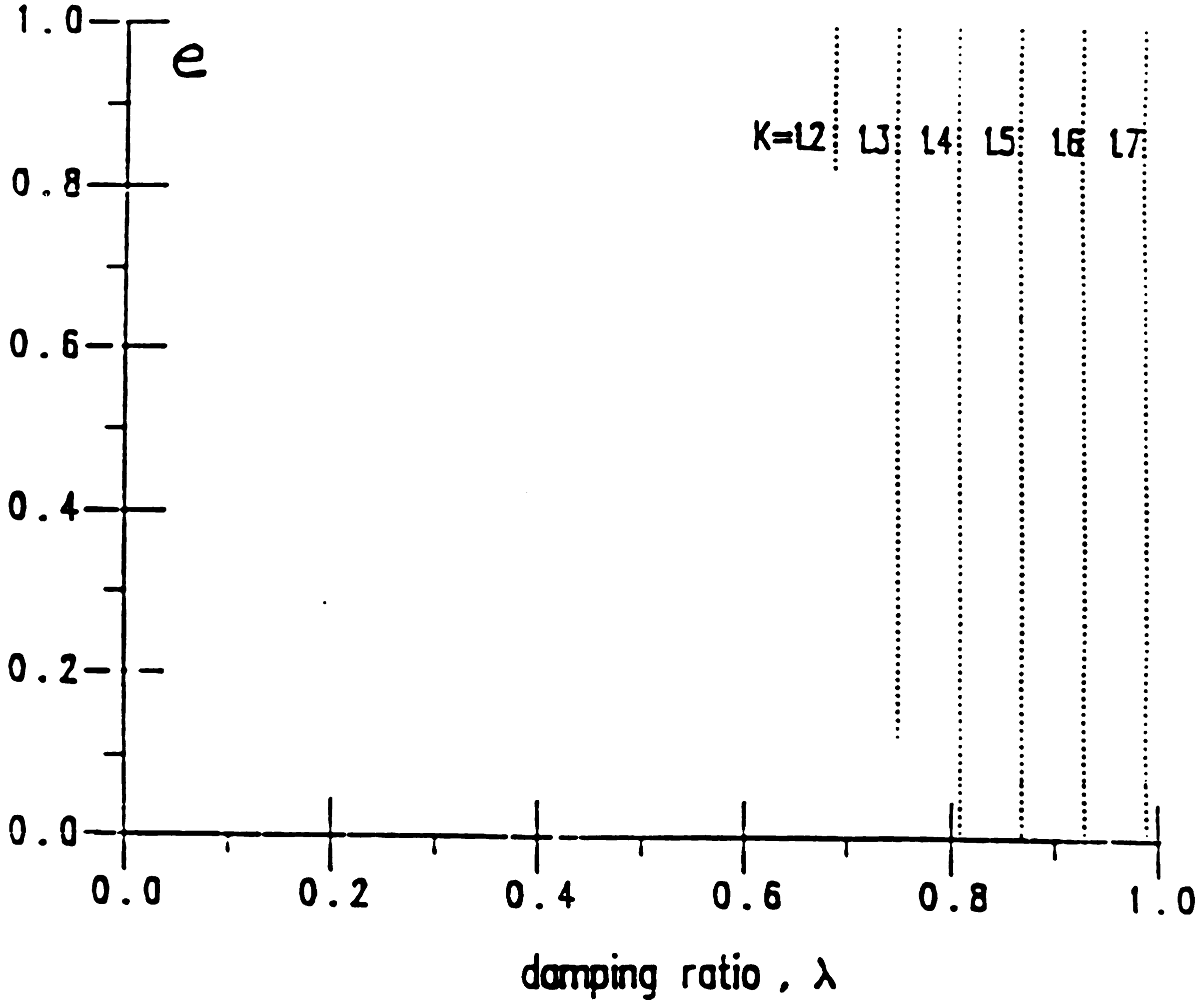

Figure 13b - Coexistence Corresponding to -5% Deviation from the Anti-resonance Frequency

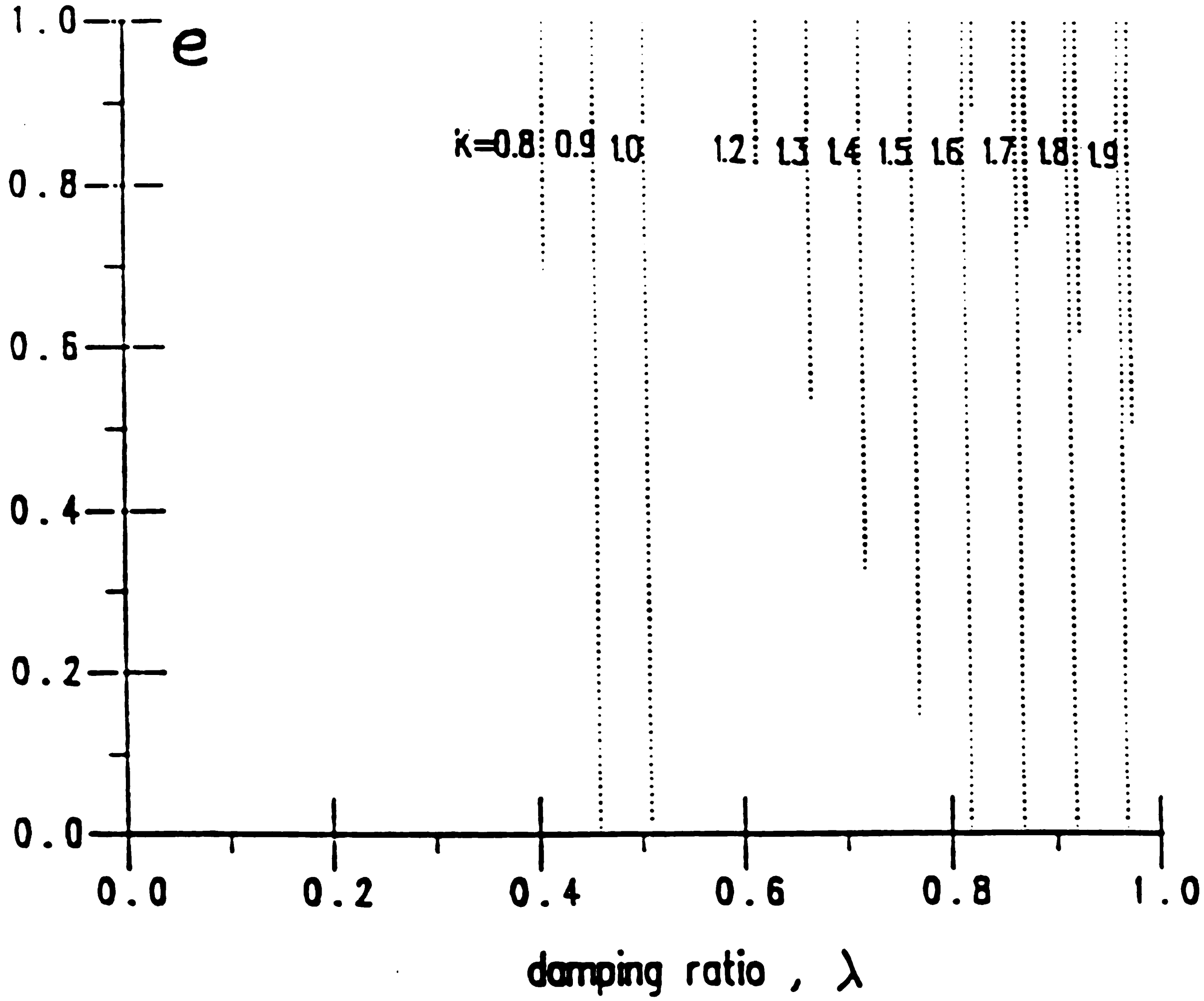

Figure 14a - Coexistence Corresponding to +10% Deviation from the Anti-resonance Frequency

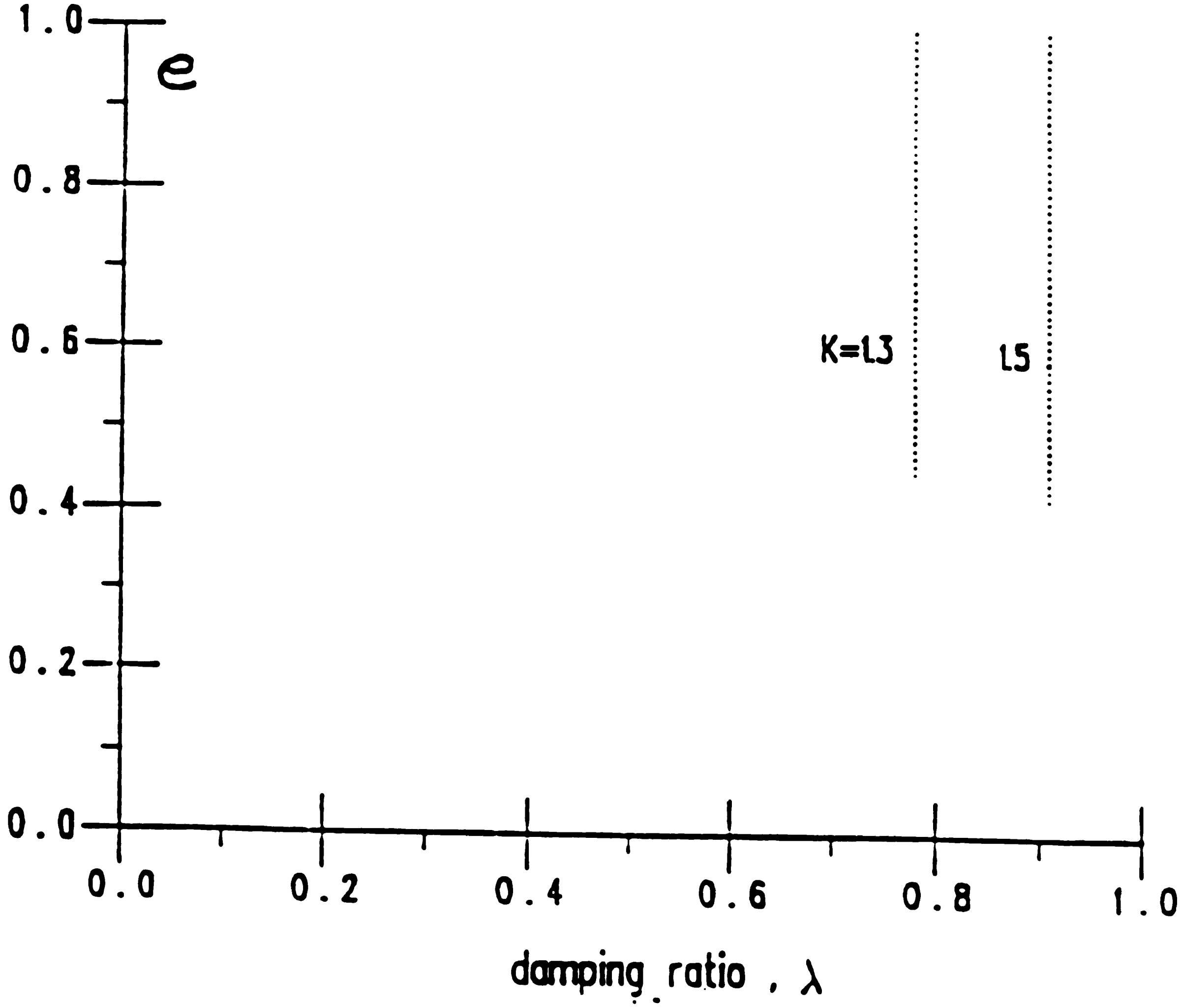

Figure 14b - Coexistence Corresponding to -10% Deviation from the Anti-resonance Frequency

(14), which are similar to Figure (11), were obtained in the following manner. The operating excitation frequency in Figure (13) has a $\pm 5\%$ variation from the anti-resonance frequency and that of Figure (14) has a $\pm 10\%$ variation. As can be observed from these Figures, the effect of detuning has a slight tendency to increase the possibility of coexistence. However, it still does not lead to coexistence at anti-resonance frequency for reasonable values of the damping ratio. This lack of sensitivity implies that tuned CPVA systems should have no problem with steady-state impacting motions.

2.4- Other Nonlinear Responses and Chaotic Motions

As mentioned earlier, in addition to the saddle-node bifurcations that result in the *jump phenomena* (see Figures 7 to 9), another form of bifurcation can occur which results in a change of stability of the SDIP response. For instance, for K=2.0, e=0.95 and λ=0.01, the frequency response is as shown in Figure (15) and it is observed that as the excitation frequency is decreased from η=2.0 the upper SDIP branch becomes unstable at about η=1.60; this is indicated as point B in Figure (15). For excitation frequencies between η=1.60 and η=1.0, where the latter frequency is close to the anti-resonance frequency (η_{AR}=0.89), there exists no stable SDIP or linear, non-impacting preioidic motions. However, a stability study reveals that as the excitation frequency is decreased past point B, an eigenvalue of the **DP** matrix passes out of the unit circle through +1 which renders the response unstable. At this frequency a super-critical pitchfork bifurcation takes place in which the stable SDIP motion becomes unstable and a pair of stable, anti-symmetric, double-impact, periodic orbits are generated. These motions then can each undergo a succession of period doubling, or flip, bifurcations, which eventually result in nonperiodic, or chaotic motions. See Shaw [28] for a more detailed bifurcation analysis for a similar, but simpler system.

Figure (16) depicts the phase trajectory of an unstable SDIP motion along with a pair of stable anti-symmetric period-one double-impact motions and Figure (17) illustrates their corresponding time responses. Plots showing the succession of period-doublings of similar anti-symmetric motions can be found in Shaw [28]. Figure (18a) is a Poincarè map indicating the existence

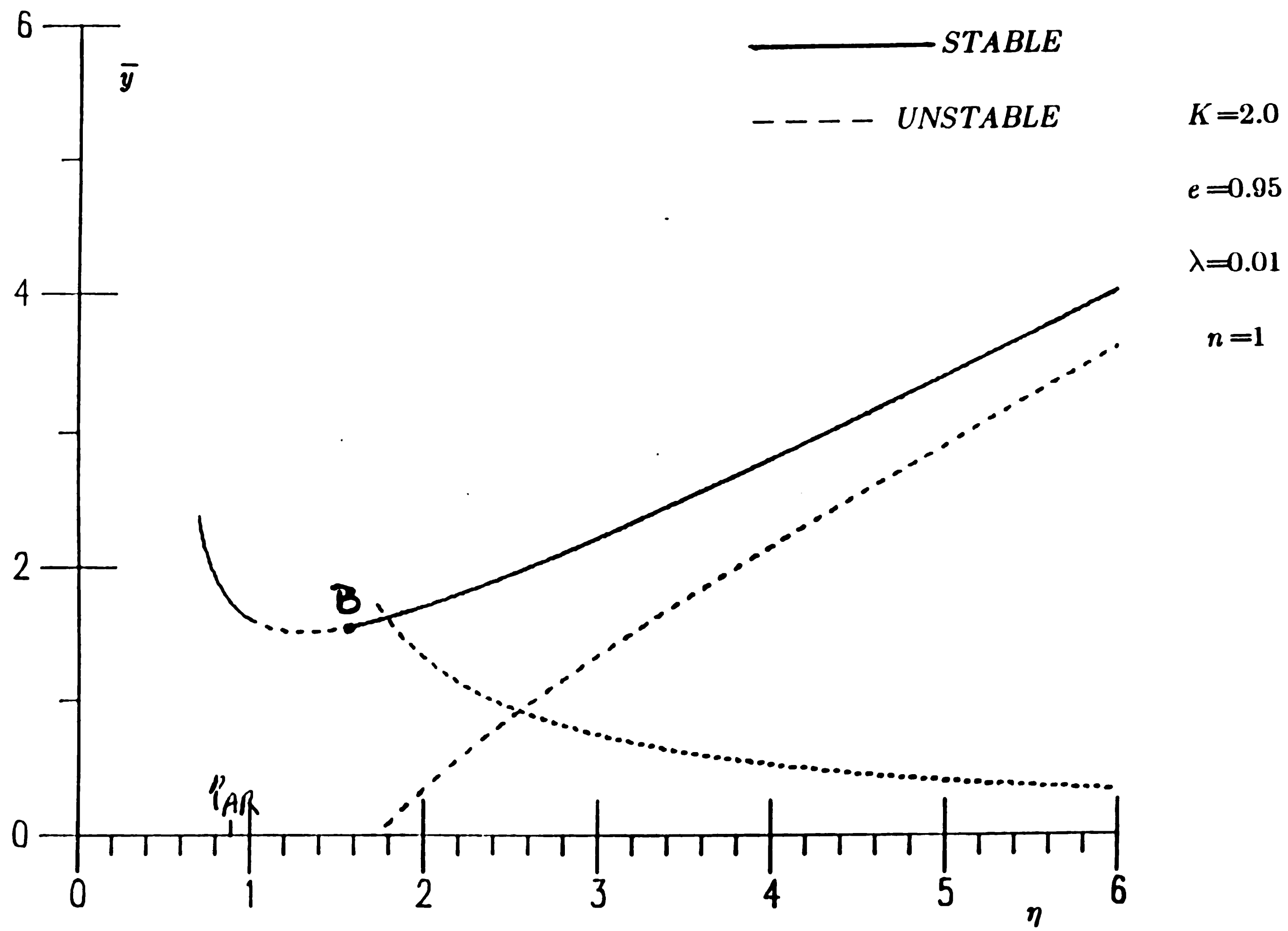

Figure 15 -Frequency Response of the Absorber

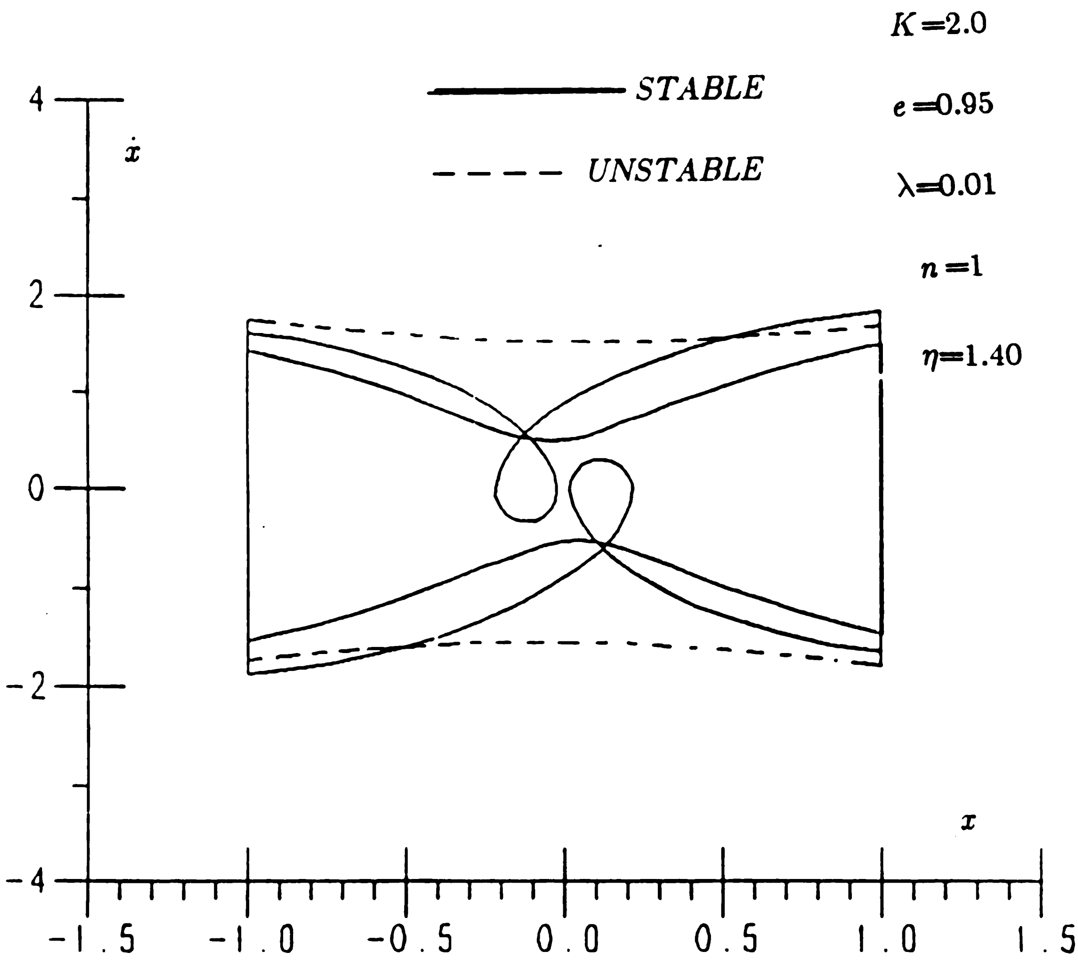

Figure 16 - Phase Trajectory of the Absorber

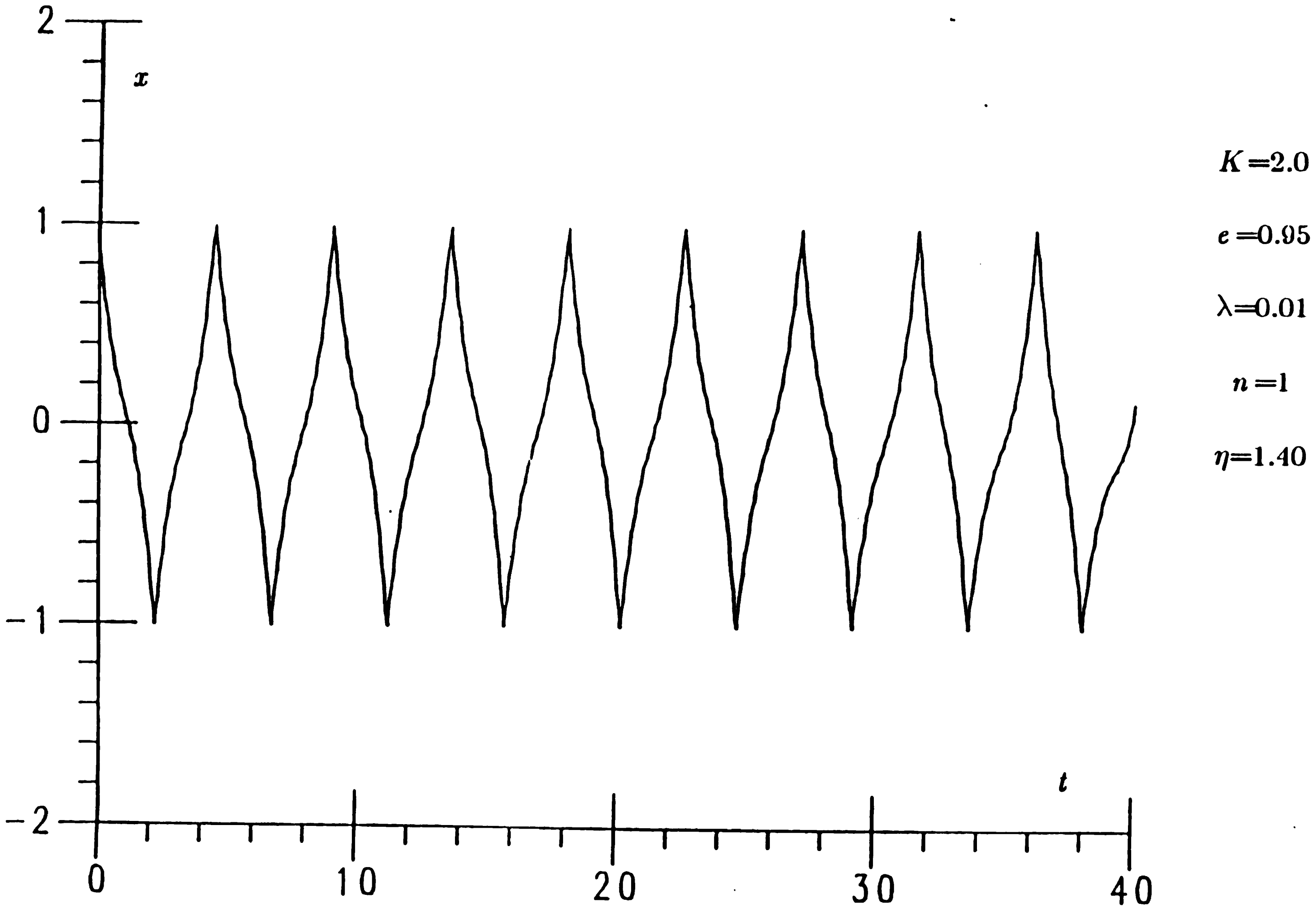

Figure 17a - Time Response of the Unstable SDIP Motion of Figure 16

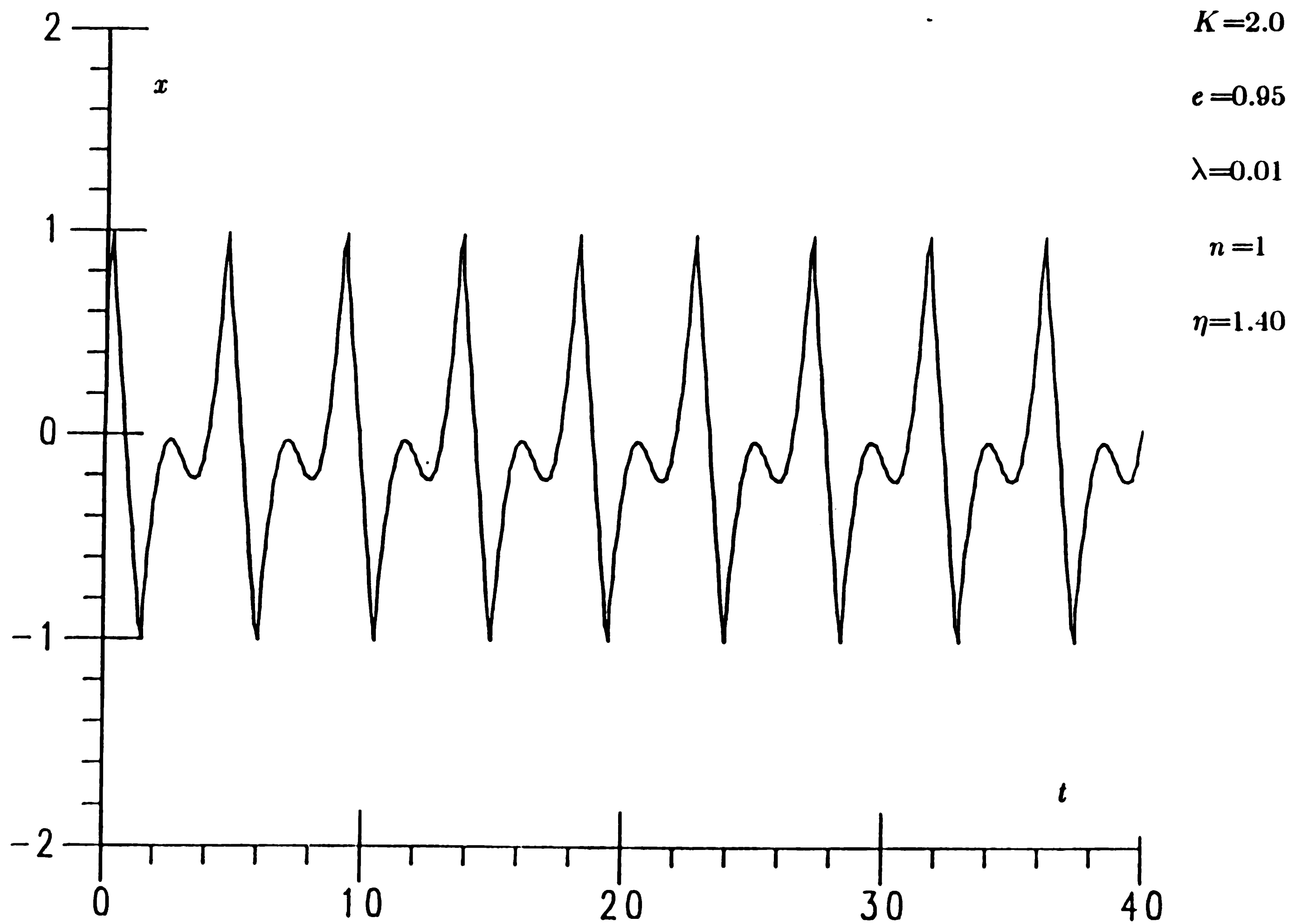

Figure 17b - Time Response of the Stable Anti-symmetric Period-one Double-Impact

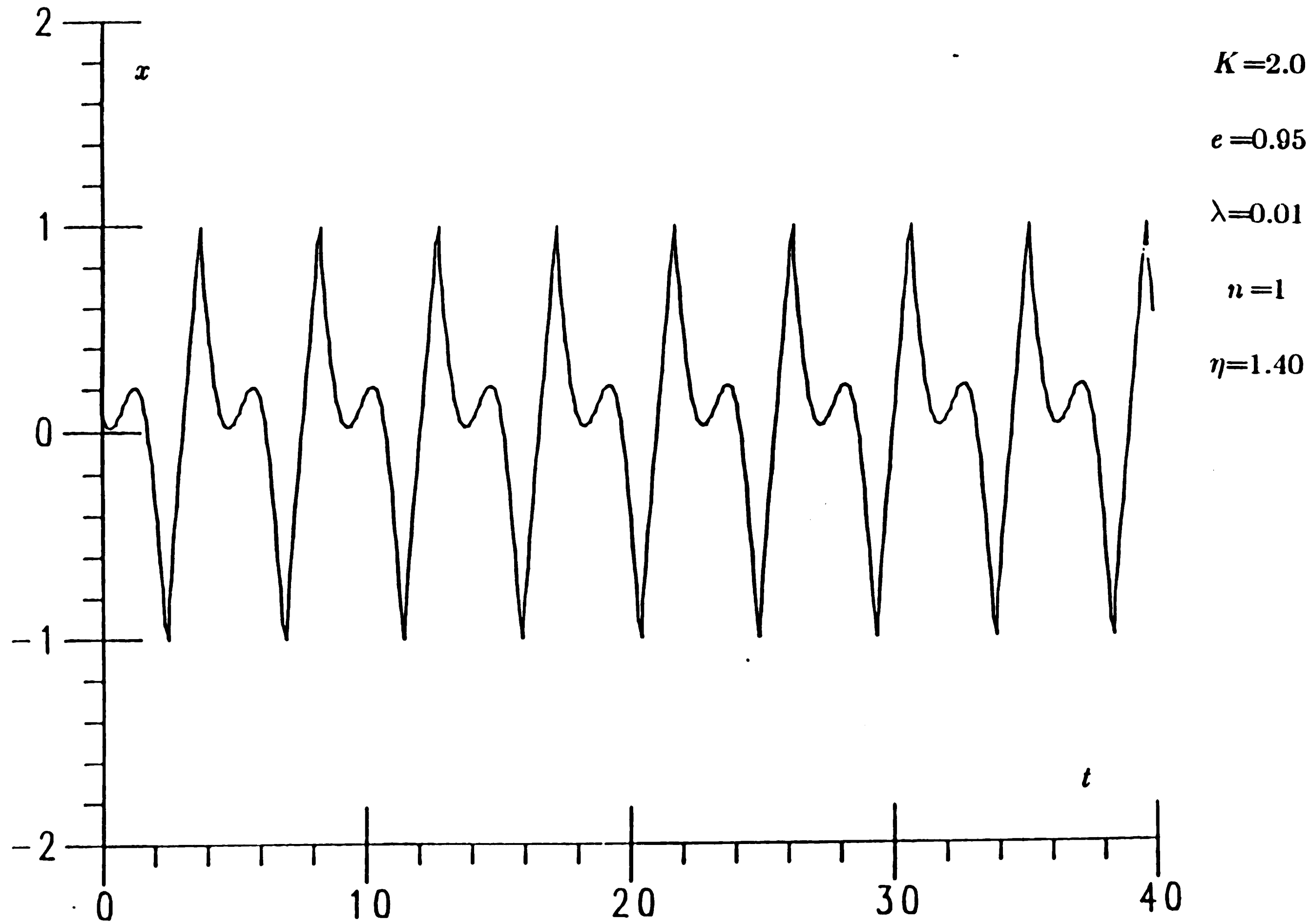

Figure 17c - Time Response of the Stable Anti-symmetric Period-one Double-Impact Motion of a strange attractor which corresponds to a chaotic motion; this occurs after the completion of the period-doubling sequence. Figure (18b) depicts a portion of a typical time response of the absorber mass for an initial condition within the strange attractor. It is noteworthy to mention that the succession of period doubling bifurcations leading to chaos occurred in such a short interval in the parameter space that actual observation of the period doubling of the trajectories turned out to be quite difficult [29]. In other words, such transition in this case does not take place as orderly as the problem considered by Shaw [28].

While chaotic motions may exist at frequencies close to the anti-resonance frequency, no chaos was found at anti-resonance for absorbers designed to operate within the linear range, *i.e.*, for $K < K_{cr}$ and λ small. However, other unmodeled disturbances may lead to chaotic responses. In particular, inputs may lead to chaotic motions near a response curve of subharmonic order n in frequency ranges from $\eta = n$ to a point analogous to point B in Figure (15).

The system is nonlinear and one cannot rule out these types of effects from disturbances, even if they are small, since superposition does not apply when impacts occur.

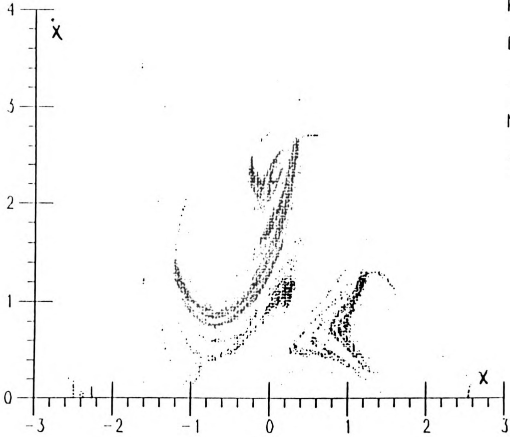

$K = 2.0000$

$E = 0.9500$

$\lambda = 0.0100$

$N = 1.0000$

$\eta = 1.2200$

Figure 18a - Poincare Map of a Strange Attractor

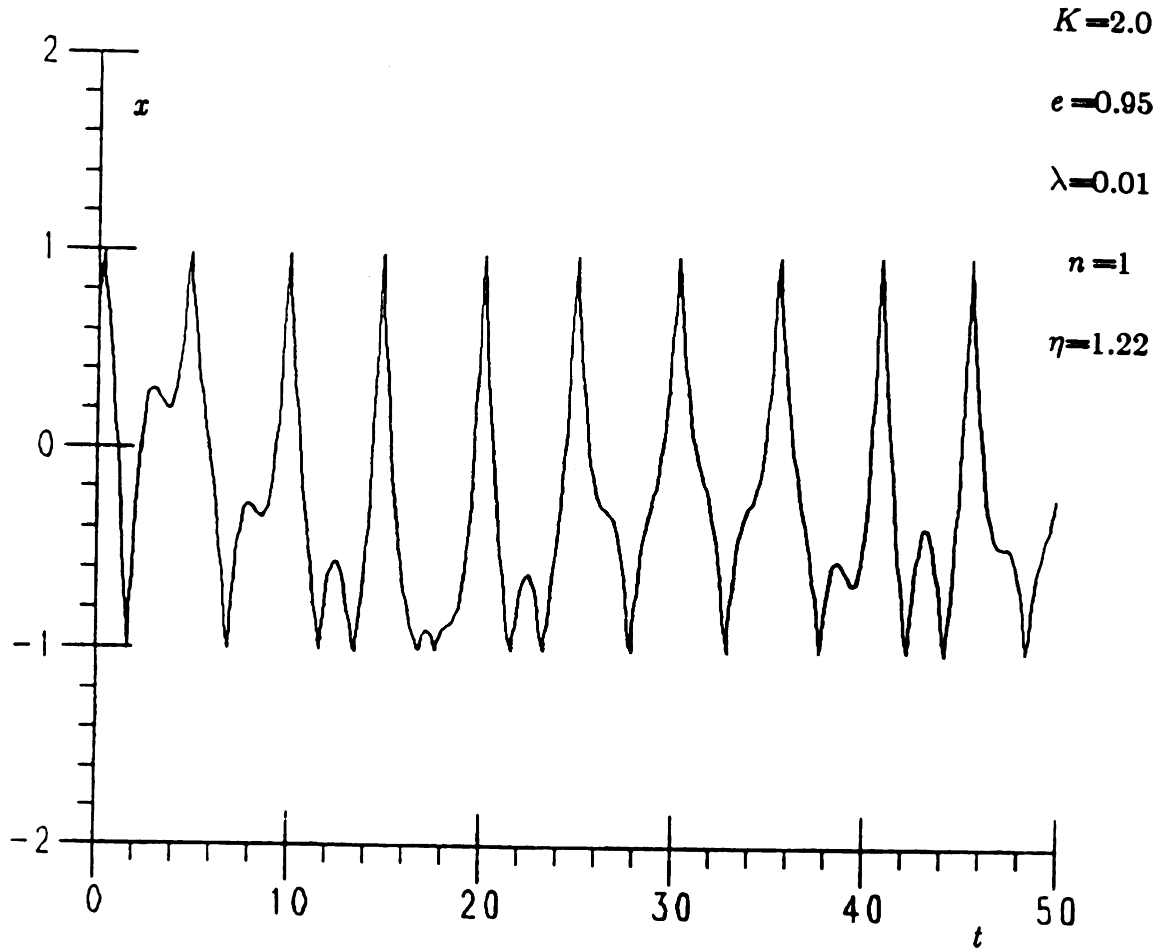

Figure 18b - Time Response of a Chaotic Motion

CHAPTER 3

EFFECTS OF NONLINEARITIES AND DAMPING ON THE DYNAMIC RESPONSE OF THE CPVA

The objective in this chapter is to gain a better understanding of the *nonlinear* dynamic response of the CPVA and the effect of damping on the system. The results enable one to obtain a broader view of the different nonlinear aspects of the response of the system along with more accurate guidelines in terms of the limitations of the linear analysis. To this effect, the nonlinear dynamic response of a centrifugal pendulum vibration absorber with damping in both the primary system and the pendulum is analyzed using the methods of harmonic balance and Floquet theory. In section 3.1 the full nonlinear equations of motion are rescaled and put into the proper form for further analysis and section 3.2 deals with the existence of periodic solutions of the system and the method of analysis. Section 3.3 is devoted to the stability analysis of the periodic solutions obtained in section 3.2 and frequency response results are presented in section 3.4. The final section of the chapter, section 3.5, describes a study of the response of the system at the anti-resonance frequency.

3.1- Equations of Motion

Rewriting the full nonlinear equations of motion (1.1.7):

$$[J+mR^2+mr^2+2mRr\cos\phi]\psi''-mr(R\cos\phi+r)\phi''+mRr\phi'^2\sin\phi-$$

$$-2mRr\psi'\phi'\sin\phi+C_c\psi'=T(\tau) \tag{3.1.1a}$$

$$-mr(R\cos\phi+r)\psi''+mr^2\phi''+C_p\phi'+mRr\psi'^2\sin\phi=0 \tag{3.1.1b}$$

where the terms in equations (3.1.1) are defined following equations (1.1.7). For simplicity, the following rescaling of the parameters is defined. Let:

$$\mu=\frac{J}{mR^2} \quad , \quad \gamma=\frac{r}{R} \tag{3.1.2a}$$

$$\tilde{\lambda}_c=\frac{C_c}{mR^2} \quad , \quad \tilde{\lambda}_p=\frac{C_p}{mR^2} \tag{3.1.2b}$$

$$\tilde{K}_0=\frac{T_0}{mR^2} \quad , \quad \tilde{K}_1=\frac{T_1}{mR^2} \quad , \tag{3.1.2c}$$

This will render the equations of motion (3.1.1) as

$$(1+\mu+\gamma^2+2\gamma\cos\phi)\psi''-\gamma(\cos\phi+\gamma)\phi''+\gamma\phi'^2\sin\phi-2\gamma\psi' \quad .$$

$$\phi'\sin\phi+\tilde{\lambda}_c\psi'=\tilde{K}_0+\tilde{K}_1\cos(\omega\tau) \tag{3.1.3a}$$

$$-\gamma(\cos\phi+\gamma)\psi''+\gamma^2\phi''+\tilde{\lambda}_p\phi'+\gamma\psi'^2\sin\phi=0 \quad . \tag{3.1.3b}$$

Note that ψ and ϕ are the angular displacements of the carrier and the absorber, respectively. In addition, as mentioned previously, primes denote differentiation with respect to time, τ. We have taken only the first term in the Fourier series of a general periodic disturbance.

The variable ψ does not appear in the equations of motion and is completely arbitrary, *i.e.*, it is an ignorable coordinate. The system has only *one—and—a—half* degrees of freedom and if equations (3.1.3) are written in first order form, only three equations will be required, *i.e.*, one each for the derivatives of ϕ, ϕ' and, ψ'. Here the system is not reducible to a second order system since we retain the constant torque and carrier damping.

As one can see, the method of rescaling of the parameters in this chapter (equations 3.1.2) is different than the one used in the previous chapter (relations following equation 2.1.20a). The scaling of chapter 2 resulted in nondimensional system parameters, while the scaling in equations (3.1.2) does not yield all the parameters as dimensionless (see equation 3.1.2b above). However, the latter scaling is employed in order to simplify the terms in the equations of motion for further analysis. Nondimensionalization is carried out below.

It is also important to note the lack of a certain symmetry in equations (3.1.3), which arises due to the damping and constant torque terms. When these terms are omitted, that is, $\tilde{\lambda}_c=\tilde{\lambda}_p=\tilde{K}_0=0$, the equations admit solutions with the following symmetry:

$$(\phi,\psi,\tau) \rightarrow (-\phi,-\psi,\tau+\frac{\pi}{\omega}) .$$

Such solutions represent motions which have zero mean and contain only odd order harmonics. When K_0 is nonzero, such symmetric solutions are not possible and in general motions will have nonzero mean and contain all harmonic orders. The physics behind this lack of symmetry is that the constant torque, $\tilde{K}_0$, and the counteracting damping, $\tilde{\lambda}_c$, bias the rotation of the carrier to a preferred direction.

To account for the fact that the system generally undergoes a gross rotational motion, we shall break ψ up as follows:

$$\psi(\tau)=\tilde{\Omega}\tau+\theta(\tau) \quad , \quad \tilde{\Omega}=constant \ ; \tag{3.1.4}$$

that is, the carrier angular displacement is composed of a nominal steady rotation and an oscillating part. The average rotational speed, $\tilde{\Omega}$, will be solved for in the course of the analysis. Substitution of equation (3.1.4) into (3.1.3) and rescaling time yields:

$$\begin{aligned}&(1+\mu+\gamma^2+2\gamma\cos\phi)\ddot{\theta}-\gamma(\cos\phi+\gamma)\ddot{\phi}+\gamma\dot{\phi}^2\sin\phi-\\ &-2\gamma\Omega\dot{\phi}\sin\phi-2\gamma\dot{\theta}\dot{\phi}\sin\phi+\lambda_c\dot{\theta}=K_1\cos(\eta t)+K_0-\lambda_c\Omega\end{aligned} \tag{3.1.5a}$$

$$\begin{aligned}&-\gamma(\cos\phi+\gamma)\ddot{\theta}+\gamma^2\ddot{\phi}+\lambda_p\dot{\phi}+\gamma\Omega^2\sin\phi+\\ &\gamma\dot{\theta}^2\sin\phi+2\gamma\Omega\dot{\theta}\sin\phi=0 \quad .\end{aligned} \tag{3.1.5b}$$

The rescaled time is defined by

$$t=\omega_n\tau$$

where

$$\omega_n=\left[\frac{\Omega^2}{\mu}\left(\frac{1}{\gamma}+\frac{\mu}{\gamma}+\gamma+2\right)\right]^{\frac{1}{2}}$$

is the nontrivial natural frequency of the carrier-absorber system. This results in the following nondimensional parameters which appear in Equations (3.1.5):

$$\lambda_p=\frac{\tilde{\lambda}_p}{\omega_n} \quad , \quad \lambda_c=\frac{\tilde{\lambda}_c}{\omega_n} \quad , \quad \Omega=\frac{\tilde{\Omega}}{\omega_n} \quad ,$$

$$\eta=\frac{\omega}{\omega_n} \quad , \quad K_0=\frac{\tilde{K}_0}{\omega_n^2} \quad and, \quad K_1=\frac{\tilde{K}_1}{\omega_n^2} \ .$$

Also, overdots denote differentiation with respect to the rescaled time t. In equation (3.1.5a), one might be tempted to immediately cancel the K_0 and $-\Omega\lambda_c$ terms by setting the average speed to be $\Omega=K_0/\lambda_c$. This will be true to first order, but it is not immediately obvious that there will be no contribution to Ω from the terms on the left hand side of the equality in equation (3.1.5a), due to the inherent asymmetric nature of the oscillations.

Two remarks about the rescaling are in order at this point. First, the numerical values of the damping ratios λ_c and λ_p used in this study are all between zero and 0.10, and are not as relatively small as one might think. In fact, if the pendulum damping ratio is greater than 0.01, the system response is drastically different when compared to that for lower damping values. This is demonstrated in section 3.4. Secondly, the numerical values of the excitation amplitude K_1 used in this analysis (typically $K_1 \leq 0.1$) represent reasonable values for the input torque. For instance, for the particular geometrical dimensions of the system used in this analysis, $K_1=0.1$ corresponds to an excitation amplitude in the system of about 5.0×10^4 $ft.lb$.

3.2- Periodic Response

The method of harmonic balance [32, 33] is employed here in order to approximate the periodic responses of the CPVA. The harmonic balance method is chosen since it provides results with relatively uniform accuracy over a wide range of frequency and is not dependent on small parameter assumptions for the equations of motion (although such an assumption is made here in order to limit the number of terms used in predicting the response; see equation 3.2.1 and the explanation following). This wide bandwidth uniformity of the results of the harmonic balance method makes it an attractive tool for analyzing nonlinear systems such as the one presented here. In fact, the limitations of the method are primarily dictated by the number of terms that one wishes to include in the analysis and also by the degree of sophistication of the computing systems at hand. In an asymptotic sense, the results of the harmonic balance obtained for problems such as the one presented here converge to the exact result as more terms are included in the analysis.

The reader should note that the method of averaging, which in its own right is a powerful method in dealing with nonlinear systems, was employed first. However, difficulties arose as one tried to obtain periodic solutions for excitation frequencies that were outside of a small neighborhood of the resonance frequency. The result was that, although the frequency response of the pendulum was predicted satisfactorily, inaccuracies in the carrier response prevented the results of the averaging to be acceptable for further analysis.

To apply the method of harmonic balance [32,33], we assume

$$\theta = A_1 \sin\eta t + B_1 \cos\eta t \tag{3.2.1a}$$

$$\phi = \alpha + A_2 \sin\eta t + B_2 \cos\eta t \tag{3.2.1b}$$

i.e., the solution is approximated by its first harmonic plus an offset in ϕ which accounts, to the first order, for the asymmetry in the solutions (the offset in ψ is given by $\Omega\tau$, a constant in θ would be meaningless).

Substitution of equations (3.1.4) and (3.2.1) into equations (3.1.5) results in two nonlinear equations in terms of α, Ω, A_1, B_1, A_2, and B_2 as follows:

$$\begin{gathered}
-\eta^2[1+\mu+\gamma^2+2\gamma f_c(t)](A_1\sin\eta t+B_1\cos\eta t)+ \\
+\gamma\eta^2[\gamma+f_c(t)](A_2\sin\eta t+B_2\cos\eta t)+\gamma\eta^2(A_2\cos\eta t-B_2\sin\eta t)^2 f_s(t)- \\
-2\gamma\Omega\eta(A_2\cos\eta t-B_2\sin\eta t)f_s(t)- \\
-2\gamma\eta^2(A_1\cos\eta t-B_1\sin\eta t)(A_2\cos\eta t-B_2\sin\eta t)f_s(t)- \\
-\lambda_c\,\eta(A_1\cos\eta t-B_1\sin\eta t)+\lambda_c\,\Omega=K_1\cos\eta t+K_0 \quad ,
\end{gathered} \tag{3.2.2a}$$

and

$$\begin{gathered}
\gamma\eta^2[\gamma+f_c(t)](A_1\sin\eta t+B_1\cos\eta t)-\gamma^2\eta^2(A_2\sin\eta t+B_2\cos\eta t)+ \\
+\lambda_p\,\eta(A_2\cos\eta t-B_2\sin\eta t)+\gamma\Omega^2 f_s(t)+ \\
+\gamma\eta^2(A_1\cos\eta t-B_1\sin\eta t)^2 f_s(t)+2\gamma\Omega\eta(A_1\cos\eta t-B_1\sin\eta t)f_s(t)=0 \quad .
\end{gathered} \tag{3.2.2b}$$

where

$$f_s(t)=\sin(\alpha+A_2\sin\eta t+B_2\cos\eta t) \tag{3.2.3a}$$

$$f_c(t)=\cos(\alpha+A_2\sin\eta t+B_2\cos\eta t) \quad . \tag{3.2.3b}$$

As one can see, the above substitution results in composite trigonometric functions $f_c(t)$ and $f_s(t)$. Expansion of equations (3.2.3) yields

$$f_c(t)=\sin\alpha[\cos(A_2\sin\eta t)\cos(B_2\cos\eta t)-\sin(A_2\sin\eta t)\sin(B_2\cos\eta t)]+$$

$$+\cos\alpha[\sin(A_2\sin\eta t)\cos(B_2\cos\eta t)+\cos(A_2\sin\eta t)\sin(B_2\cos\eta t)\quad , \tag{3.2.4a}$$

and

$$f_c(t)=-\sin\alpha[\sin(A_2\sin\eta t)\cos(B_2\cos\eta t)-\cos(A_2\sin\eta t)\sin(B_2\cos\eta t)]+$$

$$+\cos\alpha[\cos(A_2\sin\eta t)\cos(B_2\cos\eta t)-\sin(A_2\sin\eta t)\sin(B_2\cos\eta t)]\quad . \tag{3.2.4b}$$

The composite trignometric functions appearing on the right-hand sides of equations (3.2.4) can be expressed in terms of infinite series of Bessel functions as follows:

$$\cos(x\sin\eta t)=J_0(x)+2\left(J_2(x)\cos2\eta t+J_4(x)\cos4\eta t+...\right)\quad , \tag{3.2.5a}$$

$$\sin(x\sin\eta t)=2\left(J_1(x)\sin\eta t+J_3(x)\sin3\eta t+...\right)\quad , \tag{3.2.5b}$$

$$\cos(x\cos\eta t)=J_0(x)-2\left(J_2(x)\cos2\eta t-J_4(x)\cos4\eta t+...\right) \tag{3.2.5c}$$

and,

$$\sin(x\cos\eta t)=2\left(J_1(x)\cos\eta t-J_3(x)\cos3\eta t+...\right)\quad , \tag{3.2.5d}$$

where $x=A_2$ or B_2, and where $J_n(x)$ is a Bessel function of order n defined as

$$J_n(x)=\sum_{k=0}^{\infty}\frac{(-1)^k}{k!(n+k)!}\left(\frac{x}{2}\right)^{n+2k}\quad . \tag{3.2.6}$$

(The composite terms such as $\cos(A_i\sin\eta t)$, $i=1,2$ can be expressed as a power series in A_2 and B_2. The nonlinear equations will eventually be truncated at third order, *i.e.*, only linear, quadratic, and cubic terms in α, Ω, A_i and B_i are retained; this will capture first order nonlinear effects.) Utilization of equations (3.2.3), (3.2.5) in equations (3.1.5) yields two nonlinear equations in terms of the aforementioned variables as follows:

$$\lambda_c \Omega + \Big\{ -\eta^2 A_1[1+\mu+\gamma^2+2\gamma\cos\alpha J_0(A_2)J_0(B_2)] +$$

$$+\gamma\eta^2 A_2[\gamma+\cos\alpha J_0(A_2)J_0(B_2)] + 2\gamma\eta B_2 \sin\alpha J_0(A_2)J_0(B_2) -$$

$$-\lambda_c \eta B_1 \Big\} \sin\eta t + \Big\{ -\eta^2 B_1[1+\mu+\gamma^2+2\gamma\cos\alpha J_0(A_2)J_0(B_2)] +$$

$$+\gamma\eta^2 B_2[\gamma+\cos\alpha J_0(A_2)J_0(B_2)] - 2\gamma\eta A_2 \sin\alpha J_0(A_2)J_0(B_2) +$$

$$+\lambda_c \eta A_1 \Big\} \cos\eta t = K_0 + K_1 \cos\eta t \quad , \tag{3.2.7a}$$

and

$$\gamma\sin\alpha J_0(A_2)J_0(B_2) + \Big\{ \gamma\eta^2 A_1[\gamma+\cos\alpha J_0(A_2)J_0(B_2)] - \gamma^2\eta^2 A_2 -$$

$$-\lambda_p \eta B_2 + 2\gamma\cos\alpha J_0(B_2)J_1(A_2) - 2\gamma\eta B_1 \sin\alpha J_0(A_2)J_0(B_2) \Big\} \sin\eta t +$$

$$+ \Big\{ \gamma\eta^2 B_1[\gamma+\cos\alpha J_0(A_2)J_0(B_2)] - \gamma^2\eta^2 B_2 + \lambda_p \eta A_2 +$$

$$+2\gamma\cos\alpha J_0(A_2)J_1(B_2) + 2\gamma\eta A_1 \sin\alpha J_0(A_2)J_0(B_2) \Big\} \cos\eta t = 0 \quad . \tag{3.2.7b}$$

Matching the coefficients of terms multiplied by $\sin k\eta t$ and $\cos k\eta t$ for $k=0$ and 1 in equations (3.2.7) yields six equations in terms of α, Ω, A_i and, B_i , $i=1, 2$.

The constant order terms result in the following conditions:

$$\lambda_c \Omega = K_0 \quad , \tag{3.2.8a}$$

and

$$\gamma\Omega^2 \sin\alpha f(A,B) = 0 \quad , \tag{3.2.8b}$$

where

$$f(A,B) = J_0(A_2)J_0(B_2) \quad .$$

Note that $f(A,B)$ is a function of A_2 and B_2 which is nonzero (except for values of A_2 and B_2 representing large amplitude motions, *e.g.*, $\phi_{\max}>\frac{\pi}{2}$). These conditions immediately give the mean rotational speed as $\Omega=K_0/\lambda_c$ and a zero offset in pendulum oscillations, $\alpha=0$ (the $\alpha=\pi$ case is inherently unstable and not of interest here). This implies that the pendulum and the carrier oscillations can be well approximated by a zero mean, ***symmetric*** (in the sense described in section 3.1) oscillation.

The four remaining equations are in terms of the A_i and B_i and are given as follows, where we have employed conditions (3.2.8):

$$-\eta^2 A_1[1+\mu+\gamma^2+2\gamma J_0(A_2)J_0(B_2)]+$$
$$+\gamma\eta^2 A_2[\gamma+J_0(A_2)J_0(B_2)]-\lambda_c\eta B_1=0$$

$$\gamma\eta^2 A_1[\gamma+J_0(A_2)J_0(B_2)]-\gamma^2\eta^2 A_2-$$
$$-\lambda_p\eta B_2+2\gamma J_0(B_2)J_1(A_2)=0 \tag{3.2.9b}$$

$$-\eta^2 B_1[1+\mu+\gamma^2+2\gamma J_0(A_2)J_0(B_2)]+\gamma\eta^2 B_2[\gamma+$$
$$+J_0(A_2)J_0(B_2)]+\lambda_c\eta A_1=K_1$$

$$\gamma\eta^2 B_1[\gamma+J_0(A_2)J_0(B_2)]-\gamma^2\eta^2 B_2+\lambda_p\eta A_2+$$
$$+2\gamma J_0(A_2)J_1(B_2)=0\quad . \tag{3.2.10b}$$

Noting that from equation (3.2.6),

$$J_0(x)=1-\frac{x^2}{4}+\ .\ .\ .$$

and

$$J_1(x)=\frac{x}{2}-\frac{x^3}{16}+\ldots \quad .$$

All the terms in equations (3.2.9) and (3.2.10) are expanded and we keep up to cubic orders in A_i and B_i. This results in the following equations:

$$-\eta^2[1+\mu+\gamma^2+2\gamma(1-\frac{A_2^2}{4}-\frac{B_2^2}{4})]A_1+\eta^2[\gamma^2+\gamma(1-\frac{A_2^2}{4}-\frac{B_2^2}{4})]A_2-$$

$$-\lambda_c\eta B_1=0 \tag{3.2.11a}$$

$$-\eta^2[1+\mu+\gamma^2+2\gamma(1-\frac{A_2^2}{4}-\frac{B_2^2}{4})]B_1+\eta^2[\gamma^2+\gamma(1-\frac{A_2^2}{4}-\frac{B_2^2}{4})]B_2-$$

$$-\lambda_c\eta A_1-K_1=0 \tag{3.2.11b}$$

$$\eta^2[\gamma^2+\gamma(1-\frac{A_2^2}{4}-\frac{B_2^2}{4})]A_1-\gamma^2\eta^2A_2-\lambda_p\eta B_2+$$

$$+2\gamma\Omega^2(\frac{A_2}{2}-\frac{A_2B_2^2}{8}-\frac{A_2^3}{16})=0 \tag{3.2.12a}$$

$$\eta^2[\gamma^2+\gamma(1-\frac{A_2^2}{4}-\frac{B_2^2}{4})]B_1-\gamma^2\eta^2B_2-\lambda_p\eta A_2+$$

$$+2\gamma\Omega^2(\frac{B_2}{2}-\frac{B_2A_2^2}{8}-\frac{B_2^3}{16})=0 \tag{3.2.12a}$$

At this stage it is convenient to express θ and ϕ in terms of amplitude-phase variables as follows:

$$\theta=a_1\cos(\eta t-\beta_1) \tag{3.2.13a}$$

$$\phi=a_2\cos(\eta t-\beta_2) \tag{3.2.13b}$$

where

$$A_i^2+B_i^2=a_i^2 \quad , \quad A_i=a_i\sin\beta_i \quad , \quad B_i=a_i\cos\beta_i \quad , \quad i=1,2 \ .$$

Substitution of equations (3.2.11) into equations (3.2.9) and (3.2.10) (with $\Omega=K_0/\lambda_c$ and $\alpha=0$) results in the following four equations for a_1, β_1, a_2, and β_2:

$$-\eta^2\left(1+\mu+\gamma^2 2\gamma[1-\frac{a^{2_2}}{4}]\right)a_1\sin\beta_1+$$

$$+\eta^2\left(\gamma^2+\gamma[1-\frac{a_2^2}{4}]\right)a_2\sin\beta_2-\lambda_c\eta a_1\cos\beta_1=0 \quad , \tag{3.2.14a}$$

$$-\eta^2\left(1+\mu+\gamma^2 2\gamma[1-\frac{a^{2_2}}{4}]\right)a_1\cos\beta_1+$$

$$+\eta^2\left(\gamma^2+\gamma[1-\frac{a_2^2}{4}]\right)a_2\cos\beta_2+\lambda_c\eta a_1\sin\beta_1-K_1=0 \quad , \tag{3.2.14b}$$

and

$$\eta^2\left(\gamma^2+\gamma[1-\frac{a_2^2}{4}]\right)a_1\sin\beta_1-\gamma^2\eta^2 a_2\sin\beta_2-$$

$$-\lambda_p\eta a_2\cos\beta_2+2\gamma\Omega^2\left(\frac{a_2}{2}\sin\beta_2-\frac{a_2^3}{8}\sin\beta_2\cos^2\beta_2-\right.$$

$$\left.-\frac{a_2^3}{16}\sin^3\beta_2\right)=0 \quad , \tag{3.2.15a}$$

$$\eta^2\left(\gamma^2+\gamma[1-\frac{a_2^2}{4}]\right)a_1\cos\beta_1-\gamma^2\eta^2 a_2\cos\beta_2+$$

$$+\lambda_p\eta a_2\sin\beta_2+2\gamma\Omega^2\left(\frac{a_2}{2}\cos\beta_2-\frac{a_2^3}{8}\cos\beta_2\sin^2\beta_2-\right.$$

$$\left.-\frac{a_2^3}{16}\cos^3\beta_2\right)=0 \quad , \tag{3.2.15b}$$

Of these four equations, it turns out that equations (3.2.14a) and (3.2.14b) can be solved for a_1 and β_1 in terms of a_2 and β_2; that is, the equations uncouple. In terms of a_2 and β_2, a_1 and β_1 are given by:

$$a_1\sin\beta_1=\frac{1}{D}[I_1I_2a_2\sin\beta_2+\lambda_c\eta(K_1-I_2a_2\cos\beta_2)] \tag{3.2.16a}$$

and

$$a_1\cos\beta_1=\frac{-1}{D}[I_1(K_1-I_2a_2\cos\beta_2)-\lambda_c\eta I_2a_2\sin\beta_2] \tag{3.2.16b}$$

where

$$I_1=\eta^2[1+\mu+\gamma^2+2\gamma(1-\frac{a_2^2}{4})] \quad , \tag{3.2.17a}$$

$$I_2=\eta^2[\gamma^2+\gamma(1-\frac{a_2^2}{4})] \quad , \tag{3.2.17b}$$

and

$$D=I_1^2+(\lambda_c\eta)^2 \ . \tag{3.2.17c}$$

When the two expressions (3.2.16a,b) are substituted into the two equations (3.2.15a,b), the result is a pair of equations involving only a_2 and β_2:

$$\frac{I_2}{D}[I_1I_2a_2\sin\beta_2+\lambda_c\eta(K_1-I_2a_2\cos\beta_2)]-\gamma^2\eta^2a_2\sin\beta_2-\lambda_p\eta a_2\cos\beta_2$$

$$+2\gamma\Omega^2(\frac{a_2}{2}\sin\beta_2-\frac{a_2^3}{8}\sin\beta_2\cos^2\beta_2-\frac{a_2^3}{16}\sin^3\beta_2)=0 \tag{3.2.18a}$$

and,

$$-\frac{I_2}{D}[I_1(K_1-I_2a_2\cos\beta_2)+\lambda_c\eta I_2a_2\sin\beta_2]-\gamma^2\eta^2a_2\cos\beta_2+$$

$$+\lambda_p\eta a_2\sin\beta_2+2\gamma\Omega^2(\frac{a_2}{2}\cos\beta_2-\frac{a_2^3}{16}\cos^3\beta_2-\frac{a_2^3}{8}\sin^2\beta_2\cos\beta_2)=0 \tag{3.2.18b}$$

This uncoupling simplifies the equations considerably. Equations (3.2.18a) and (3.2.18b) can be solved for the pendulum amplitude and phase (a_2 and β_2) and the latter substituted into equations (3.2.16a) and (3.2.16b) to yield those of the carrier, namely, a_1 and β_1. This is carried out numerically.

The case of zero damping and zero constant torque, $\lambda_p=\lambda_c=K_0=0$, is useful for certain analyses and is presented here. For this case equations (3.2.16a,b) and (3.2.18a,b) reduce to:

$$a_1\sin\beta_1=\frac{I_2a_2\sin\beta_2}{I_1} \tag{3.2.19a}$$

$$a_1\cos\beta_1=\frac{-(K_1-I_2a_2\cos\beta_2)}{I_1} \tag{3.2.19b}$$

$$\frac{I_2}{I_1}I_2a_2\sin\beta_2-\gamma^2\eta^2a_2\sin\beta_2+$$

$$+2\gamma\Omega^2\left(\frac{a_2}{2}\sin\beta_2-\frac{a_2^3}{8}\sin\beta_2\cos^2\beta_2-\frac{a_2^3}{16}\sin^3\beta_2\right)=0 \tag{3.2.19c}$$

$$-\frac{I_2}{I_1}(K_1-I_2a_2\cos\beta_2)-\gamma^2\eta^2a_2\cos\beta_2+$$

$$+2\gamma\Omega^2\left(\frac{a_2}{2}\cos\beta_2-\frac{a_2^3}{16}\cos^3\beta_2-\frac{a_2^3}{8}\sin^2\beta_2\cos\beta_2\right)=0 \tag{3.2.19d}$$

3.3- Stability Analysis

In this section we consider the dynamic stability of the approximate solutions which are obtained. This analysis uses Floquet theory (see [32] or [34]). The idea is to determine the dynamics (actually only the growth or decay) of small perturbations to a periodic solution. This is accomplished by linearizing the full equations of motion about the periodic solution and studying the resulting linear, time varying differential equations.

We denote the periodic solution as $(\bar{\theta},\bar{\phi})$, and let $\tilde{\theta}$ and $\tilde{\phi}$ represent small perturbations of $\bar{\theta}$ and $\bar{\phi}$. Substitution of $\theta=\bar{\theta}+\tilde{\theta}$ and $\phi=\bar{\phi}+\tilde{\phi}$ into equations of motion (3.1.3a,b), and noting that $\sin\tilde{\phi}$ and $\cos\tilde{\phi}$ can be approximated by $\tilde{\phi}$ and 1, respectively, one obtains

$$[1+\mu+\gamma^2+2\cos\bar{\phi}-\tilde{\phi}\sin\bar{\phi}](\ddot{\bar{\theta}}+\ddot{\tilde{\theta}})-\gamma[\cos\bar{\phi}-\tilde{\phi}\sin\bar{\phi}+\gamma](\ddot{\bar{\phi}}+\ddot{\tilde{\phi}})+$$

$$+\gamma(\dot{\bar{\phi}}+\dot{\tilde{\phi}})^2(\sin\bar{\phi}+\tilde{\phi}\cos\bar{\phi})--2\gamma\Omega(\dot{\bar{\phi}}+\dot{\tilde{\phi}})(\sin\bar{\phi}+\tilde{\phi}\cos\bar{\phi})-$$

$$-2\gamma(\dot{\bar{\theta}}+\dot{\tilde{\theta}})(\dot{\bar{\phi}}+\dot{\tilde{\phi}})(\sin\bar{\phi}+\tilde{\phi}\cos\bar{\phi})+\lambda_c(\dot{\bar{\theta}}+\dot{\tilde{\theta}})=K_1\cos\eta t \quad , \tag{3.3.1a}$$

$$-\gamma[\cos\bar{\phi}-\tilde{\phi}\sin\bar{\phi}+\gamma](\ddot{\bar{\theta}}+\ddot{\tilde{\theta}})+\gamma^2(\ddot{\bar{\phi}}+\ddot{\tilde{\phi}})+\lambda_p(\dot{\bar{\phi}}+\dot{\tilde{\phi}})+$$

$$+\gamma\Omega^2(\sin\bar{\phi}+\tilde{\phi}\cos\bar{\phi})+\gamma(\dot{\bar{\theta}}+\dot{\tilde{\theta}})^2(\sin\bar{\phi}+\tilde{\phi}\cos\bar{\phi})+$$

$$+2\gamma\Omega(\dot{\bar{\theta}}+\dot{\tilde{\theta}})(\sin\bar{\phi}+\tilde{\phi}\cos\bar{\phi})=0 \quad . \tag{3.3.1b}$$

Note that, by definition, $\bar{\theta}$ and $\bar{\phi}$ satisfy the equations of motion (3.1.5), and also keeping only terms linear in the tilde variables in equations (3.3.1), we obtain:

$$-2\gamma\tilde{\phi}\sin\overline{\phi\ddot{\theta}}+[1+\mu+\gamma^2+2\gamma\cos\bar{\phi}]\ddot{\tilde{\theta}}+\gamma\tilde{\phi}\sin\overline{\phi\ddot{\phi}}-$$

$$-\gamma(\gamma+\cos\bar{\phi})\ddot{\tilde{\phi}}+2\gamma\dot{\bar{\phi}}\dot{\tilde{\phi}}\sin\bar{\phi}-2\gamma\Omega\dot{\tilde{\phi}}\sin\bar{\phi}-$$

$$-2\gamma\Omega\dot{\bar{\phi}}\tilde{\phi}\cos\bar{\phi}-2\gamma(\dot{\bar{\theta}}\dot{\tilde{\phi}}+\dot{\bar{\phi}}\dot{\tilde{\theta}})\sin\bar{\phi}+\lambda_c\dot{\tilde{\theta}}=K_1\cos\eta t \quad , \tag{3.3.2a}$$

$$\gamma\tilde{\phi}\sin\overline{\dot{\phi}\dot{\theta}}-\gamma[\gamma+\cos\bar{\phi}]\ddot{\tilde{\theta}}+\gamma^2\ddot{\tilde{\phi}}+\lambda_p\dot{\tilde{\phi}}+$$

$$+\gamma\Omega^2\tilde{\phi}\cos\bar{\phi}+2\gamma\dot{\bar{\theta}}\dot{\tilde{\theta}}\sin\bar{\phi}+2\gamma\Omega\dot{\bar{\theta}}\tilde{\phi}\cos\bar{\phi}+$$

$$+2\gamma\Omega\dot{\bar{\theta}}\sin\bar{\phi}=0 \quad . \tag{3.3.2b}$$

Solving equations (3.3.2) for $\ddot{\tilde{\theta}}$ and $\ddot{\tilde{\phi}}$ yields

$$\ddot{\tilde{\theta}}=\frac{1}{D}[\gamma^2L_\theta+\gamma(\gamma+C)L_\phi] \tag{3.3.3a}$$

$$\ddot{\tilde{\phi}}=\frac{1}{D}[L_\phi(1+\mu+\gamma^2+2\gamma c)+\gamma(\gamma+c)L_\theta] \tag{3.3.3b}$$

where

$$L_\theta=+2\gamma\tilde{\phi}\sin\overline{\dot{\phi}\dot{\theta}}-\gamma\tilde{\phi}\sin\overline{\dot{\phi}\dot{\phi}}-2\gamma\dot{\bar{\phi}}\dot{\tilde{\phi}}\sin\bar{\phi}+2\gamma\Omega\dot{\tilde{\phi}}\sin\bar{\phi}+$$

$$+2\gamma\Omega\dot{\bar{\phi}}\tilde{\phi}\cos\bar{\phi}+2\gamma(\dot{\bar{\theta}}\dot{\tilde{\phi}}+\dot{\bar{\phi}}\dot{\tilde{\theta}})\sin\bar{\phi}-\lambda_c\dot{\tilde{\theta}} \quad , \tag{3.3.4a}$$

$$L_\phi=-\gamma\tilde{\phi}\sin\overline{\dot{\phi}\dot{\theta}}-\lambda_p\dot{\tilde{\phi}}-\gamma\Omega^2\tilde{\phi}\cos\bar{\phi}-2\gamma\dot{\bar{\theta}}\dot{\tilde{\theta}}\sin\bar{\phi}-$$

$$-2\gamma\Omega\dot{\bar{\theta}}\tilde{\phi}\cos\bar{\phi}-2\gamma\Omega\dot{\tilde{\theta}}\sin\bar{\phi} \quad . \tag{3.3.4b}$$

and

$$\bar{D}=\gamma^2(1+\mu-\cos^2\bar{\phi}) \tag{3.3.4c}$$

Equations (3.3.3a) and (3.3.3b) can be put into first order form to obtain four first order linear differential equations for $\tilde{\theta}$, $\dot{\tilde{\theta}}$, $\tilde{\phi}$, and $\dot{\tilde{\phi}}$ with time-periodic coefficients. These equations are then numerically integrated through one period of the forcing with initial conditions equal to successive columns of the 4$\times$4 identity matrix. The four resulting vectors can be assembled to form the 4×4 monodromy matrix. According to the Floquet theory, a periodic solution $(\overline{\theta},\overline{\phi})$ is stable if all the eigenvalues of its monodromy matrix, *i.e.*, the Floquet multipliers, have moduli less than unity; otherwise it is unstable. Bifurcations occur as eigenvalues pass through the unit circle in the complex plane, and we shall predict post-stability behavior wherever possible using concepts from bifurcation theory. We shall use as $\overline{\theta}$ and $\overline{\phi}$ our approximate solutions obtained using harmonic balance.

It must be re-emphasized that the variable θ appears nowhere in the governing equations. The system under consideration has actually only *one—and—a—half* degrees of freedom and can be represented by three first order differential equations. The effect of this on the stability analysis is that one of the four eigenvalues will always be identically one, due to the inherently neutral nature of θ. Thus, all stability considerations are based on the remaining three eigenvalues. Another way to see this is to note that we only need to consider the differential equations for $\dot{\tilde{\theta}}$, $\tilde{\phi}$, and $\dot{\tilde{\phi}}$, and after solving them $\tilde{\theta}$ can be obtained by direct integration, *i.e.*, the $\tilde{\theta}$ dynamics are uncoupled.

In regards to symmetries, it must be noted that the linearized equations (3.3.3a,b) are symmetric in the following sense:

$$(\tilde{\phi},\tilde{\theta},t)\rightarrow(-\tilde{\phi},-\tilde{\theta},t+\frac{\pi}{\eta})$$

leaves the equations unchanged only if the periodic solutions $(\overline{\phi},\overline{\theta})$ have the following symmetry:

$$(\overline{\phi},\overline{\theta},t)\rightarrow(-\overline{\phi},-\overline{\theta},t+\frac{\pi}{\eta}) \quad .$$

The original equations of motion do not admit such solutions, but it is important to note that our approximate solutions have such a symmetry. This will be a crucial point used in interpreting the stability results.

3.4- Frequency Response

Figures (19a) and (19b) show typical frequency response curves for the pendulum and the carrier, respectively, and Figure (19c) depicts the corresponding phase difference of the carrier and the absorber. The solid lines indicate stable periodic motions and the dashed lines indicate unstable ones. Superimposed on these plots are the results from simulations of the full nonlinear equations of motion (3.1.3a) and (3.1.3b), shown as circles.

As can be observed, the results of the harmonic balance agree well with the simulation results and only when the absorber amplitude response (Figure 19a) becomes quite large does one see a difference in the analytical and simulation results. In particular, the results of the analysis start to diverge from those of the simulation of the equations of motion when the absorber sweeps through about 90 degrees in each direction during the steady-state operation, well beyond the range of practical applications. This is primarily due to the fact that in the harmonic balance analysis, the solution was assumed to consist of only its first harmonic while the actual response contains many harmonics, and as the amplitude of the oscillation grows, the effect of these harmonics becomes more pronounced. Also, the effects of terms ignored in the series expansions of the Bessel functions may become non-negligible. As a test of the validity of our approximate solutions, the Fourier spectrum of the response of the carrier obtained through the simulation of the full nonlinear equations of motion was analyzed over a range of frequencies. It was found that at low amplitude, oscillation energy is primarily stored in the first harmonic, while as the amplitude grows, the higher harmonics (in fact up to the fourth) acquire

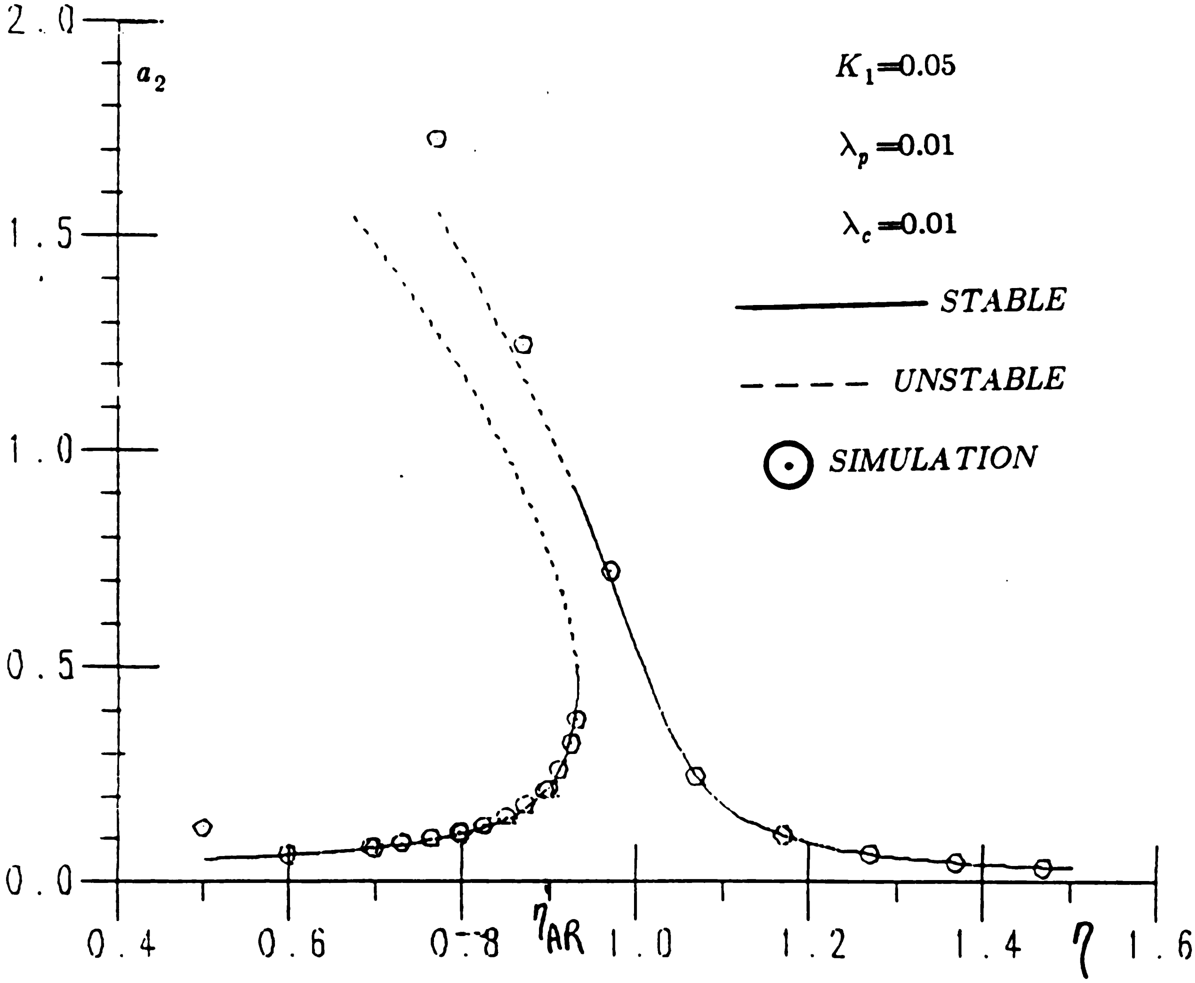

Figure 19a - Frequency Response of the Absorber - Analysis and Simulation

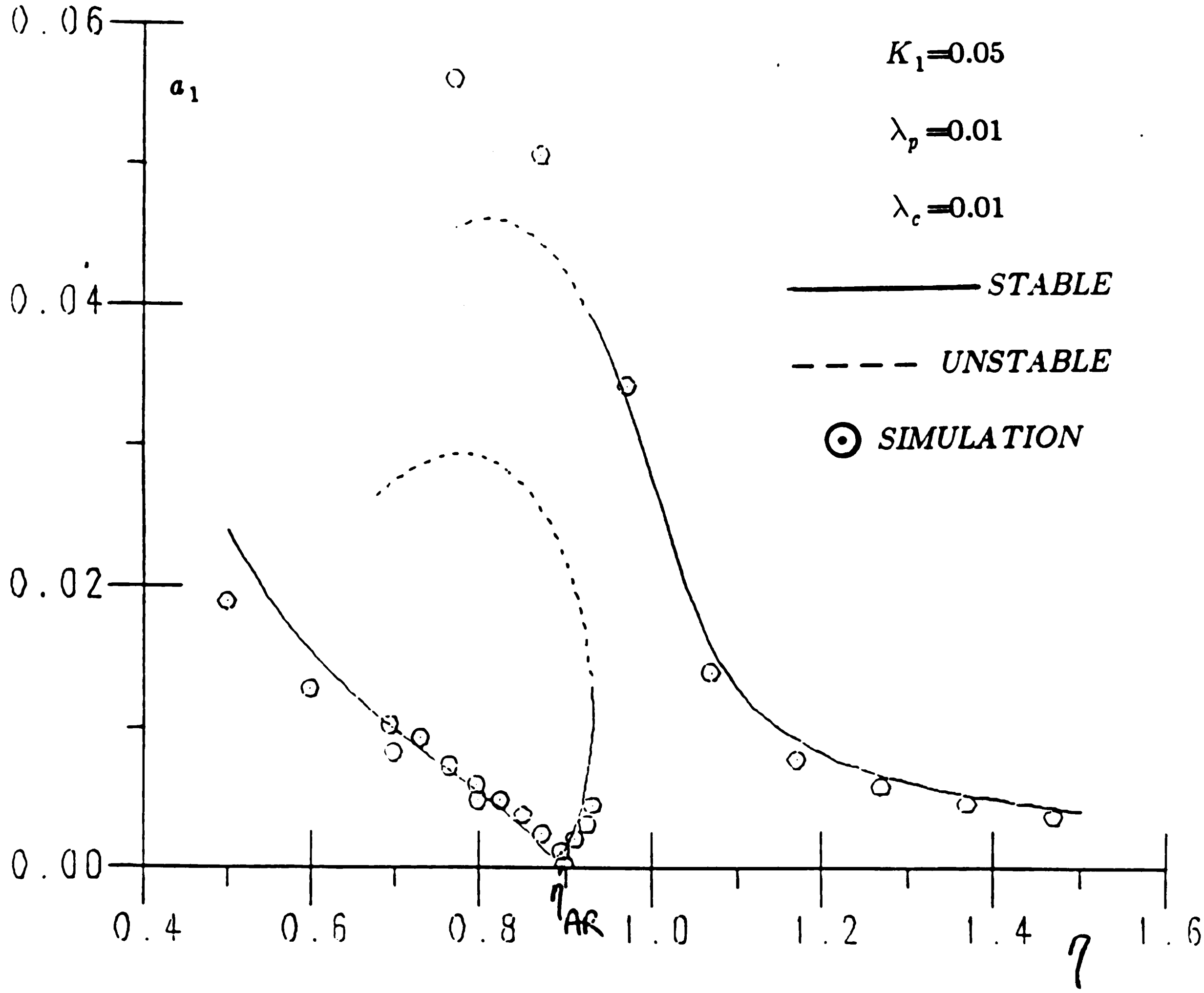

Figure 19b - Frequency Response of the Carrier - Analysis and Simulation

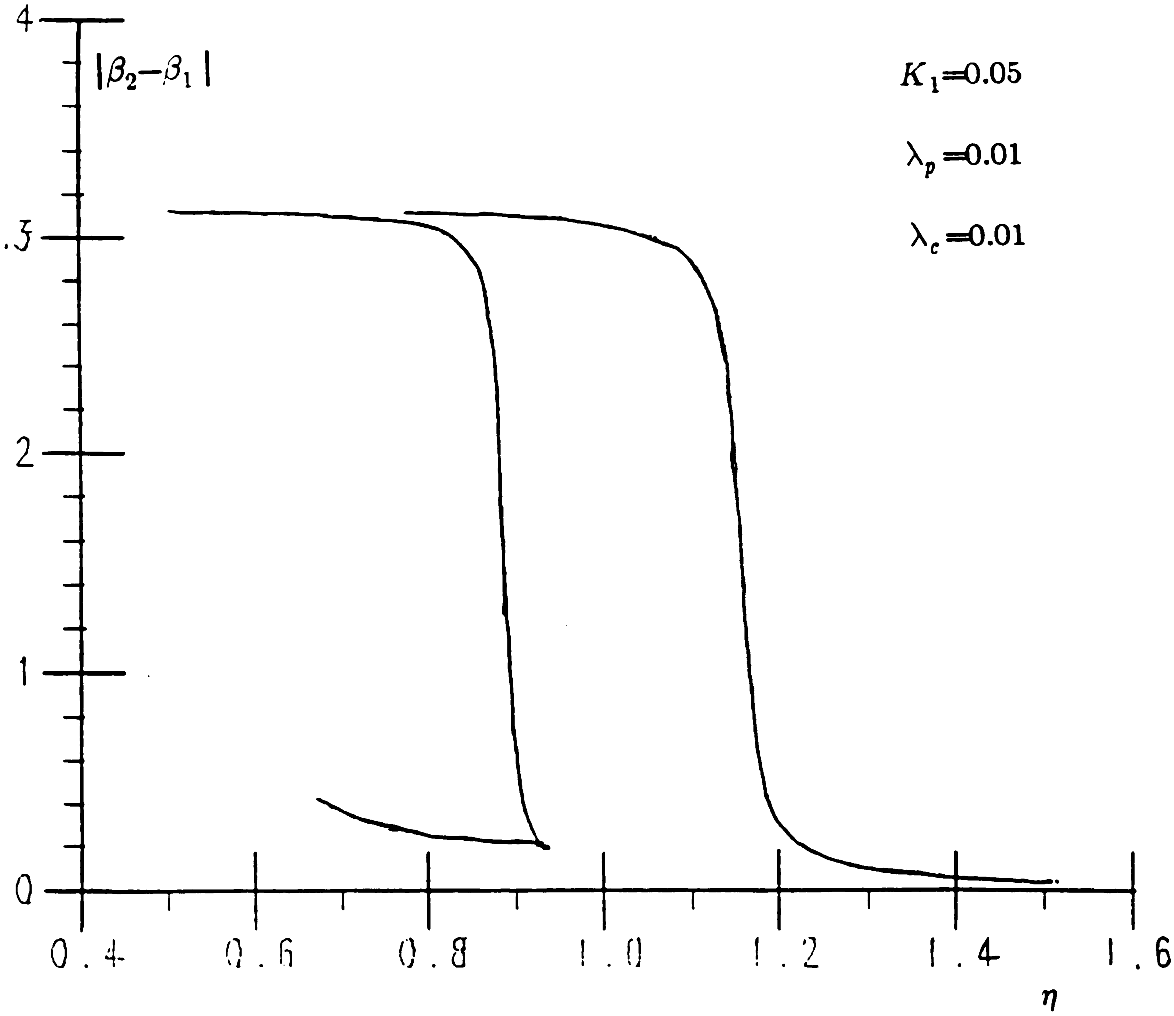

Figure 19c - Phase Difference of the Carrier and the Absorber enough energy to significantly affect the motion of the carrier.

The numerical value of the anti-resonance frequency for the example system used in this analysis is determined from the linearized system to be $\eta_{AR}=0.89$, which is close to the resonance frequency of the system, $\eta=1.0$. As is shown in section 3.5, the nonlinear anti-resonance frequency for the damped, nonlinear system will differ from η_{AR}. Figures (20a) and (20b) illustrate the frequency response of the absorber and the carrier, respectively, for several values of the excitation amplitude, K_1.

The frequency at which the *slope* of the response curves of the pendulum and the carrier are vertical is referred to as the turning frequency, η_t. From Figure (19a) one can observe that the turning frequency should not be too close to the anti-resonance frequency for a feasible design. Obviously, if the frequency of the excitation is slightly increased above η_{AR} the resulting response of the system will be drastically different than expected and the absorber will not function properly.

The initial conditions play a major role in the response of the CPVA in certain cases. For instance, in Figure (19) one can see that there exists more than one steady-state periodic solution for the system at the anti-resonance frequency, η_{AR}. In other words, depending on the initial conditions, the system either responds as predicted by the linear analysis (the lower branch on Figure 19) or oscillates with much larger amplitude (the upper branch in Figure 19). The middle branch in Figure (19) represents unstable, and unobservable, periodic solutions of the CPVA.

The numerical value of the turning frequency can be obtained as described by Stoker [34] and outlined here. As mentioned earlier, at η_t the slope of the frequency response of the pendulum is vertical, $i.e., \dfrac{\partial \eta}{\partial a_2}=0 \ at \ \eta=\eta_t$. This property can be exploited to find η_t by

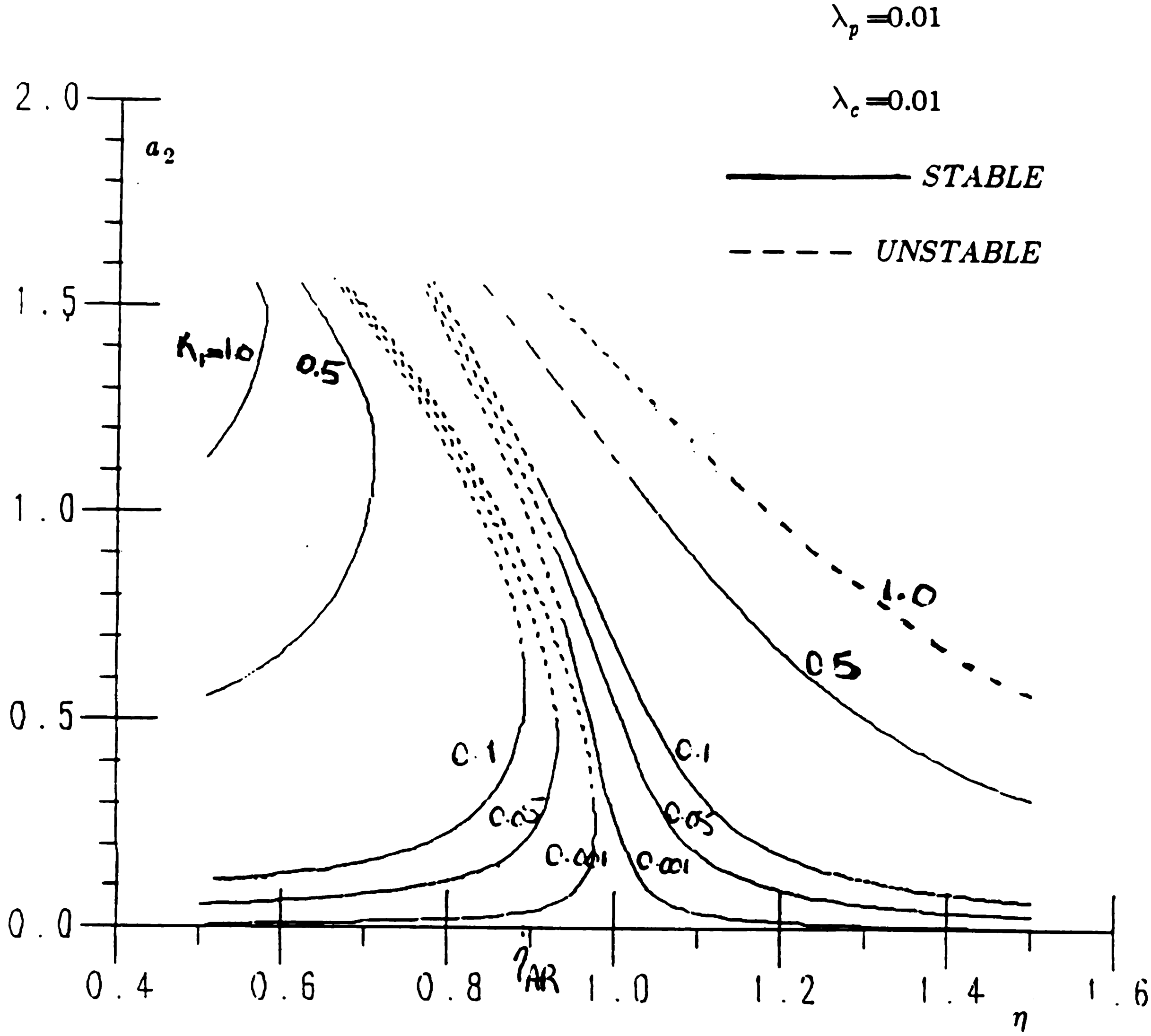

Figure 20a -Variation of the Frequency Response of the Absorber With Respect to the Excitation Amplitude

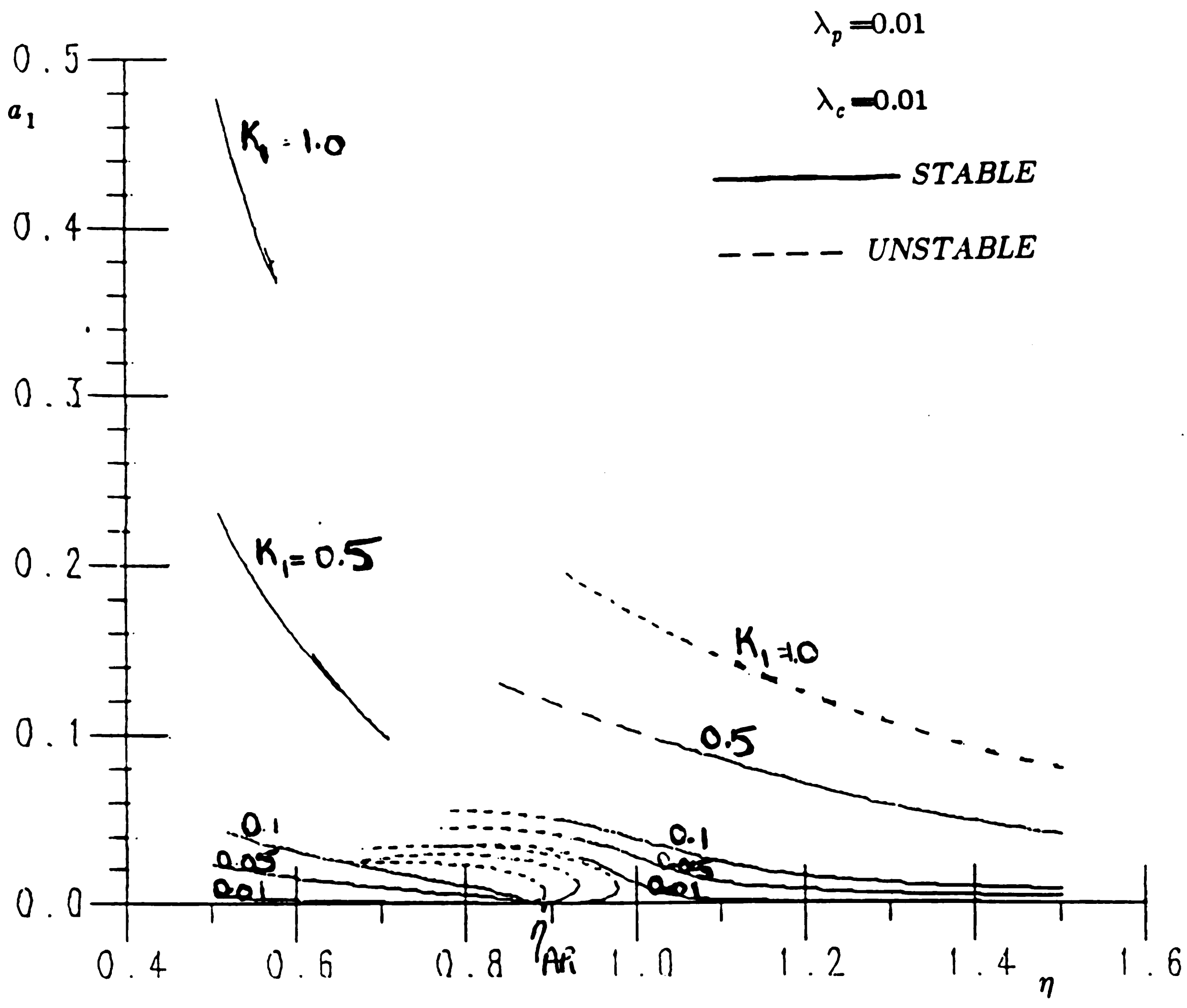

Figure 20b -Variation of the Frequency Response of the Carrier With Respect to the Excitation Amplitude

differentiating equations (3.2.18a) and (3.2.18b) with respect to a_2. Two equations result in terms of η_t, a_2, β_2, and $\dfrac{\partial\beta_2}{\partial a_2}$ as follows:

$$\frac{1}{D^2}\Big([I_1' I_2^2 a_2\sin\beta_2+2I_1I_2I_2' a_2\sin\beta_2+I_1I_2^2\sin\beta_2+I_1I_2^2a_2\beta_2'\cos\beta_2+$$
$$+\lambda_c\eta I_2'(K_1-I_2a_2\cos\beta_2)+\lambda_c\eta I_2(-I_2' a_2\cos\beta_2-I_2\cos\beta_2+$$
$$+I_2a_2\beta_2'\sin\beta_2)]D-D'[I_1I_2^2a_2\sin\beta_2+I_2\lambda_c\eta(K_1-I_2a_2\cos\beta_2)]\Big)-$$
$$-\gamma^2\eta^2\sin\beta_2-\gamma^2\eta^2a_2\beta_2'\cos\beta_2-\lambda_p\eta\cos\beta_2+\lambda_p\eta a_2\beta_2'\sin\beta_2+$$
$$+2\gamma\Omega^2[\frac{1}{2}\sin\beta_2+\frac{a_2}{2}\beta_2'\cos\beta_2-\frac{3a_2^2}{8}\sin\beta_2\cos^2\beta_2-$$
$$-\frac{a_2^3}{8}\beta_2'\cos^3\beta_2+\frac{a_2^3}{4}\beta_2'\sin^2\beta_2\cos\beta_2-\frac{3a_2^2}{16}\sin^3\beta_2-$$
$$-\frac{3a_2^3}{16}\beta_2'\sin^2\beta_2\cos\beta_2]=0 \quad , \tag{3.4.1a}$$

and

$$\frac{-1}{D^2}\Big(D[I_1' I_2(K_1-I_2a_2\cos\beta_2)+I_1I_2'(K_1-I_2a_2\cos\beta_2)+$$
$$+I_1I_2(-I_2' a_2\cos\beta_2-I_2\cos\beta_2+I_2a_2\beta_2'\sin\beta_2)+$$
$$+2\lambda_c\eta I_2I_2' a_2\sin\beta_2+\lambda_c\eta I_2^2\sin\beta_2+\lambda_c\eta I_2^2a_2\beta_2'\cos\beta_2]-$$
$$-D'[I_1I_2(K_1-I_2a_2\cos\beta_2)+\lambda_c\eta I_2^2a_2\sin\beta_2]\Big)-$$
$$-\gamma^2\eta^2\cos\beta_2+\gamma^2\eta^2a_2\beta_2'\sin\beta_2+\lambda_p\eta\sin\beta_2+\lambda_p\eta a_2\beta_2'\cos\beta_2+$$
$$+2\gamma\Omega^2[\frac{1}{2}\cos\beta_2-\frac{a_2}{2}\beta_2'\sin\beta_2-\frac{3a_2^2}{16}\cos^3\beta_2+\frac{3a_2^3}{16}\beta_2'\sin\beta_2\cos^2\beta_2-$$
$$-\frac{3a_2^2}{8}\sin^2\beta_2\cos\beta_2-\frac{a_2^3}{4}\beta_2'\sin\beta_2\cos^2\beta_2+\frac{a_2^3}{8}\beta_2'\sin^3\beta_2]=0 \quad . \tag{3.4.1b}$$

where

$$I_1' = -\gamma\eta^2 a_2 \quad ,$$

$$I_2' = \frac{I_1'}{2}$$

and

$$D' = 2I_1 I_1' \quad .$$

Equations (3.4.1a,b) along with equations (3.2.18a) and (3.2.18b) form a system of four nonlinear equations in terms of four unknowns, namely, $(a_2, \beta_2, \frac{\partial \beta_2}{\partial a_2}, \eta_t)$. Here, a_2 and β_2 are the absorber's amplitude and phase, respectively, at η_t and $\frac{\partial \beta_2}{\partial a_2}$ is the rate of change of the relative phase of the absorber with respect to the absorber amplitude. Given a set of system parameters such as damping ratios and excitation amplitudes, these equations can be solved numerically to yield the corresponding turning frequency, η_t.

Figure (21) shows a plot of the turning frequency versus the amplitude of the oscillating component of the excitation, K_1 (the $\hat{\eta}$ curve in Figure (21) is explained in section 3.5). It was found through numerous simulations and analysis that the damping ratios of the carrier and the pendulum have little effect on the turning frequency compared to the effect of varying K_1. Hence Figure (21) depicts the result for zero damping with the fact in mind that similar curves for other sets of damping values (within practical range) all lie in a small neighborhood of the curve shown in Figure (21). As described in the next section, the turning frequency η_t can cross over the anti-resonance frequency, $\hat{\eta}$, resulting in a drastic change in response.

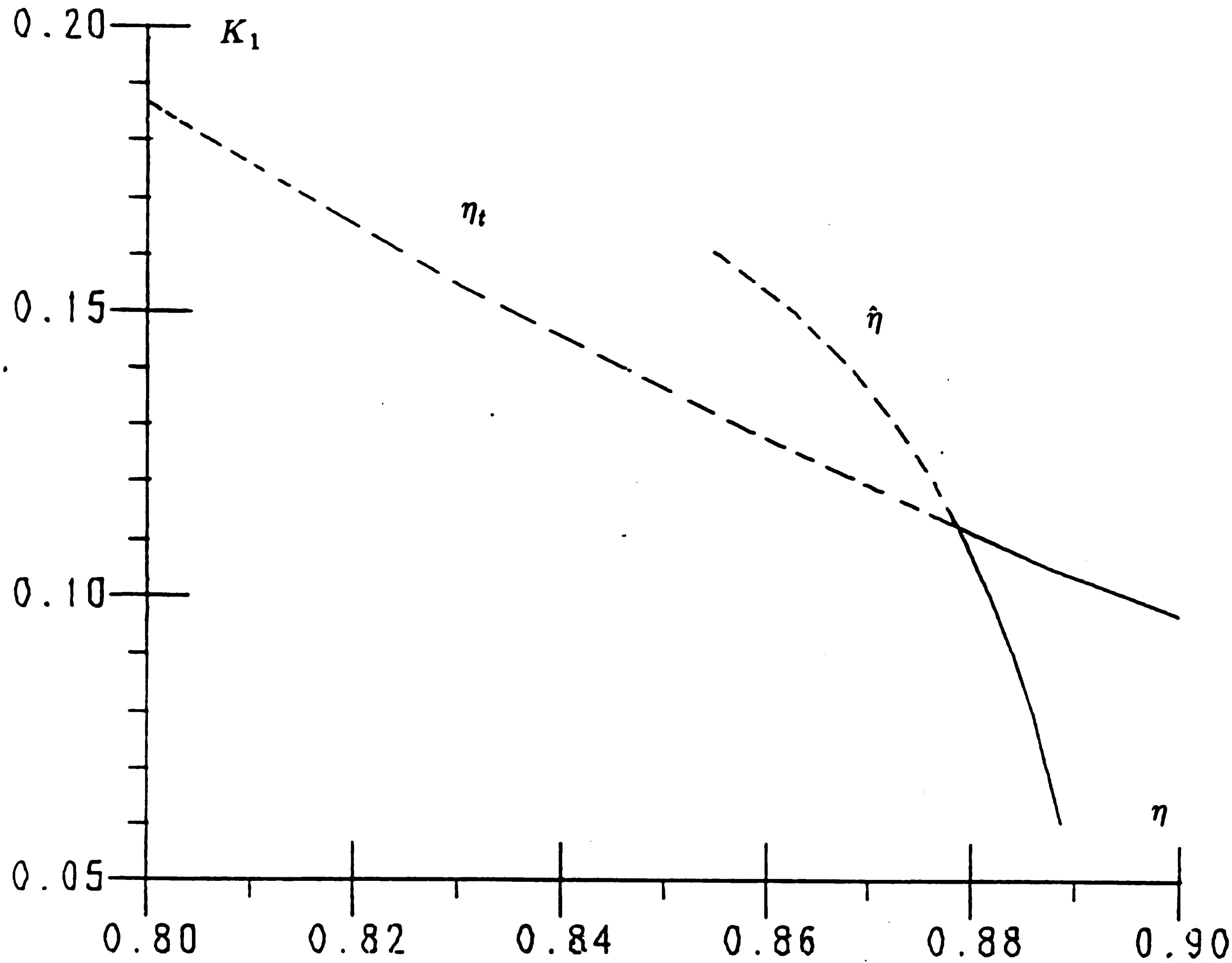

Figure 21 - Turning Frequency and the Anti-resonance Frequency

There are two dynamic instabilities observed in Figure (19). There exists one at the turning frequency; this is a straightforward, simple saddle-node bifurcation (Guckenheimer and Holmes [26]). The more interesting one occurs on the upper branch of the response curve. It corresponds to an eigenvalue passing through +1 in an increasing manner as η is decreased. Such a transition corresponds in the generic case to a simple saddle-node bifurcation, but this does not occur here. The instability results in a symmetric saddle-node, or pitchfork, bifurcation which results in a pair of anti-symmetric motions [26]. This bifurcation is predicted from our analysis, which yields *symmetric* approximate solutions, which cannot occur in the actual, nonsymmetric system. By considering a small, unsymmetric variation in the predicted instability, we predict that near this point a large deviation from symmetry will occur. That is, solutions will be nearly symmetric up to the instability, and above the instability the asymmetry of the solutions will be amplified quite sharply (see section 7.1 of Guckenheimer and Holmes [26] for a more thorough explanation). Figures (22a,b) show the variation of the mean values of $\dot{\theta}$ and ϕ, that is, deviations from $\Omega = \frac{K_0}{\lambda_c}$ and $\alpha = 0$, as computed from direct simulations of the steady-state solutions of equations (3.1.5) while following the upper branch of the response curve. The sharp rise in the mean value of $\dot{\theta}$ near the instability indicates that our approximation for Ω is breaking down. In Figures (23a,b) we show a series of periodic motions as limit cycles in the three dimensional phase space $(\phi, \dot{\phi}, \dot{\theta})$ for η varying near the point of loss in symmetry; it clearly shows the breakdown in symmetry as η is decreased near the instability.

Another point of interest is that there should exist another branch of solutions arising via a saddle-node bifurcation near the predicted pitchfork bifurcation point. We were unable to find any evidence of these motions,

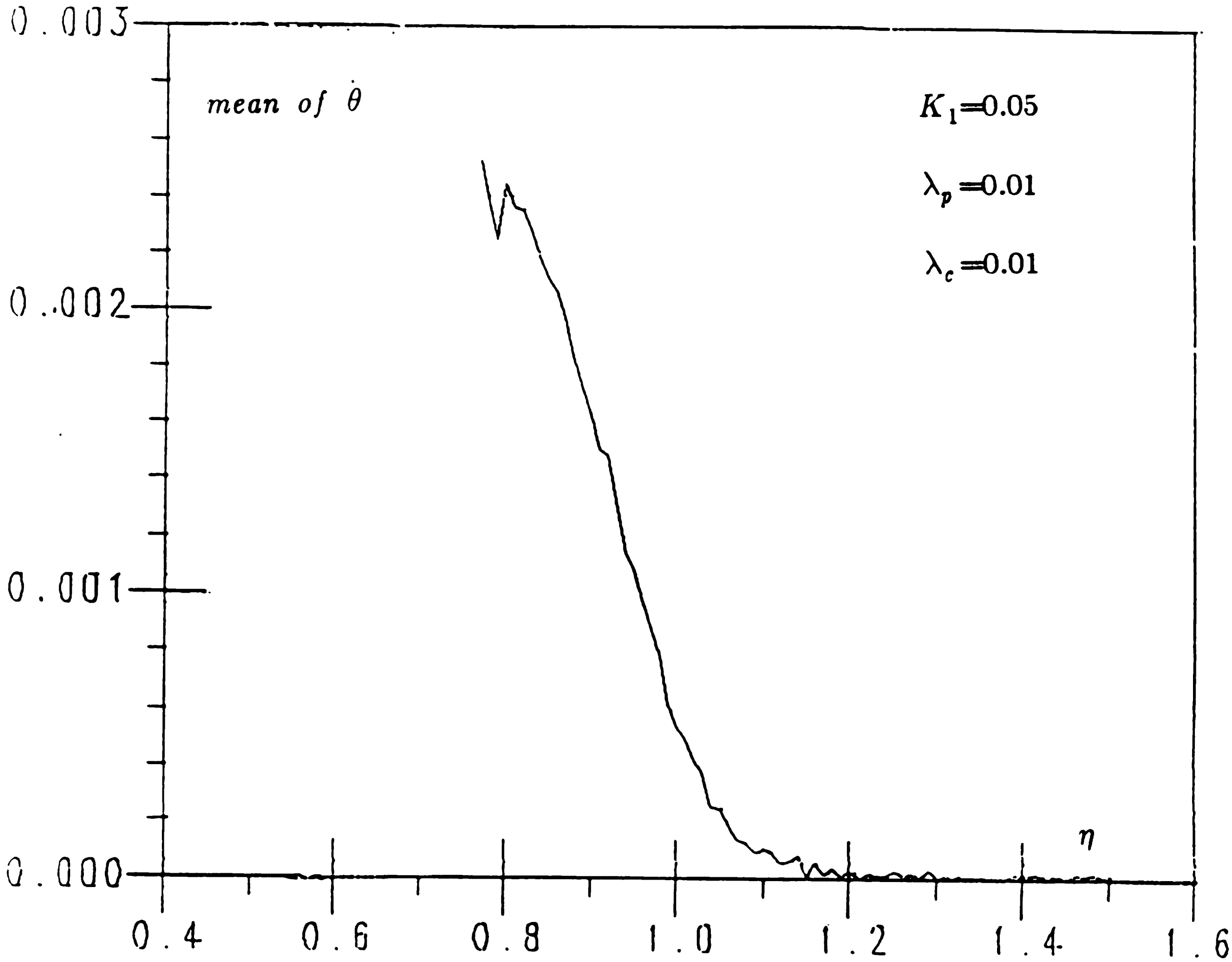

Figure 22a - Variation of the Mean Value of the Carrier Velocity

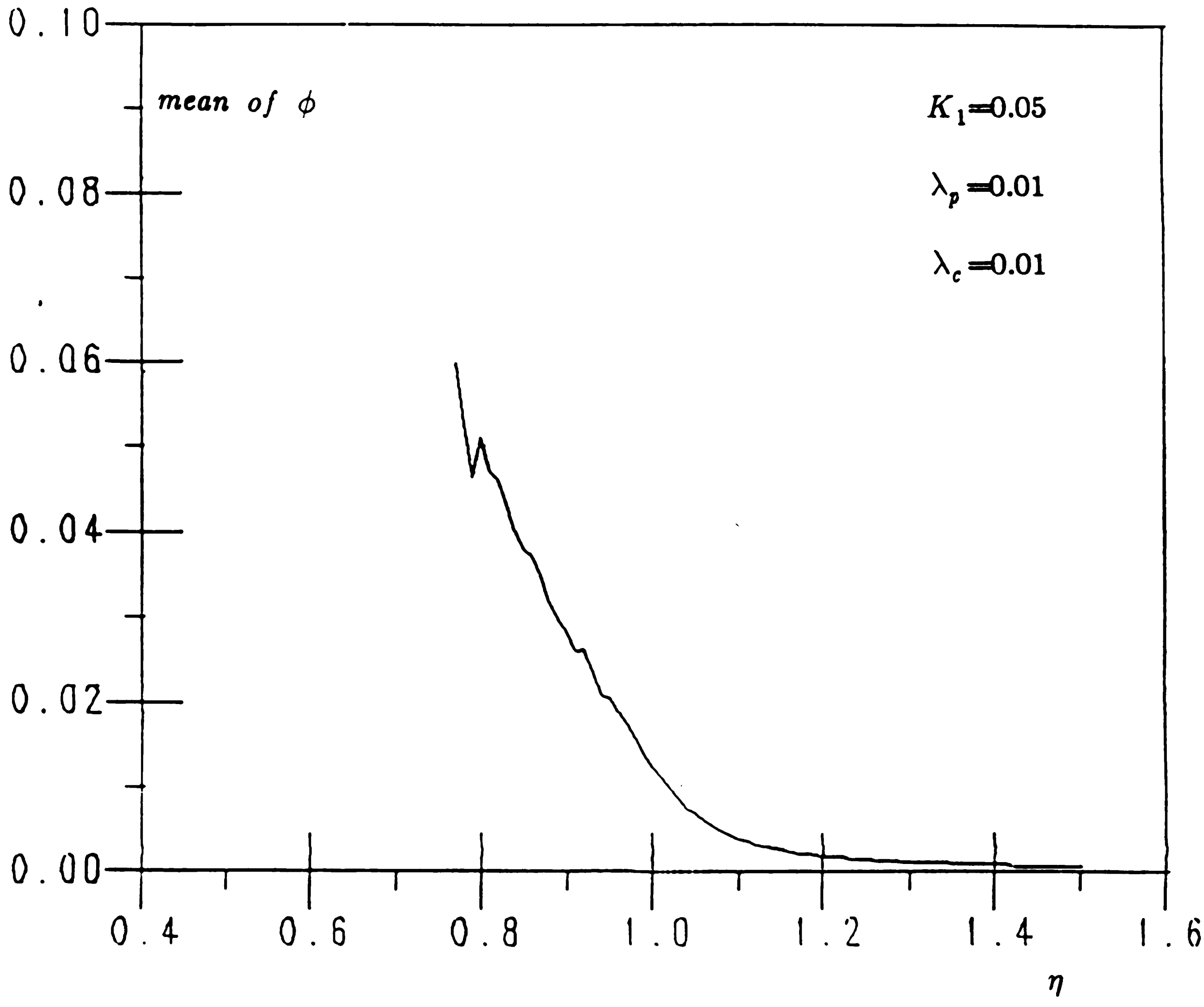

Figure 22b - Variation of the Mean Value of the Absorber Angular Displacement

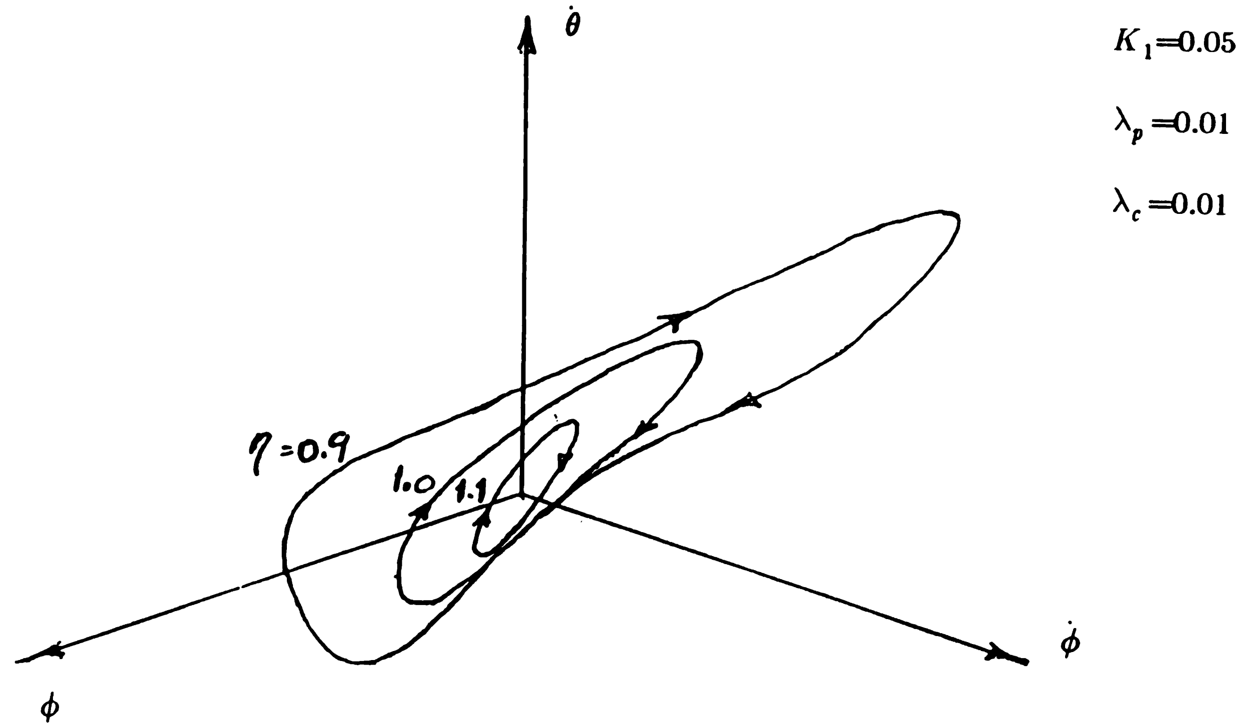

Figure 23a - Phase Trajectory of the CPVA in Three-Dimensional Space

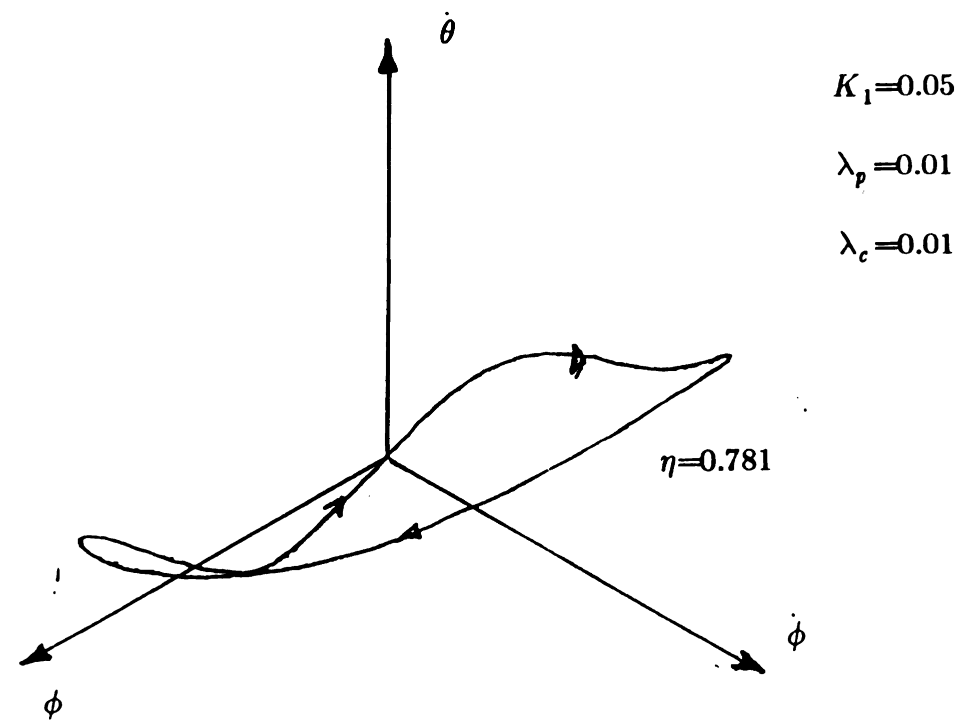

Figure 23b - Phase Trajectory of the CPVA in Three-Dimensional Space although they may well, and should, exist. Figure (24) depicts the effects of small symmetry deviations on a pitchfork bifurcation.

Finally, we remind the reader that the rescaling of time and other system parameters that led to the equations of motion (3.1.5) results in a scaling down of the damping values. In Figure (25) we show a set of response curves corresponding to $\lambda_c=\lambda_p=0.1$ and $K_1=0.1$. Note that for these apparently moderate damping values the response has no usual resonance peak or anti-resonance point. Such response curves were found to occur for λ_p greater than about .01 over a wide range of K_1 and λ_c values. A reason for this is provided in the following section.

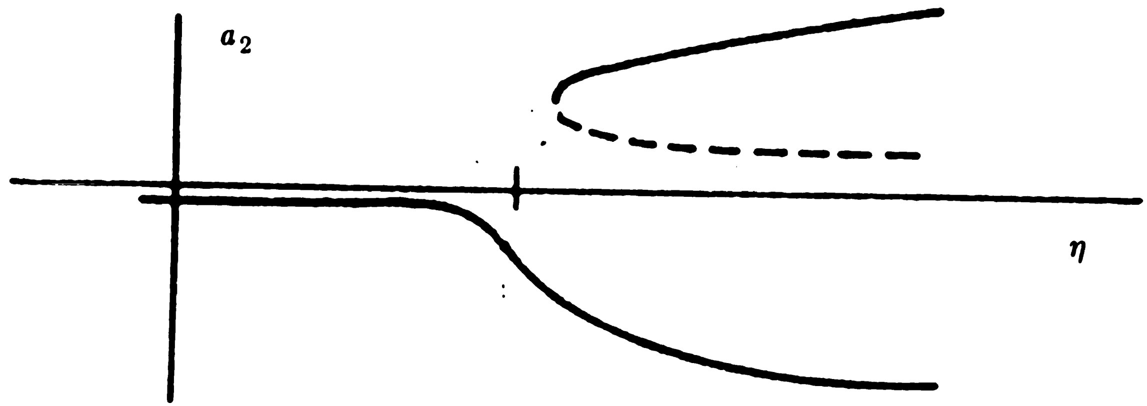

Figure 24 - Effects of Small Symmetry Deviations on a Pitchfork Bifurcation

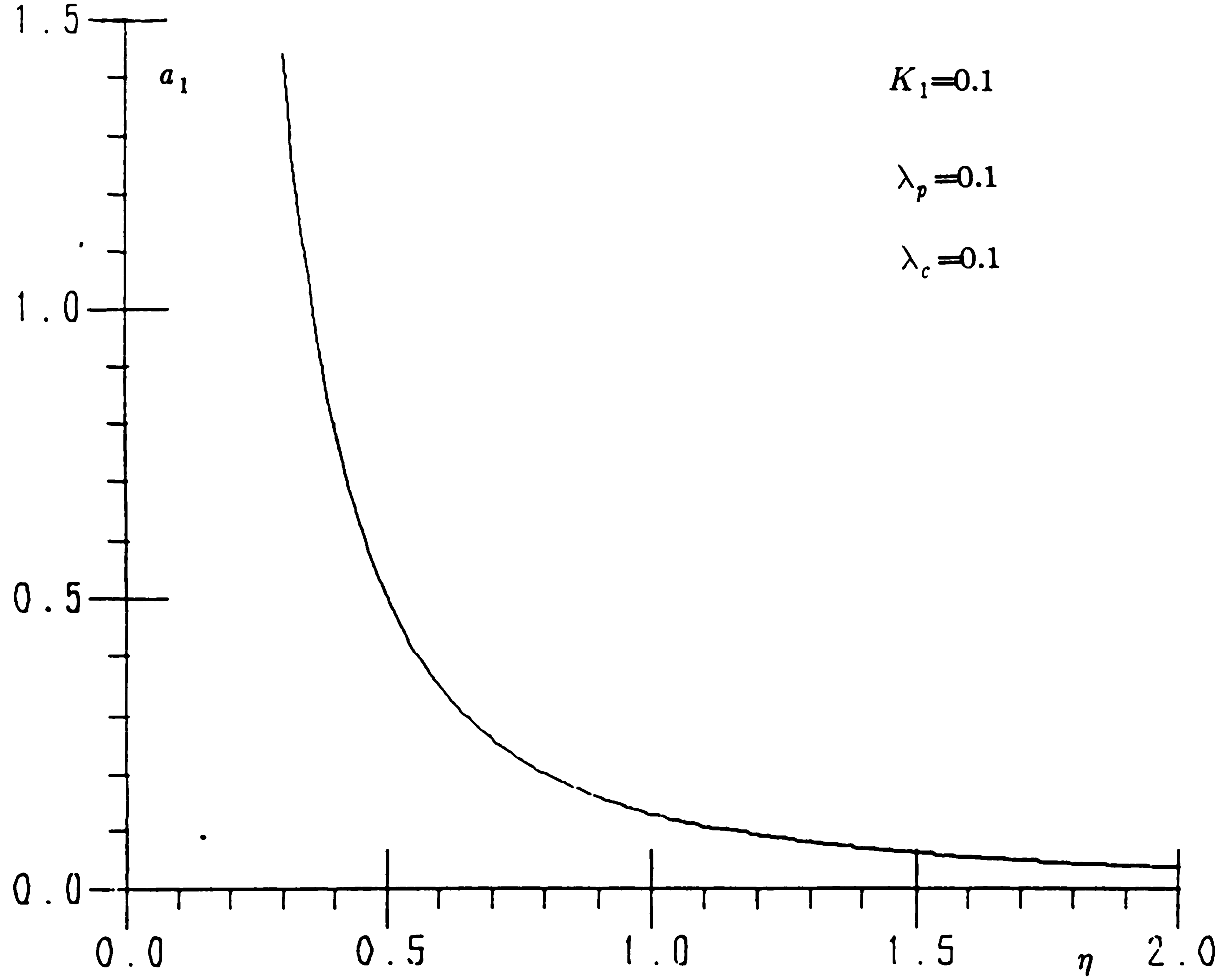

Figure 25a - Frequency Response of .the Carrier

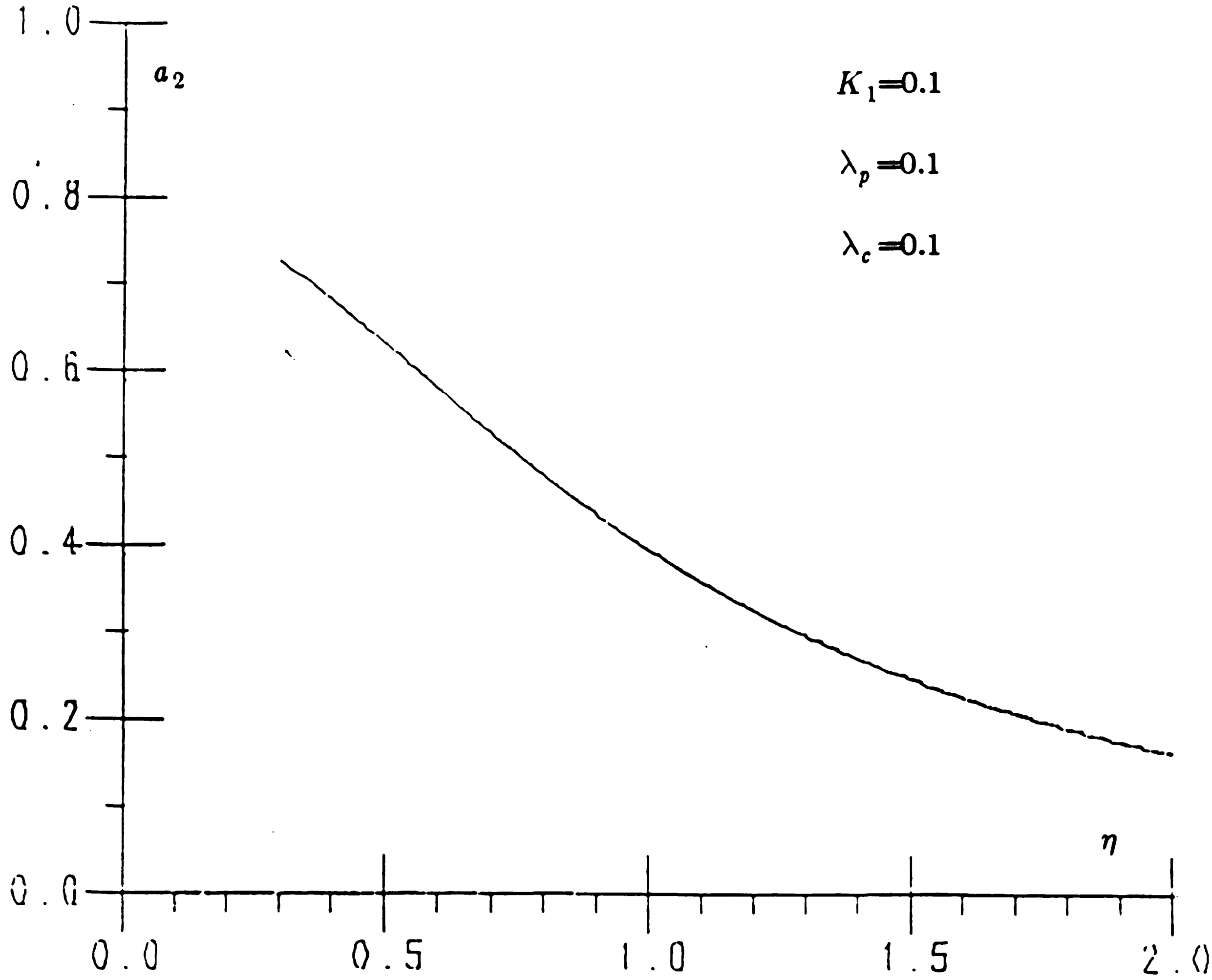

Figure 25b - Frequency Response of the Absorber

3.5- The Response at the Anti-resonance Frequency

A study was done on the behavior of the carrier near the predicted anti-resonance frequency for a range of damping and excitation amplitude values. The variations of the carrier amplitude at η_{AR} as a function of K_1, λ_p and, λ_c are shown in Figures (26a), (26b) and, (26c), respectively. From these Figures one can observe that the carrier amplitude at the anti-resonance frequency, η_{AR}, varies almost linearly as a function of the excitation amplitude, K_1. It depends strongly on the pendulum damping λ_p for $0 \leq \lambda_p < 0.02$ and is relatively insensitive for $\lambda_p > 0.02$. The carrier amplitude at η_{AR} remains essentially constant as λ_c is varied. The sensitivity of the response to changes in λ_p as shown in Figures (25) and (26b) indicate that the pendulum damping should be kept as low as possible.

As shown immediately below, the actual desired operating point may vary away from η_{AR} due to nonlinear and/or damping effects. This is crucial from a design standpoint. Thus, the sensitivity of the value of the anti-resonance frequency itself to the variation of the system parameters was also investigated.

A first order approximation of nonlinear effects on the anti-resonance frequency can be obtained by assuming that the carrier and the pendulum dampings are small enough so as to be neglected. The absence of damping implies that the carrier amplitude can be identically zero at a single value of η, the true anti-resonance frequency, denoted by $\hat{\eta}$. This value is exactly at η_{AR} only for the linear, undamped system.

The condition for anti-resonance in the undamped system is $a_1=0$, *i.e.*, the carrier has no oscillatory response. Imposing $a_1=0$ on the undamped response conditions (3.2.19) yields the following conclusions. From equation

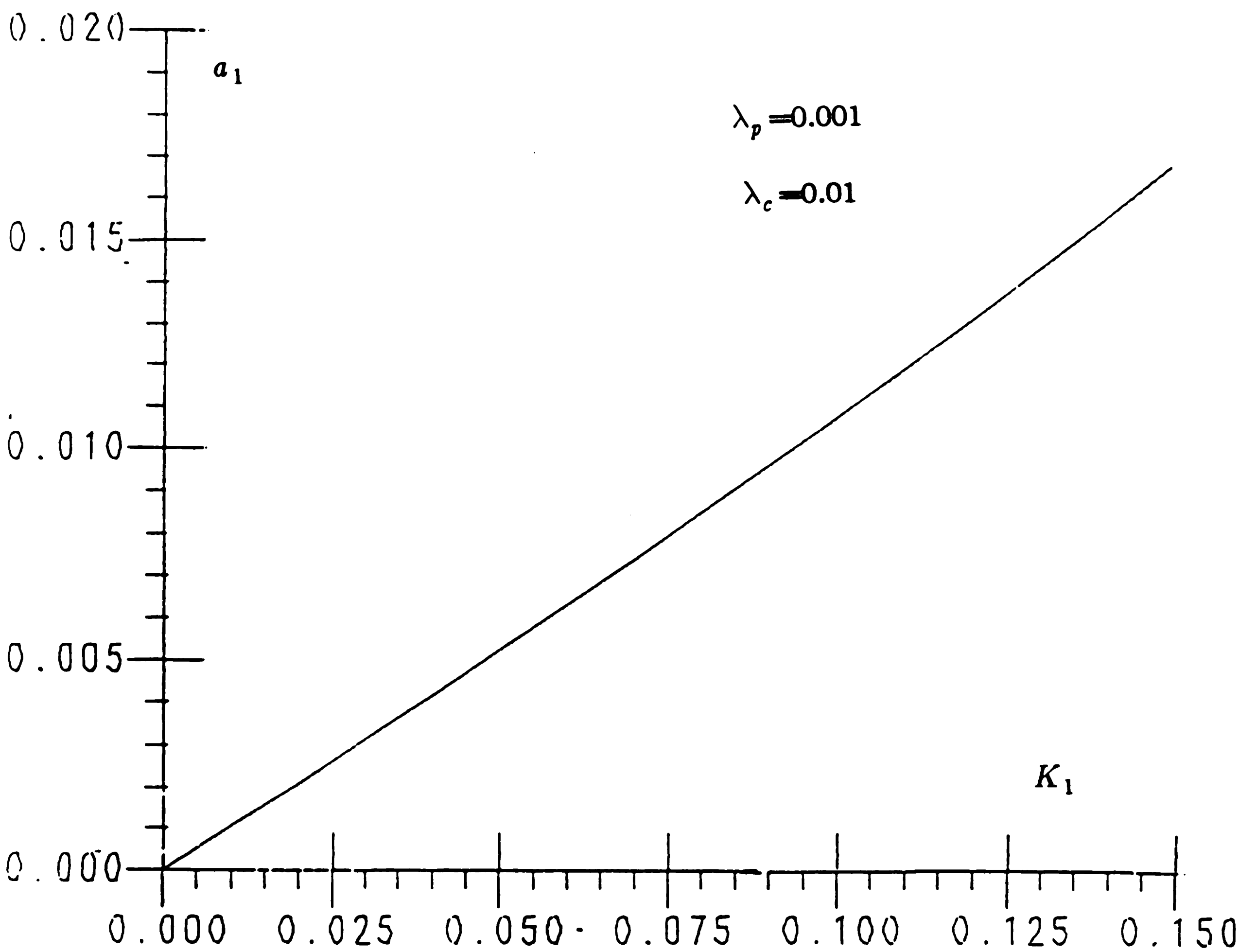

Figure 26a - Variation of the Carrier Amplitude at the Anti-resonance Frequency with Respect to the Excitation Amplitude

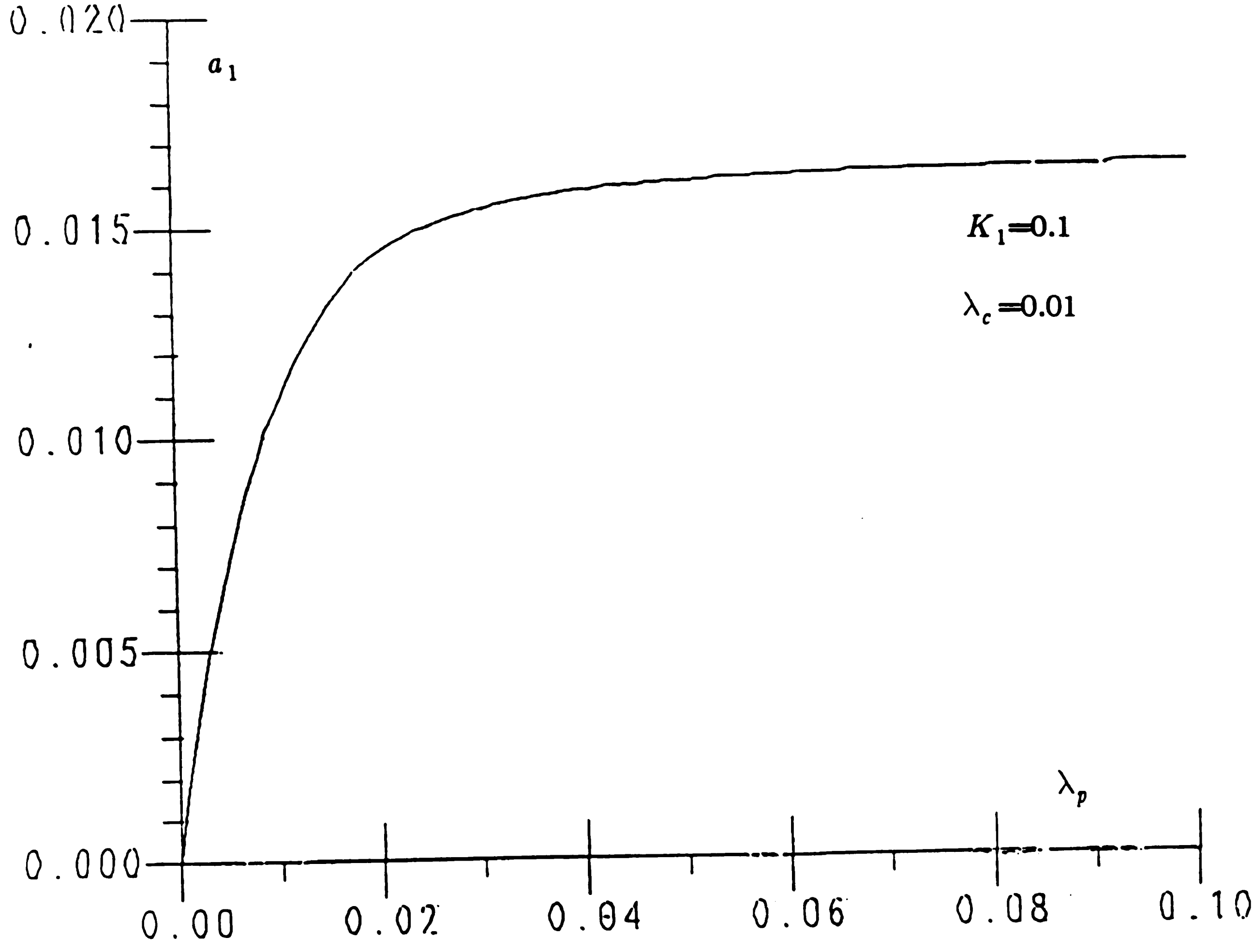

Figure 26b - Variation of the Carrier Amplitude at the Anti-resonance Frequency with Respect to the Absorber Damping

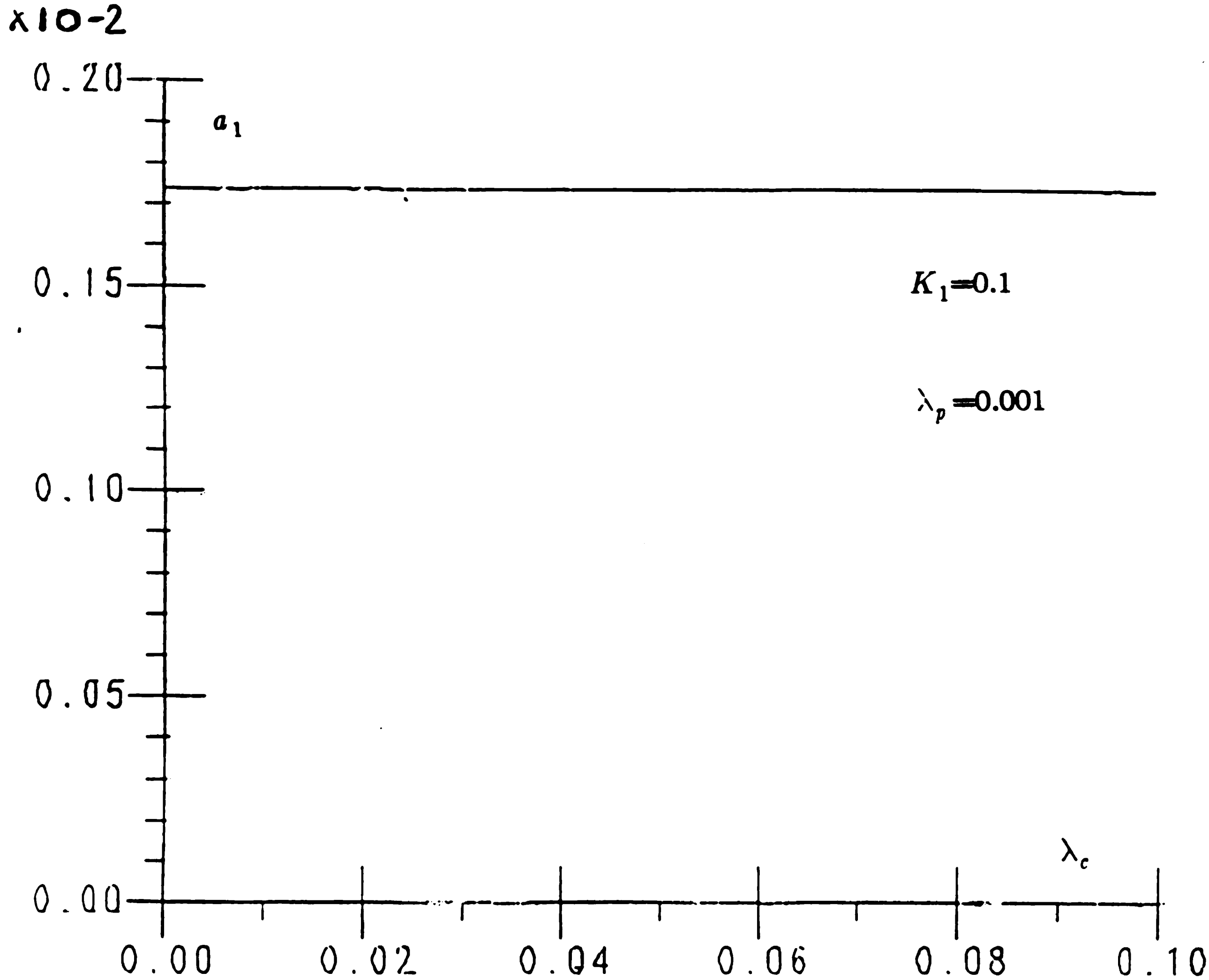

Figure 26c - Variation of the Carrier Amplitude at the Anti-resonance Frequency with Respect to the Carrier Damping

(3.2.19a) it is concluded that either $a_2=0$ or $\beta_2=0$ or π ($I_2=0$ corresponds to $a_2=2$ which is beyond the range of our approximation, *i.e.*, $\phi_{\max}>\frac{\pi}{2}$). The $a_2=0$ solution is unfeasible with $a_1=0$. Note that due to the particular configuration of the directions of the excitation and the rotation of the carrier and the motion of the absorber (Figure 2b), the $\beta_2=\pi$ solution represents the upper branch of the response curve and the $\beta_2=0$ solution represents the desired solution on the lower branch of the response curve; this, in fact, corresponds to the pendulum moving out of phase with respect to the forcing, as it must in order to act as an absorber. Equation (3.2.19c) is automatically satisfied for $\beta_2=0$. Equation (3.2.19b) reduces to

$$K_1-I_2\hat{a}_2=0 \tag{3.5.1a}$$

where I_1 and I_2 are as in equations (3.2.17a) and (3.2.17b), respectively, with $\eta=\hat{\eta}$ and $a_2=\hat{a}_2$ where $\hat{a}_2$ is the pendulum amplitude at the anti-resonance frequency, $\hat{\eta}$. Equation (3.2.19d) simplifies to the following expression by imposing $a_1=0$, $\beta_2=0$ and equation (3.5.1a):

$$\gamma\hat{\eta}^2-\Omega^2(1-\frac{\hat{a}_2^2}{8})=0 \tag{3.5.1b}$$

Note that if $\hat{a}_2$ is small, *i.e.*, if we linearize, then $\hat{\eta}=\eta_{AR}$ is recovered from equation (3.5.1b) and (3.5.1a) yields the linear pendulum response amplitude at η_{AR}.

Equations (3.5.1) were solved numerically for the unknowns $\hat{a}_2$ and $\hat{\eta}$ as a function of the excitation amplitude K_1. Figure (21) illustrates the result of this analysis for $\hat{\eta}$. As can be observed, the anti-resonance frequency, $\hat{\eta}$, decreases in value as the excitation amplitude is increased. According to Figure (21), for $K_1>0.12$ the anti-resonance frequency is predicted to be larger than the turning frequency, η_t. When $\eta_t<\hat{\eta}$ is predicted from our approximate analysis, no $\hat{\eta}$ can actually occur since $a_1=0$ cannot exist at a frequency above η_t . In such a case no low amplitude carrier motion can exist, and a steady-state response at $\eta=\hat{\eta}$ will occur which corresponds to the upper branch of the response curve. This effect renders the absorber useless, and it cannot be captured from a linearized system analysis. Figure (27) depicts the predicted and simulated carrier response for $K=0.5$. Note that in this situation no range of η values exists for which the system acts as an absorber. The conclusion is that these devices will have a limited torque range.

When damping is taken into account the amplitude of the carrier at the anti-resonance frequency can be no longer set identically to zero. Instead, the derivative of the carrier amplitude with respect to the excitation frequency at the anti-resonance frequency can be set to zero since the carrier response curve, by definition of the anti-resonance frequency, has a minimum at that frequency. Accordingly, equations (3.2.16) and (3.2.18) can be differentiated with respect to the excitation frequency, η, resulting in four coupled partial differential equations. The subsequent eight unknowns (*i.e.*, a_1, a_2, β_1, β_2, and their partial derivatives with respect to η, with $\frac{\partial a_1}{\partial \eta}$ set to zero, and $\hat{\eta}$ which is not known) can be solved (in principle) using the four equations (3.2.16) and (3.2.18) and the four partial differential equations mentioned above. However, the resulting equations are complicated enough (and are not shown here) that results obtained directly from the simulation of the equations of motion (3.1.5) proved more practical. It was found as a general rule that increasing the absorber damping tends to shift the $\hat{\eta}$ curve in Figure (21) slightly to the left, while the carrier damping has no detectable effect on the shifting of the anti-resonance frequency (for $\lambda_c<0.1$).

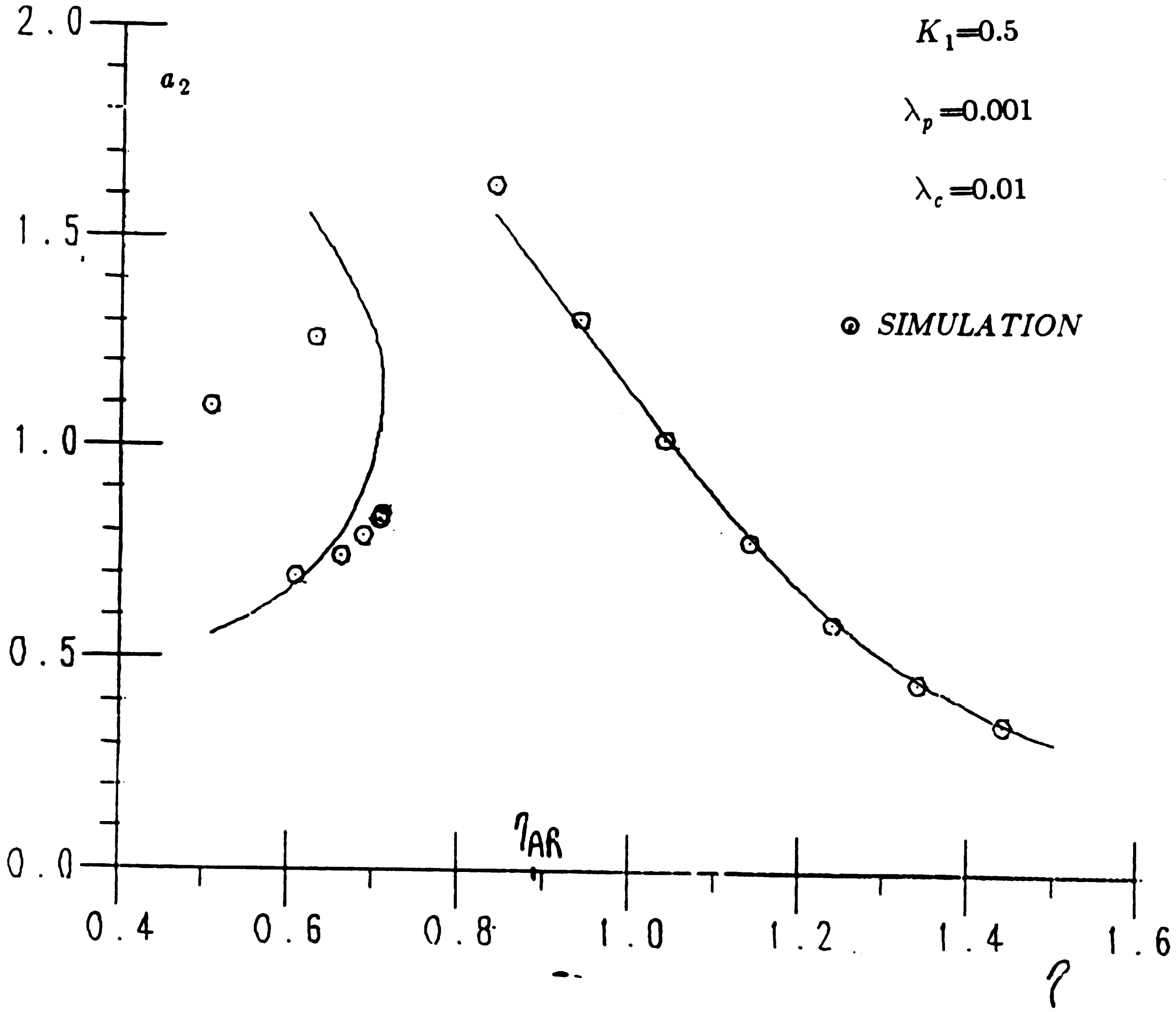

Figure 27a - Frequency Response of the Absorber

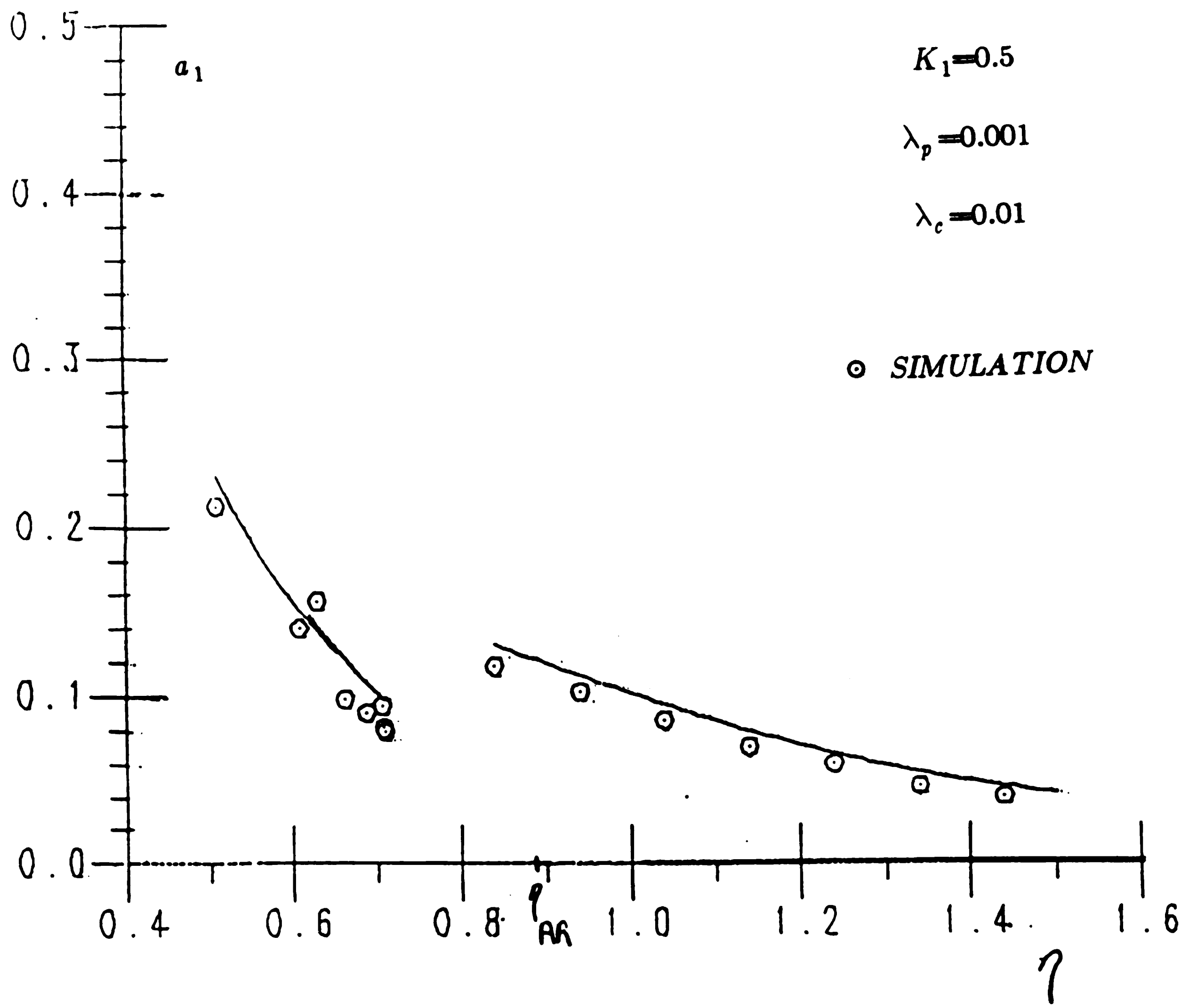

Figure 27b - Frequency Response of the Carrier

CHAPTER 4

CONCLUSIONS

The dynamic response of a centrifugal pendulum vibration absorber was investigated in terms of the effectiveness and range of applications of the device. The nonlinear methods of analysis undertaken in this work have revealed some aspects of the dynamics of the CPVA which have not been understood before.

4.1- The Effects of Motion Limiting Stops

The main conclusion drawn from the first part of the thesis is that motion limiting stops can be effectively employed when placed at amplitudes larger than the steady-state response predicted from the linear system at the anti-resonance frequency. This is so due to the fact that steady-state impacting motions can occur at the anti-resonance frequency only if the damping between the pendulum and the carrier is unreasonably large. The impact dynamics of the system can be very complicated when it is subjected to frequencies above anti-resonance; this can include chaotic motions and/or a variety of periodic responses. The satisfactory performance of the centrifugal absorber with motion limiting stops is dependent on the amplitudes of the excitation that is inducing the undesirable vibration on the primary system (carrier). If the excitation amplitude becomes larger than the *free−flight* threshold, the absorber will interact with the stops resulting in poor, if not damaging, performance.

Recent experiments have been carried out on a simple, non-rotating, impacting pendulum which is governed by the same equations of motion as the linearized system with stops (equations 2.1.20a,b). These demonstrated the existence of SDIP motions, pitchfork bifurcations and chaotic dynamics [36]. Frequencies near the corresponding anti-resonance frequency were not, however, attainable in that system since η was restricted to be 1.0 or higher by equipment limitations.

The SDIP motions are a very specific type of periodic motion. An *infinite* number of other types of periodic motions exist for this system. This is known since the presence of chaotic dynamics indicates the existence of horseshoe sets for the map **P** which in turn contain this infinity of periodic motions along with nonperiodic motions [37]. Thus a *complete* study of the impacting dynamics is out of the question. However, SDIP motions are the most common; this has been observed in experiments [36] and simulations. In addition, they are a good indicator of where other impacting motions exist since many (although not all) of the other types arise out of bifurcations which are directly tied to an SDIP motion.

If stops are not employed at all, and the pendulum is allowed to swing over the top (an extreme situation which is rarely, if ever, seen in applications), the system can undergo chaotic motions in which the pendulum undergoes chaotic sequences of clockwise and counter-clockwise rotations [35].

4.2- The Effects of Nonlinearities and Damping

In the second part of the study, the nonlinear response of a centrifugal pendulum vibration absorber was studied using harmonic balance and Floquet theory. Although specific geometrical dimensions for the model were used in this report, some general conclusions can be drawn from the results.

The method of analysis applied to the basic model resulted in sufficiently accurate results and their agreement with the simulation of the full nonlinear equations of motion was satisfactory. The results depict how the true response of the system can be drastically different than what is predicted from the linear analysis. Hence, it is well advised that when designing a CPVA that the undamped, linear analysis should be used as a means of first trial of the required system dimensions and geometric properties. However, once designed, the model must be analyzed using a nonlinear method such as the one outlined in this study to account for the nonlinear and damping characteristics of the system, which affect the dynamic response of the CPVA. This can be true even in some cases where one might think that the mere presence of low amplitude motions justifies using the linear analysis results.

Nonlinear characteristics of the system such as the shifting of the anti-resonance frequency and the jump phenomena must be considered in the design of the CPVA since if ignored, the absorber's effectiveness can be reduced, or it might even result in larger oscillatory amplitudes in the primary system.

It is often assumed that carrier damping has negligible effect on the response of the CPVA since, when properly working, the carrier runs at constant speed, and hence the carrier damping is completely counteracted by the mean component of the torque. Based on the results indicated in Figure (23c), it appears that such an assumption is reasonable since the response at the anti-resonance is quite insensitive to the values of λ_c. However, the anti-resonance response is extremely sensitive to the magnitude of pendulum damping. It may be possible to lump the carrier damping in with the pendulum damping, resulting in some increased value for the effective pendulum damping, due to the system's insensitivity to λ_c at anti-resonance.

Several other researchers have investigated the nonlinear dynamic response of the CPVA. Den Hartog [38], Crossley [20], and Newland [7, 25] seem to have contributed the most. A brief comparison is presented here between the results obtained in this report and those of these references. The model used in this report is a generalization of the one used by Crossley [20] except that damping is neglected in [20]. Although the equations of motion in both reports are equivalent (with the exception of damping terms), the final expressions for the nonlinear dynamic response of the pendulum and the carrier are different. Since Crossley models the system without damping, the equations of motion are integrable and the result is an expression for the angular displacement of the pendulum in terms of hyperelliptic functions. Also, no stability analysis was carried out by Crossley and the subjects of jump phenomena and the turning frequency were not considered. The conclusion drawn from Crossley's analysis is that, due to the wide angle of swing of the absorber, the designed aborber should never be too long and they should be of a length somewhat shorter than the value given by the linear analysis. The results in this report show in a more detailed manner as to the reason that the pendulum should be designed with a shorter length than predicted by the linear analysis. This is performed by the computation of the shifting in the anti-resonance frequency and as noted, η_{AR} has a tendency to *decrease* as K_1,, and consequently the absorber amplitude, is increased. Keeping in mind that the excitation frequency is fixed at $\eta = j\Omega$, and since the minimum amplitude of oscillation of the carrier occurs at a value below $j = \left(\frac{R}{r}\right)^{1/2}$, then the ratio $\frac{R}{r}$ should be adjusted in such a manner as to increase the frequency at which the minimum oscillation amplitude of the carrier takes place, *i.e.*, the frequency at which the absorber is most effective. By the virtue of the fact that the carrier effective radius, R, is essentially fixed, the only parameter over which the designer can have effective control is the pendulum length, r. An increase in the effective frequency of the absorber (a right-ward shift of the anti-resonance frequency) then necessarily implies a decrease in the effective radius of the absorber. This fact, as mentioned earlier, is in agreement with Crossley's results.

Den Hartog [38] uses a model equivalent to Crossley's. The equations are linearized and the concept of anti-resonance frequency for small angle displacement is discussed through the definition of the equivalent inertia of the system. The effects of pendulum damping and nonlinearities are briefly touched upon and expressions are presented for the dynamic response of the absorber in terms of hyperelliptic functions. As far as the shift in the anti-resonance frequency is concerned, remarks similar to those given by Crossley [20] are presented, indicating an increase in the anti-resonance frequency due to the wide angle of swing of the pendulum. No stability analysis is presented by Den Hartog [38] or Crossley [19, 20].

Newland [7, 25] has presented the most comprehensive study on this subject. However, his model does not consider the effects of damping. Newland obtains an approximate solution using the Ritz minimization method. Some stability analysis is presented in Newland [7] which explains the unstable nature of the middle branch of the frequency response. The stability results presented in this report extend those of [7] in the sense that in addition it has been shown that there can be breakdown in the stability of the periodic motions on the upper branch of the frequency response curve. The effect of jump phenomena is dealt with extensively in [25].

In this work it is shown that the method of harmonic balance with nonlinear terms of up to cubic order yields quite accurate and satisfactory results when compared to the results obtained from simulations of the full nonlinear equations of motion (Equations 3.1.1). The method of averaging [33] was also applied to the present system. This effort was not fruitful, however, due to the fact that the low-amplitude carrier response near the anti-resonance frequency could not be captured using first-order averaging.

4.3- Suggestions for Future Work

A limiting factor in many designs of the CPVA is that the steady-state pendulum angle amplitudes must become large when the disturbing torque amplitudes are large. If the system is driven out of the region of validity for linearization, then nonlinear effects can lead to catastrophic failures [7]. This is currently dealt with by making the effective pendulum path non-circular. Cycloidal paths are common in helicopter applications; more optimal paths are currently being worked on in the automotive industry

[18]. It is found, through research and experiments, that many of the undesirable nonlinear properties of the conventionaly circular-path CPVAs (for example, the jump phenomena) can be eliminated by incorporating non-circular paths in the design of the CPVA. Also worthy of note is the work of Mouzakis [23] on a monofilar pendulous absorber in conjunction with helicopter rotor torsional vibrations.

An obvious study complementary to the one presented in this thesis is an experimental investigation of the response of the CPVA. Further research can also be carried out on other aspects of the dynamics of the CPVA. For instance, more detailed analysis of the response of the absorber with respect to non-circular paths deserves more attention. Also, the use of multiple-pendula sets on shafts that are subject to excitations with more than one dominant frequency needs to be investigated. From a design point of view, one can study the range of system parameters for which an absorber with *optimal* performance characteristics can be designed. In particular, one can study the effects of combining the results of the two parts of this thesis to obtain guidelines and data for the response of the CPVA with motion limiting stops with respect to the turning frequency, anti-resonance frequency and possible interactions with the stops. Also, the dynamic interactions which result when multiple pendula are used on a shaft is of interest, as are the effects of the coupling between vibrations due to shaft flexibility and/or translations of the entire structure. Furthermore, during simulations of the full nonlinear equations of motion of the CPVA it was observed that a subharmonic of order two occured near η=0.5 (chapter 3 of the thesis) and has a significant effect on the response of the system at that frequency. This characteristic of the CPVA is one which deserves further study.

LIST OF REFERENCES

1. E. S. Taylor, 1936, *Transactions of the Society of Aeronautical Engineers* **38**, 81. Eliminating Crankshaft Vibration in Radial Aircraft Engines.

2. Moore, 1942, *Journal of Aeronautical Science* **9** 229. The Control of Torsional Vibration in Radial Aircraft Engines by Means of Tuned Pendulums.

3. C. F. Taylor, 1982, *The Internal Combustion Engine in Theory and Practice, Vol. 2: Combustion, Fuels, Materials, Design*. M.I.T. Press.

4. O'Connor, 1947, *Society of Automotive Engineers Quarterly Transactions* **1**, 87. The Viscous Torsional Vibration Damper.

5. Pierce, 1945, *Transactions of Society of Automotive Engineers* **53**, 480. Rubber Mounted Dampers, Examples of Application.

6. W. F. Paul, 1969, *25th American Helicopter Society Forum*, 1-9. Development and Evaluation of the Main Rotor Bifilar Absorber.

7. D. E. Newland, 1963, *Nonlinear Vibrations: A Comparative Study with Applications to Centrifugal Pendulum Vibration Absorbers. Ph.D. Thesis, M.I.T.* .

8. R. W. Zdanowich, T. S. Wilson, 1945, *Proceedings of Institute of Mechanical Engineers* **143**, 182-210. The Elements of Pendulum Dampers.

9. J. P. Den Hartog, 1947, *Mechanical Vibrations*,McGraw-Hill Book Company. New York.

10. T. C. Lim, 1986, *Dynamics of Systems with Rotating Pendulums as Vibration Absorbers*. M.S. Thesis, University of Missouri-Rolla.

11. Robert Plunkett, 1953, *Applied Mechanics Review* **6**, 7, 313-315. Vibration Damping.

12. R. J. Harker, 1944, *Journal of Aeronautical Science* **11**, 246,197-204. Theory of the Centrifugally Tuned Vibration Absorber.

13. C. A. Meyer, H. B. Saldin, 1942, *Journal of Applied Mechanics* **9**, A59-A64. Model Tests of Two Types of Vibration Absorbers.

14. R. E. Reed, 1949, *Journal of Applied Mechanics*, 190-194. The Use of the Centrifugal Pendulum Absorber for the Reduction of Linear Vibration.

15. R. R. Sarazin, 1930, *Rotating Pendulum Absorbers with Bifilar Suspension*, British Patent 379, 165, 1930.

16. R. Chilton, Reed Propeller Company, *Rotating Pendulum Absorbers with Bifialr Suspension Using Crankweb Counterweights as Pendulum Masses.* British Patent 460, 088, 1935.

17. Butler, B. A. C., *Rotating Pendulum Absorbers Using One or More Shell Balls as Pendulum Masses, Rolling on Elliptical and Paraboidal Tracks,* British Patent 520, 787, 1938.

18. H. H. Denman, 1988,*Ford Motor Company Report #88-08-01,* Tautochronic Bifilar Pendulum Torsional Absorber in Reciprocating Engines.

19. F. R. E. Crossley, 1952, *Journal of Applied Mechanics,* 315-319. The Free Oscillation of the Centrifugal Pendulum with Wide Angles.

20. F. R. E. Crossley, 1953, *Journal of Applied Mechanics* **75,** 41-47. The Forced Oscillation of the Centrifugal Pendulum with Wide Angles.

21. W. L. Miao, T. Mouzakis, 1981,*37th American Helicopter Society Forum.* Nonlinear Characteristics of the Rotor Bifilar Absorber.

22. B. Kelly, et al, *Device to Alter Dynamic Characteristics of Rotor Systems,* U. S. Patent 3,035, 643, May22, 1962.

23. T. Mouzakis, 1981, *American Helicopter Society NorthEast Region National Specialists' Meeting on Helicopter Vibration, "Technology for the Jet Smooth Ride".* Monofilar- A Dual Frequency Rotorhead Absorber, Hartford, Connecticut.

24. S. F. Masri, 1972, *Journal of Applied Mechanics* **39,** 563-568. Theory of Dynamic Vibration Neutralizer with Motion Limiting Stops.

25. D. E. Newland, 1964, *Journal of Engineering for Industry* **86,** 257-263. Nonlinear Aspects of the Performance of Centrifugal Pendulum Vibration Absorber.

26. J. Guckenheimer, P. Holmes, 1983, *Nonlinear Oscillations, Dynamical Systems and Bifurcations of Vector Fields.* Springer-Verlag, New York.

27. H. Poincarè, 1899, *Les Methodes Nouvelles de la Mecanique Celeste,* 3 vols. Gauthier-Villars, Paris.

28. S. W. Shaw, 1985, *Journal of Applied Mechanics,* 453-458. The Dynamics of a Harmonically Excited System Having Rigid Constraints, Part I: Subharmonic Motions and Local Bifurcations.

29. G. S. Whiston, 1987, *Journal of Sound and Vibration* **118**(3), 395-424. Global Dynamics of a Vibro-Impacting Linear Oscillator.

30. S. F. Masri, T. K. Caughey, 1966, *Journal of Applied Mechanics* **33,** 586-592. On The Stability of the Impact Damper.

31. M. W. Hirsch, S. Smale, 1974, *Differential Equations, Dynamical Systems and Linear Algebra*. Academic Press, Inc. Florida.

32 Ali. H. Nayfeh, D. T. Mook, 1979, *Nonlinear Oscillations*. John Wiley and Sons. New York.

33. Jack H. Hale, 1969, *Ordinary Differential Equations*. John Wiley and Sons. New York.

34. J. J. Stoker, 1957, *Nonlinear Vibrations*. Interscience. New York.

35. S. W. Shaw, S. W. Wiggins, 1988, *ASME Journal of Applied Mechanics*, to appear. Chaotic Motions of a Torsional Vibration Absorber.

36. D. W. Moore, S. W. Shaw, 1988, *International Journal of Nonlinear Mechanics*. The Dynamic Response of an Impacting Pendulum System. Experiments. To appear.

37. S. W. Shaw, 1985, *Journal of Applied Mechanics* **52**, 459-464.The Dynamics of a Harmonically Excited System Having Rigid Constraints, Part II: Chaotic Motions and Global Bifurcations.

38. J. P. Den Hartog, 1938, *S. Timoshenko 60th Anniversary*, **17-26**. Tuned Pendulums as Torsional Vibration Absorbers. McMillan Company. New York.